# UNIVERSITAT DE VALÈNCIA

## Doctoral Program in Neurosciences

## Faculty of Biological Sciences


# Immunoelectron microscopy labeling for the identification of oligodendrocytes and their precursor cells

PhD thesis presented by María José Ulloa Navas

and supervised by Prof. José Manuel García Verdugo, PhD

and Vicente Herranz Pérez, PhD

Valencia, November 2021

José Manuel García Verdugo, Catedrático del Departamento de Biología Celular, Biología Funcional y Antropología Física de la Facultad de Ciencias Biológicas de la Universitat de València:

INFORMA

Que Dª María José Ulloa Navas ha realizado en el Laboratorio de Neurobiología Comparada del Instituto Cavanilles de Biodiversidad y Biología Evolutiva de la Universitat de València, bajo mi dirección, el trabajo experimental que ha llevado a la redacción de la presente memoria de Tesis Doctoral presentada como compendio de publicaciones, titulada "Immunoelectron microscopy labeling for the identification of oligodendrocyte and its precursors".

Revisado el trabajo, autorizo su presentación para optar al grado de Doctor, y para que así conste y surta los efectos oportunos, firmo el presente informe en Valencia,

Firmado: José Manuel García Verdugo

Vicente Herranz Pérez, Doctor en Biología e investigador postdoctoral del Centro de Investigación en Red en Enfermedades Neurodegenerativas (CIBERNED):

INFORMA

Que Dª María José Ulloa Navas ha realizado en el Laboratorio de Neurobiología Comparada del Instituto Cavanilles de Biodiversdad y Biología Evolutiva de la Universitat de València, bajo mi dirección, el trabajo experimental que ha llevado a la redacción de la presente memoria de Tesis Doctoral presentada como compendio de publicaciones, titulada "Immunoelectron microscopy labeling for the identification of oligodendrocyte and its precursors".

Revisado el trabajo, autorizo su presentación para optar al grado de Doctor, y para que así conste y surta los efectos oportunos, firmo el presente informe en Valencia,

Firmado: Vicente Herranz Pérez


Yo, María José Ulloa Navas, declaro que soy autora del presente trabajo de investigación realizado en el Laboratorio de Neurobiología Comparada del Instituto Cavanilles de Biodiversdad y Biología Evolutiva de la Universitat de València, bajo la dirección del Dr. D. José Manuel García Verdugo, Catedrático del Departamento de Biología Celular, Biología Funcional y Antropología Física de la Universitat de València y el Dr. D. Vicente Herranz Pérez, investigador postdoctoral del Centro de Investigación en Red en Enfermedades Neurodegenerativas (CIBERNED).

Y para que así conste y surta los efectos oportunos, firmo el presente certificado en Valencia,

Firmado: María José Ulloa Navas

The present thesis was funded by a McDonald Fellowship granted by the Multiple Sclerosis International Federation and by the Nano-scaffolding for neuronal migration and generation project (PCI2018-093062) granted by the Spanish Ministry of Science (CIBERNED).

*Per aspera, ad astra.*

**AGRADECIMIENTOS**

Quiero agradecer primero a Dios, a mis papás, a mi hermana y a mis abuelitos. En especial a mi abuelita Anita que ha estado conmigo apoyándome siempre y estoy segura de que ahora me apoya desde el cielo. A mi papá por ser un ejemplo siempre, por quererme, perdonarme y enseñarme tanto. Espero que todo su sacrificio se vea al menos parcialmente retribuido en esta tesis. A mi mamá que siempre tiene paciencia conmigo, me ama incondicionalmente y siempre se adelanta a mis necesidades. Gracias por todo lo que has hecho por mí en todos estos años. A mi hermana que ha sido mi compañera y mi cómplice en todo, que siempre me escucha y me apoya. Dios no me pudo haber regalado una mejor compañera de infancia y ahora de vida.

A mi profesor Verdugo, que siempre vio algo bueno y especial en mi para hacer ciencia. Gracias por dejarme hacer mil preguntas desde segundo curso en organización de la célula, gracias por enseñarme a tener paciencia y a ver que la ciencia y las cosas más bonitas están en los detalles pequeños. Sobre todo, gracias por apoyarme en cada experimento loco que se me ha ocurrido. Gracias porque eso me ayudó a entender la ciencia y a ser independiente. Gracias, profesor por las risas, por los buenos momentos, por las comidas y por los mil estudiantes. Gracias por su ejemplo de amor a la ciencia ante la adversidad y la enfermedad. Lo quiero muchísimo mi profe y siempre estará en mi corazón, en mis oraciones y en mi hipocampo.

A Vicente, por guiarme en este camino, por estar disponible 24/7 para mí, tanto para mis preguntas científicas, como para apoyarme en los problemas personales. Gracias por ayudarme a crecer y ayudarme a ver las cosas desde varios puntos de vista. Gracias por todas las risas, el fútbol, las miles de correcciones y los refranes apuntados en estos años.

A mi Patri, mi cielo en el laboratorio y en la vida. No puede existir mejor amiga, ni oficial de laboratorio para mí. Gracias por tenerme paciencia y enseñarme a que hay que pegar los tarugos para arrancar. Gracias porque estas manos parkinsonianas aprendieron a cortar ultrafinos arrancados gracias a ti. Gracias por todas las enseñanzas de vida, los bailes infinitos y las

canciones aprendidas en la sala de ultracuts. Gracias por los viajes, por los perros y las aventuras vividas y contadas. Siempre estás en mi corazón y en mis pensamientos. Aunque somos polos opuestos, siempre estaremos juntas.

A Susana, por abrirme el grifo cada vez que lo he necesitado. Gracias por acompañarme en este camino, por enseñarme que la vida es mejor en parafina. Gracias por todas las risas compartidas, por los almuerzos, por los cumpleaños, por todos los secretos compartidos en la cafetería. Gracias por tu amistad y tu cariño a lo largo de estos años.

A todas mis mentoras que han pasado por el laboratorio, en especial a Arantxa y Paula. Por enseñarme la pasión por la ciencia y a saber que al laboratorio se va a pasárselo bien. A todos los estudiantes que han pasado por mi vida y mi corazón a mis An(n)as que me enseñaron a enseñar, a Jorge, a mi Raquel que me ha sacado de tantos apuros científicos y me ayuda a avanzar siempre. A Luci y a Marina, por la confianza, el cariño y la paciencia cada día. Les dejo mi lugar feliz, mi laboratorio para que sigan disfrutando del cerebro.

A todas las personas del Cavanilles y de la Universidad gracias a cuyo trabajo, para mí casi invisible he podido hacer esta tesis.

A Peter que me ha ayudado a conseguir las muestras humanas y a todos los pacientes que han puesto sus muestras en nuestras manos, con la confianza de que vamos a hacer lo mejor con ellas.

To Dr Q's lab members especially to Emily and Rawan who have supported and loved me unconditionally during my visit. I'll never find the words to thank you enough for what you have done for me. I hope our friendship lasts forever. We'll run to Saudi one day.

## INDEX

**FIGURE INDEX**

## ABBREVIATIONS

**A2B5** Antibody that recognizes ganglioside GT3 in OPCs

**AAV** Adenovirus

**ABCD1** ATP-Binding cassette subfamily D member 1

**APC [CC1]** Antibody that recognizes quaking 7 in oligodendrocytes

**ASPA** Aspartoacylase

**ARSA** Arylsulfatase A

**BCAS1** Brain enriched myelin associated protein 1

**BMP** Bone morphogenic factor

**CNS** Central nervous system

**CRISPR-Cas** Clustered regularly interspaced short palindromic repeat-CRISPR-associated protein

**DLX2** Distal-Less Homeobox 2

**EGFR** Epidermal growth factor receptor

**EIF2B** Eukaryotic protein complex which exerts the function on guaninenucleotide exchange factor.

**GALC** Galactosylceramidase

**GFAP** Glial fibrillary acidic protein

**Gsh2** Glutathione synthetase 2

**HIV** Human immunodeficiency virus

**JC Virus** John Cunningham virus

**m-OLS** Myelinating oligodendrocytes

**MAG** Myelin associated glycoprotein

**MBP** Myelin basic protein

**MLC1** Modulator of VRAC current 1

**MRI** Magnetic resonance imaging

**MS** Multiple sclerosis

**NKX 2.1** NK2 Homeobox 1

**NKX2.2 NK2** Homeobox 2

**NG2** Neuron-glial antigen 2

**NeuN** Neuronal nuclei/ Hexaribonucleotide binding protein 3

**ODG** Oligodendroglioma

**Olig1** Oligodendrocyte transfection factor 1

**Olig2** Oligodendrocyte transfection factor 2

**OPCs** Oligodendrocyte progenitor cells

**PDGFRα** Platelet derived growth factor alpha

**PLP1** Proteolipid protein 1

**pre-OLs** Pre-oligodendrocytes

**SHH** Sonic Hedgehog

**Sox10** Sry-related HMg-Box gene 10

**SpCas9** *Streptococcus pyogenes* Cas9

**TEM** Transmission electron microscopy

**TSA** Tyramide signal amplification

**Tuj1** Anti-beta-tubulin III antibody

**VRAC** Volume-regulated anion channel

**V-SVZ** Ventricular-subventricular zone

**WHO** World health organization

**ABSTRACT**

Oligodendrocytes are the myelinating cells of the central nervous system. Besides myelination, they provide metabolic and trophic support to neurons. These cells originate from oligodendrocyte progenitor cells (OPCs) that are widely distributed in the white and gray matter. Oligodendrocytes and OPCs are severely affected in different pathologies in the human brain. These impairments are caused by several different pathogenic mechanisms such as genetic mutations, infections, neoplastic mutations, autoimmunity and traumatic injuries. Most of these dysfunctions result demyelination. Among the multiple techniques to study demyelination/remyelination, transmission electron microscopy (TEM) has emerged as the gold standard. However, in human tissue and in some cases in rodent tissue, the lack of optimal fixation difficult TEM characterization of the cells and their analysis. Hence, in the present thesis presented as a compendium of publications, we have used TEM to study several aspects of oligodendrocytes and OPCs. In the first article presented we studied and characterized the fine structure of human oligodendrocytes and OPCs via immunogold labeling. Our results suggest that there are 3 different ultrastructural differentiation stages in oligodendrocytes. The second publication is a book chapter in which we developed a tyramide-based amplification method to enhance immunogold labeling to detect oligodendrocyte lineage markers such as PDGFRa, NG2 and BCAS1. This method displays a better specificity than standard pre-embedding immunogold and can be performed in less time and using lower concentrations of antibodies. The third publication describes the existence of a clustered population of BCAS1-positive cells in a case of human oligodendroglioma for the first time. This points out the importance of oligodendrocyte progenitor markers in glial neoplastic entities. The last article, shows how immunoelectron microscopy can be used for subcellular tracking of the novel CRISPR system in hard to manipulate cells such as OPCs. Our results show how nuclear transportation is hardly achieved in primary OPCs compared to control standardized cell lines. Interestingly, OPCs package and process the enzyme Cas9 into endosomal compartments rather than directing it for nuclear transportation.

**RESUMEN**

Los oligodendrocitos son las células mielinizantes del sistema nervioso central. Además de la mielinización, proporcionan apoyo metabólico y trófico a las neuronas. Estas células se originan a partir de células progenitoras de oligodendrocitos (OPC) que están ampliamente distribuidas en la sustancia blanca y gris. Los oligodendrocitos y las OPC se ven gravemente afectados en diferentes patologías del cerebro humano. Estas enfermedades son causadas por patologías con diferentes mecanismos, como mutaciones genéticas, infecciones, mutaciones que dan lugar a neoplasias, autoinmunidad y lesiones traumáticas. La mayoría de estas disfunciones resultan en desmielinización. De entre las múltiples técnicas para analizar desmielinización y remielinización, la microscopía electrónica de transmisión (MET) es el estándar. Sin embargo, en tejido humano y en algunos casos en tejido de roedor, la falta de una fijación óptima dificulta la caracterización de las células y el análisis a través de MET. Por lo tanto, en la presente tesis presentada como un compendio de publicaciones hemos utilizado MET para estudiar varios aspectos de los oligodendrocitos y las OPC. En el primer artículo presentado, estudiamos y caracterizamos la ultraestructura de los oligodendrocitos y OPC humanos mediante inmunomarcaje. Nuestros resultados sugieren que hay 3 diferentes etapas de diferenciación ultraestructural en los oligodendrocitos. La segunda publicación es un capítulo de un libro en el que desarrollamos un método basado en amplificación con tiramidas para mejorar el marcaje inmunohistoquímico con el fin de detectar marcadores del linaje oligodendroglial como PDGFRa, NG2 y BCAS1. Este método muestra una mejor especificidad que el estándar de inmuno-oro preinclusión y se puede realizar en menor tiempo y utilizando concentraciones más bajas de anticuerpos. La tercera publicación describe la existencia de una población definida de células positivas para BCAS1 en un caso de oligodendroglioma humano por primera vez. Esto señala la importancia de los marcadores progenitores de oligodendrocitos en las entidades neoplásicas gliales. El último artículo muestra cómo se puede utilizar la inmuno-oro y el análisis por microscopía electrónica para el seguimiento subcelular del novedoso sistema CRISPR en células difíciles de manipular como las OPC. Nuestros resultados

muestran cómo el transporte nuclear apenas se logra en las OPC primarias en comparación con las líneas celulares estandarizadas de control. Curiosamente, los OPC empaquetan y procesan la enzima Cas9 en compartimentos endosomales, en lugar de transportar la enzima al núcleo.

## INTRODUCCIÓN

### Oligodendrocitos y oligodendrogénesis en el cerebro

La composición celular del sistema nervioso central (CNS) se compone de cinco tipos de células principales: 1) neuronas, que son las principales células ejecutoras del cerebro (Gowers 1897); 2) astrocitos, las células de apoyo que desempeñan su papel en la función física, metabólica y reparadora dentro del CNS (Parpura y Verkhratsky 2012). Además, las células madre en los nichos neurogénicos (es decir, la zona ventricular-subventricular (V-SVZ) y el giro dentada del hipocampo) pertenecen al linaje astroglial (Kriegstein y Alvarez-Buylla 2009); 3) microglía, consideradas las células fagocíticas inmunes del SNC (Penfield 1925); 4) células ependimarias, que son células ciliadas que separan el parénquima cerebral y los ventrículos llenos de líquido. Se ha propuesto el movimiento coordinado en forma de látigo de los cilios ependimarios para dirigir el líquido cefalorraquídeo a través del sistema ventricular del SNC en roedores (Sawamoto et al. 2006); y 5) los oligodendrocitos que son células gliales cuya función principal es la mielinización. La mielinización es un proceso que favorece la optimización de la conducción saltatoria de los potenciales de acción de propagación (McLaurin y Yong 1995). Además, los oligodendrocitos realizan otras actividades de apoyo como el metabolismo de la glucosa (Amaral et al. 2016; Saab et al. 2016), la entrada / salida de calcio hacia el axón para impedir la degeneración (Witte et al. 2019) y la regulación del pH y el equilibrio iónico (Inouye y Kirschner 1988).

En el cerebro humano, los oligodendrocitos, como cualquier otra célula del cerebro derivada del linaje neural, se originan a partir de células gliales radiales tempranas (Anthony et al. 2004). Estudios recientes que utilizan estudios histológicos combinados con perfiles transcriptómicos en tejidos fetales han establecido que el origen exacto de los oligodendrocitos y sus progenitores es la glía radial externa (Huang et al., 2020). Además, esta población tiene el potencial de producir oligodendrocitos *in vitro* (Mo y Zecevic 2009). Más. No obstante, las regiones donde se generan las células

progenitoras de oligodendrocitos (OPC) y sus vías de migración son diversas a lo largo del desarrollo fetal. Tres ondas oligodendrogénicas con diferente origen y destino se suceden durante el desarrollo del cerebro (Kessaris et al. 2006). Se cree que el primer evento masivo de generación de OPC se origina en las eminencias ganglionares laterales anteriores durante las semanas 17-22 de gestación en el humano. Las células derivadas de esta primera ola se caracterizan por la expresión citoplasmática de DLX2 junto con otros marcadores específicos de OPC como PDGFRa, NG2 y Olig1. Se cree que estas células migran a través de una corriente discreta hacia la V-SVZ cortical. La segunda oleada de OPC surge de la eminencia ganglionar medial alrededor de la semana 23 de gestación. Las células de esta región se caracterizan por la expresión de NKX2.1 como marcador distintivo. Se cree que la tercera región de la generación de OPC es la corteza. Las OPC corticales expresan únicamente marcadores de linaje específico (Rakic y Zecevic 2003; Jakovcevski y Zecevic 2005).

Por otro lado, en el cerebro del ratón, se han estudiado mejor las bases moleculares de la oligodendrogénesis. La oligodendrogénesis del desarrollo comienza y depende del establecimiento de gradientes de *Sonic hedgehog* (SHH), un factor de transcripción que induce la ventralización del tejido al inhibir la acción de la proteína morfogénica ósea (BMP) (Figura 1A-B). SHH es secretada por la notocorda y la placa del piso del tubo neural, por lo tanto, tiene un efecto más robusto en las áreas ventrales (Takebayashi e Ikenaka, 2015). En el dominio de los progenitores de la neurona motora de la zona ventricular, las células sufren especificación debido a la alta concentración de SHH. Este estímulo les induce a comenzar a expresar Olig2 en E9.5 en este dominio. Estas células tienen el potencial de diferenciarse en neuronas motoras, oligodendrocitos o astrocitos (Masahira et al. 2006). Las células Olig2-positivas (Olig2 +) que se diferenciarán en oligodendrocitos maduros pasan a través de un estado transitorio de OPC indiferenciado que puede identificarse mediante la expresión de PDGFRα. Un subconjunto de estos progenitores persiste en un estado inactivo en el cerebro postnatal y adulto (Woodruff et al. 2001).

En E12.5, la porción ventral del dominio de los progenitores de la neurona motora expresa Nkx 2.2 además de Olig2 y PDGFRα, dando así lugar a la primera onda de migración u onda ventral de OPC (Fu et al. 2002). Esta onda celular migra hacia las estructuras dorsal y rostral de la médula espinal temprana, el rombencéfalo y el telencéfalo (Woodruff et al., 2001). En el telencéfalo, cuando todas las áreas de la eminencia ganglionar están completamente diferenciadas (E14.5), hay una segunda ola (primera ola telencefálica) de migración de progenitores. Estas células emergen del área medial de la eminencia ganglionar (células positivas para Nkx2.1) como marcador diferencial. Las OPC que expresan Nkx2.1 migran y ocupan la mayoría de las áreas telencefálicas y la corteza cerebelosa (Spassky et al. 1998).

En E15.5 (segunda onda telencefálica), otras áreas de la eminencia ganglionar como la eminencia gangliónica lateral y la eminencia gangliónica caudal dan lugar a un nuevo subconjunto de OPC, que se caracteriza por la expresión de Gsh2. Se pueden encontrar células positivas para GSH2 en la corteza en la etapa de desarrollo E16.5 (Kessaris et al. 2006). La tercera ola proliferativa telencefálica de OPC tiene lugar en fases embrionarias tardías y perinatalmente. Se caracterizan por la expresión de Emx1 (Vallstedt et al. 2005) y su función es reemplazar las OPC Nkx2.1 + generadas en etapas tempranas de desarrollo.

La generación de mielina y nuevos oligodendrocitos juega un papel fundamental en el cerebro adulto, en el que la remodelación y la plasticidad son un fenómeno constante y necesario. Una vez que se completa el desarrollo del SNC, existe una población de células NG2 positivas que permanecen distribuidsa por todo el cerebro adulto. Esta población de OPC tiene una capacidad de proliferación lenta o inactiva y actúa como reservorio, pudiendo diferenciarse en oligodendrocitos mielinizantes durante la vida posnatal (Dimou et al. 2008). Además de estas OPC distribuidas por todo el parénquima cerebral, las células madre neurales ubicadas en la V-SVZ pueden generar nuevas OPC en el cerebro adulto. Curiosamente, estas células también se encuentran en lesiones desmielinizantes como las placas de esclerosis múltiple (Wilson et al. 2006).

La dinámica y la ultraestructura de los oligodendrocitos en el cerebro de los roedores se encuentran más estudiadas ya que existe una mayor disponibilidad de muestras y diversidad de animales transgénicos. La morfología y la estructura fina de los oligodendrocitos se han caracterizado previamente en roedores como células ramificadas cuyo soma es pequeño, electrodenso, con citoplasma irregular que se adapta a axones amielínicos y que contiene un retículo endoplásmico dilatado y corto; presentan núcleo esférico y cúmulos de cromatina adheridos a la membrana nuclear interna. (Luskin et al. 1993; Olude et al. 2018). Sus progenitores, por otro lado, se han caracterizado por el marcado Olig2 en el V-SVZ de ratones lesionados como células con un citoplasma relativamente denso en electrones, con numerosas mitocondrias, aparato de Golgi y retículo endoplásmico corto. Su morfología es similar a la de las células de tipo C (o progenitores amplificadores de tránsito) de la V-SVZ (Menn et al. 2006).

Por el contrario, en la investigación en tejido humano existen varios problemas relacionados con la conservación de muestras, especialmente para los estudios ultraestructurales, en los que la fijación es un paso fundamental para los procedimientos experimentales posteriores. Teniendo en cuenta que el estándar para los estudios de mielinización / remielinización se basa en el análisis de microscopía electrónica, caracterizar los oligodendrocitos y sus progenitores en el tejido humano es un hito para la investigación básica y aplicada de oligodendrocitos.

**Patologías relacionadas con la oligodendroglia**

La importancia de estudiar los oligodendrocitos y su generación en el CNS se basa en la diversidad de patologías que puede generar la disfunción de los oligodendrocitos. Existe una amplia variedad de causas que resultan en desmielinización y deterioro de oligodendrocitos, tales como bases genéticas, infecciosas, traumáticas y autoinmunes.

Las causas genéticas no son las más frecuentes, pero sí representan los casos más graves. Se han reportado deficiencias o mutaciones en diferentes genes como:

- Mutaciones en la proteína ácida fibrilar glial (GFAP), localizada en 17q21, que provocan la enfermedad de Alexander en el cerebro neonatal e infantil. Los signos y síntomas de esta leucodistrofia no son homogéneos. Sin embargo, en todos los pacientes da como resultado una desmielinización crónica que conduce a un deterioro físico y cognitivo que finalmente conduce a la muerte en un promedio de 10 años después del inicio (Messing 2018).

- Las mutaciones en la proteína proteolípida1 (PLP1), localizada en Xq22, provocan la enfermedad de Pelizaeus-Merzbacher, una leucodistrofia infantil / joven mortal que comienza durante la primera infancia y conduce a la muerte prematura durante la niñez (Renier et al. 1981).

- Las mutaciones en la aspartoacilasa (ASPA), ubicada en el cromosoma 17p13, son la causa de la enfermedad de Canavan, cuyas características se muestran durante la primera infancia e incluyen una amplia gama de defectos neurológicos desde la atonía hasta la ceguera y, en última instancia, causan la muerte del bebé a los 18 meses.

- Las mutaciones en el gen de la galactosilceramidasa (GALC), ubicado en el cromosoma 14q31, provocan la enfermedad de Krabbe. Esta patología se manifiesta principalmente en bebés con pronóstico fatal a los 2 años. Los signos y síntomas neurológicos son variados, pero el resultado es común en todos los pacientes infantiles. La enfermedad de Krabbe da como resultado un deterioro motor y mental, que conduce a la descerebración (Tappino et al. 2010).

- Las mutaciones en cualquiera de los 5 genes que codifican las subunidades del factor de iniciación de la traducción EIF2B, ubicado en 1p34, 2p23, 3q27, 12q24 o 14q2, causan leucoencefalopatía con pérdida de la sustancia blanca. Dada la variabilidad de las mutaciones dentro de los genes, los síntomas neurológicos y el pronóstico pueden no coincidir entre los

pacientes (van der Knaap et al. 1998; Biancheri et al. 2003; Labauge et al. 2009). El único síntoma común es la desmielinización progresiva.

- Las mutaciones en el gen modulador de la corriente 1 de VRAC (MLC1), ubicado en 22q13, provocan la enfermedad de Van der Knaap también conocida como leucoencefalopatía megalencefálica con quistes subcorticales. Esta leucodistrofia afecta principalmente a los lactantes que mueren prematuramente y comprende características neurológicas como megalencefalia, ataxia progresiva lenta, espasticidad y convulsiones (van der Knaap et al. 1995; Van der Knaap et al. 1996).

- Las mutaciones en el gen de la arilsulfatasa A (ARSA), ubicado en 22q13, provocan leucodistrofia metacromática. Las formas infantil y juvenil exhiben síntomas motores junto con incapacidad mental o retraso (Greenfield 1933). Las formas adultas de la enfermedad comienzan con sintomatología psiquiátrica (Propping et al. 1986).

- La adrenoleucodistrofia ligada al cromosoma X es el resultado de mutaciones en el gen ABCD1, ubicado en Xq21. Esta mutación da como resultado una falla en la transferencia de ácidos grasos a los peroxisomas prolongada en el tiempo. Una de las formas de la enfermedad da como resultado una forma cerebral que incluye una desmielinización extensa (Moser et al. 1991).

Las enfermedades infecciosas del SNC también son una causa de desmielinización. Los agentes infecciosos clásicos que causan desmielinización son los virus. Los virus pueden inducir la desmielinización de cuatro formas diferentes: 1) Al infectar directamente a los oligodendrocitos, lo que conduce a la muerte celular. 2) Una respuesta persistente hacia agentes virales que causa alteraciones homeostáticas y metabólicas en el cerebro y finalmente produce la muerte de oligodendrocitos. 3) Inflamación inducida por citocinas que afecta al entorno oligodendroglial. 4) La respuesta inmune a través de mimetismo antigénico hacia proteínas específicas de oligodendrocitos o mielina secundaria a una infección viral (Stohlman y Hinton 2001).

Las enfermedades producidas por virus que involucran uno o más mecanismos de los descritos anteriormente son: panencefalitis esclerosante subaguda, leucoencefalopatía multifocal progresiva y encefalomielitis posinfecciosa.

La panencefalitis esclerosante subaguda es una enfermedad rara provocada por el virus del sarampión o la vacuna contra el sarampión atenuado. Ocurre en 1 caso por millón y causa desmielinización crónica severa en los niños (Modlin et al. 1977). La persistencia de este virus dentro de las neuronas y oligodendrocitos se asocia con varias mutaciones que impiden el ensamblaje viral y la salida de las células (Stohlman y Hinton 2001).

La leucoencefalopatía multifocal progresiva es una enfermedad mortal causada por el virus JC. Este virus es un virus ubicuo adquirido por los seres humanos durante la infancia y cuyo reservorio se cree que es el riñón. En pacientes inmunodeprimidos y en pacientes coinfectados por el VIH, este virus escapa a la vigilancia inmunitaria e infecta a los oligodendrocitos, provocando así desmielinización (Hou y Major 2000).

Finalmente, encefalomielitis post infecciosa, un subgrupo de enfermedades asociadas con varias infecciones virales diferentes como: paperas, varicela y virus de influenza. En este caso, el agente viral no puede relacionarse directamente con la desmielinización (Stohlman y Hinton 2001).

Las lesiones cerebrales también pueden inducir desmielinización. Varias causas pueden conducir a lesiones cerebrales, pero los mecanismos comunes son lesiones hemorrágicas o isquémicas. Las lesiones hemorrágicas son causadas por lesiones traumáticas o accidentes cerebrovasculares intracerebrales. Este tipo de lesiones resulta en un ambiente inflamatorio en la zona dañada, que deteriora el equilibrio homeostático de las células. En modelos animales de hemorragia, los oligodendrocitos y la mielina se ven afectados dentro del área hemorrágica y, en la periferia, la desmielinización con mala recuperación axonal y oligodendrocitaria son características clásicas de este tipo de lesiones (Wasserman y Schlichter 2008).

Por otro lado, las lesiones isquémicas pueden ser causadas por un ictus durante la edad adulta o por hipoxia cerebral que conduce a encefalopatía isquémica hipóxica o leucomalacia en lactantes (Chavali et al. 2020). En modelos de isquemia de adultos, los oligodendrocitos parecen ser una población afectada selectivamente en los primeros momentos después del infarto y mueren rápidamente por necrosis (Petito et al. 1998). El mismo fenómeno se observa en modelos de leucomalacia, donde los oligodendrocitos se ven particularmente afectados (Back et al. 2002). Esto se ha corroborado en cerebros de pacientes que presentan leucomalacia en lactantes humanos, en los que la maduración de los oligodendrocitos está gravemente comprometida (Volpe 2001).

Las enfermedades autoinmunes incluyen síndromes desmielinizantes raros y alteraciones neurodegenerativas frecuentes como la esclerosis múltiple (EM) y la neuritis óptica. La EM es la principal causa neurodegenerativa de discapacidad entre los adultos jóvenes. Se estima que la prevalencia mundial real de EM es de 1 / 3.000 personas, de las cuales el 1,5% corresponde a casos de EM pediátrica (personas menores de 18 años). En promedio, 7/10 pacientes con EM son mujeres. La incidencia varía entre países; por lo tanto, los países desarrollados presentan 2-3 veces más casos en comparación con los países subdesarrollados. Dado que en los países subdesarrollados el acceso a la asistencia sanitaria no es óptimo, se considera que los datos epidemiológicos (incidencia y prevalencia) aún están subestimados (MS Atlas 2020).

Además, los estudios sugieren la participación de OPC y oligodendrocitos en patologías neoplásicas como gliomas difusos y glioblastomas (Dufour et al. 2018). Dado que las OPC son la población cíclica y proliferativa más abundante en el cerebro, se cree que pueden desempeñar un papel importante en el desarrollo de gliomas y glioblastomas (Geha et al. 2010). En la misma línea, estudios ómicos de última generación han señalado que cuando los programas transcripcionales tipo OPC están activos, los oligodendrogliomas tienden a ser más agresivos y presentan un peor pronóstico (Bielle et al. 2017).

Dado que existen tratamientos para detener o al menos disminuir las causas de la desmielinización en enfermedades infecciosas, traumáticas y autoinmunes, las terapias viables para mejorar la remielinización siguen siendo la prioridad en el campo de la investigación. Las estrategias para evaluar la remielinización aún están en desarrollo, sin embargo, el estándar de oro para medir la remielinización en los tejidos es el *g-ratio* medido por microscopía electrónica de transmisión (MET). Por tanto, el estudio de la ultraestructura de los oligodendrocitos, sus progenitores y la mielina, especialmente en el tejido humano, es un aspecto relevante en biología celular y neurobiología.

### 1.3 El sistema CRISPR-Cas9 y las alteraciones de los oligodendrocitos

La ingeniería genómica se ha convertido en uno de los campos de estudio más destacados en las últimas cinco décadas. Particularmente, desde que se demostró por primera vez que los sistemas CRISPR-Cas funcionan en células eucariotas para la aplicación de edición genómica durante la última década, las posibilidades de ediciones genómicas fáciles, precisas y poderosas han dado como resultado un aumento en el número de estudios biológicos y clínicos básicos para lograr con éxito tratar o mejorar una amplia variedad de condiciones genéticas.

Cuando se descubrieron por primera vez, los sistemas CRISPR-Cas se describieron como un sistema inmunológico adaptativo que permitía a las bacterias y arqueobacterias defenderse de plásmidos y fagos (Barrangou et al. 2007). A día de hoy, los sistemas CRISPR-Cas se utilizan no solo para editar el genoma y el epigenoma, sino también para apuntar, rastrear y regular la expresión génica (Sander y Joung 2014), lo que maximiza las posibilidades de modelar y apuntar no solo a condiciones genéticas.

En cuanto a las patologías oligodendrogliales, el sistema CRISPR-Cas9 se ha utilizado en la enfermedad de Alexander para corregir las mutaciones en el gen GFAP, mejorando así el fenotipo de hipomielinización causado por esta condición (Li et al. 2018). Además, el uso de esta nueva herramienta genómica y oligonucleótidos antisentido ha demostrado ser una estrategia terapéutica eficaz para rescatar la corta vida útil del mutante PLP1, también conocido como ratones jimpy (modelo de enfermedad de Pelizaeus-Merzbacher) y el fenotipo de hipomielinización resultante (Elitt et al.2020).

Sin embargo, ambas enfermedades mencionadas anteriormente son condiciones genéticas raras que comprenden una minoría de las posibles causas desmielinizantes. La efectividad del tratamiento de la desmielinización como síntoma, especialmente en pacientes adultos, a pesar de la etiología, sigue siendo difícil de alcanzar. Esto es especialmente importante para los numerosos pacientes que se ven afectados por la EM, en los que muchas funciones cerebrales nunca se recuperan después de la desmielinización.

Para ello, modificar transitoriamente los patrones de expresión génica en progenitores de oligodendrocitos en el cerebro para activar programas pro-mielinizantes o modificar estos progenitores ex vivo para su posterior injerto son algunas de las alternativas a explorar en este campo. Aprovechar los sistemas de edición del genoma CRISPR-Cas para estos fines es todavía una posibilidad poco explorada. Para trazar mejores estrategias, el primer paso es caracterizar y estudiar cómo se comporta este sistema en este linaje celular tanto *in vivo* como *ex vivo*.

## RESUMEN DE LOS RESULTADOS OBTENIDOS POR EL ARTÍCULO

### Caracterización ultraestructural de oligodendrocitos humanos y sus células progenitoras mediante inmuno marcaje con oro pre-inclusión.

En este artículo, nuestro principal objetivo fue estudiar y describir la ultraestructura de los oligodendrocitos y sus progenitores en el tejido humano. Los estudios de análisis ultraestructurales de estas células son escasos principalmente debido al difícil acceso a muestras humanas con una fijación óptima para el inmunomarcaje combinado con el análisis TEM.

En este estudio, analizamos y caracterizamos los oligodendrocitos y sus progenitores utilizando 10 muestras humanas pediátricas y adultas de sustancia blanca humana. Estas muestras se obtuvieron de resecciones quirúrgicas de pacientes que presentaban epilepsia refractaria y fueron diagnosticados además de displasia cortical focal en la que la sustancia blanca no presentaba alteraciones. Los pacientes fueron intervenidos mediante craneotomía y escisión de la lesión en el Hospital Universitari i Politècnic La Fe. Realizamos inmunofluorescencia y marcaje inmunológico con 9 marcadores diferentes expresados por células de linaje de oligodendrocitos (NG2, PDGFRa, A2B5, Sox10, Olig2, BCAS1, APC [CC1], MAG y MBP) y GFAP como control para el marcaje astrocítico.

Nuestros resultados sugirieron que los oligodendrocitos constituyen una población muy heterogénea dentro de la sustancia blanca humana. Según los marcadores moleculares utilizados, identificamos tres etapas diferentes de diferenciación. Las OPC comprenden la primera etapa de diferenciación y se identificaron por la expresión de Olig2, PDGFRa, NG2 y A2B5. Los pre-oligodendrocitos (pre-OL) se definieron como la segunda etapa de diferenciación. Estas células se caracterizaron por la expresión de BCAS1, SOX10 y Olig2. La etapa final de diferenciación corresponde a oligodendrocitos mielinizantes completamente diferenciados (m-OLs) que expresan Olig2 y APC [CC1] como marcadores moleculares para su identificación. La mielina se marcó con MAG y MBP, sin embargo, debido a la baja penetración de los anticuerpos secundarios conjugados con oro, no pudimos detectar la ubicación exacta de estas proteínas.

El análisis ultraestructural de las OPC reveló que las proteínas analizadas estaban ubicadas en diferentes compartimentos subcelulares. Se observó marcaje de NG2 en el citoplasma, retículo endoplásmico (ER) y filamentos intermedios presentes en los procesos OPC. Se detectó que PDGFRa formaba pequeños grupos en la membrana plasmática. Se observó la marca de A2B5 en el citoplasma, proximal al ER. Finalmente, se observó Olig2 en los núcleos de las OPC. Esta subpoblación mostró una morfología

estrellada con núcleo electro lúcido y eucromatina no condensada. Su porción citoplasmática muestra varios procesos filamentosos, abundante retículo endoplásmico corto dilatado, mitocondrias y ribosomas.

En el caso de los pre-OL, encontramos Sox10 y Olig2 como marcadores nucleares característicos. Se observó BCAS1 en la membrana plasmática de estas células en contacto directo con la mielina. Nuestras observaciones señalaron que los pre-OL presentan un citoplasma electro lúcido y cromatina ligeramente condensada.

La porción citoplasmática muestra a los polirribosomas como el orgánulo más frecuente; también presentan pocas mitocondrias y RE corto dilatado. Los m-OL mostraron la expresión del marcador Olig2 en los núcleos, como el resto de las etapas de maduración oligodendroglial. La distribución de este factor de transcripción se asoció con la cromatina no condensada dentro del núcleo. Por el contrario, la proteína de unión al ARN7 marcado con APC-[CC1] se encontró asociado tanto a eucromatina y heterocromatina como en el citoplasma. La estructura nuclear de los m-OL presentaba cromatina condensada unida a la membrana nuclear interna. Por otro lado, el citoplasma presentaba RE, mitocondrias, vesículas densas de degradación y polirribosomas característicos de RE corto y dilatado.

En conclusión, este estudio arrojó luz sobre la ultraestructura del linaje oligodendroglial en diferentes etapas de diferenciación. Estos resultados son una valiosa contribución al campo, ya que esta caracterización se puede utilizar más como una herramienta para identificar oligodendrocitos en alta resolución por TEM.

Uno de los problemas más frecuentes relacionados con en el inumomarcaje para microscopía es que algunos antígenos no se conservan bien debido a la fijación. Esto provoca una baja intensidad de la marca y, por lo tanto, la marca no se puede distinguir del ruido de fondo.

**Amplificación de la señal con tiramidas para inmunomarcaje y microscopía electrónica**

En este capítulo del libro, nuestro objetivo era establecer un sistema confiable y robusto que nos permita detectar proteínas en el cerebro humano y de ratón a través de TEM. Por lo tanto, aprovechamos el sistema de amplificación de señal de tiramidas (TSA) con el fin de mejorar el marcaje y optimizar el tiempo de procesamiento y la concentración de anticuerpos para microscopía electrónica. Además, esta técnica permite la visualización precisa de algunos antígenos que no fueron detectados por inmunomarcaje para microscopía electrónica estándar.

Nuestro método utiliza TSA, una enzima reportera dependiente de analito que mejora la sensibilidad de detección de cualquier antígeno dado catalizando el depósito de tiramida marcada que se une covalentemente cerca de la molécula diana, proporcionando una señal de alta densidad. La mejora en el marcaje se produce después de la incubación del anticuerpo secundario biotinilado que posteriormente se incuba con estreptavidina-HRP. El enzima HRP cataliza la activación de tiramidas biotiniladas. Luego, usamos un anticuerpo que reconoce la biotina para realizar inmunomarcaje estándar pre-inclusión.

Nuestros resultados muestran que al utilizar este enfoque fuimos capaces de detectar oligodendrocitos humanos y de ratón con mayor precisión. En el caso de NG2, hubo una diferencia notable entre el marcaje de la membrana plasmática mejorada con inmunomarcaje con oro estándar y con TSA en tejido de ratón. Lo mismo sucedió con PDGFRa en tejido humano y de ratón; sin el aumento de TSA, este antígeno no podría detectarse. Finalmente, TSA también mejoró la calidad del etiquetado de BCAS1 en tejido humano y de ratón.

La relevancia de nuestros resultados se basa en la mejora del inmunomarcaje, que permite una mejor caracterización ultraestructural de las células del SNC, especialmente de los oligodendrocitos, no solo en el ratón sino también en el tejido humano.

Utilizamos TSA para estudiar más a fondo la ultraestructura de las células en otros tejidos patológicos humanos. En particular, nuestro objetivo era utilizar el marcaje para microscopía electrónica-TSA para estudiar marcadores como BCAS1 en tumores como el oligodendroglioma.

**Patrón de diferenciación heterogéneo con expresión de BCAS1 / NABC1 en un caso de oligodendroglioma**

En este trabajo se presentó la caracterización de un ejemplo de una enfermedad humana relacionada con el deterioro de los oligodendrocitos, como el oligodendroglioma (ODG), identificando la expresión del nuevo marcador BCAS1. Los ODG se han definido como gliomas difusos codificados con codificación 1p / 19q de IDH según la Clasificación de tumores del sistema nervioso central de la OMS de 2016 (Weller et al.2017; Wesseling y Capper 2018; Wesseling et al.2015). La histogénesis subyacente a los gliomas aún es difícil de alcanzar y la célula de origen de los gliomas no se ha definido con claridad.

En este caso estudiamos un tumor cerebral de una mujer de 65 años neurológicamente asintomática, a la que se le realizó una resonancia magnética antes de la cirugía oral. La paciente presentaba una masa hiperintensa en T2 sin contraste en el lóbulo frontal derecho, de 55 mm en su mayor dimensión, rodeada de edema. Se realizó resección quirúrgica completa en bloque.

Parte del tumor se embebió en parafina para el análisis patológico y para el marcaje de marcadores neuronales y de oligodendrocitos. El resto del tumor se conservó en formalina para análisis TEM. Realizamos análisis inmunohistoquímico para los marcadores neuronales: sinaptofisina, NeuN, Tuj1 y doblecortina. En cuanto al linaje oligodendroglial, realizamos análisis inmunohistoquímicos para: BCAS1, NG2 y Olig2. Los filamentos intermedios

analizados fueron: GFAP y Vimentina. Finalmente, estudiamos los factores de crecimiento EGFR y PDGFRa.

Nuestros hallazgos muestran que las células tumorales dentro de este oligodendroglioma presentan tres subconjuntos diferentes de células según su morfología y organización. El primer subconjunto comprendía un componente principal del oligodendroglioma clásico, que crecía de manera difusa en láminas de células tumorales uniformes muy compactas con escaso citoplasma, núcleos redondos y halos claros perinucleares. Esta población también invadió de manera difusa la corteza adyacente, mostrando satelitosis perineuronal y perivascular. La segunda subpoblación celular correspondió a pequeños nódulos relativamente bien definidos en la sustancia blanca superficial. Estos nódulos estaban en transición directa con el crecimiento tumoral cortical difuso en forma de lámina. Mostraron una población de células tumorales poco cohesiva, incrustadas en un fondo microvacuolado. Estas células presentaban un citoplasma más abundante y vacuolado, y núcleos moderadamente pleomórficos de contorno irregular y raras mitosis. La tercera subpoblación de células tumorales invadió la sustancia blanca subcortical formando filas o columnas mal definidas, así como vagas rosetas.

El principal hallazgo de este artículo fue la expresión del marcador de oligodendrocitos inmaduros BCAS1 en los pequeños nódulos localizados en la sustancia blanca superficial en un oligodendroglioma. Ésta es la primera descripción de este marcador en el cáncer de cerebro. Este descubrimiento ha llevado a un mayor análisis de la expresión de BCAS1 en una cohorte más grande de gliomas difusos.

Un enfoque interesante para estudiar la función de moléculas relacionadas con oligodendrocitos mediante modificación genética es el sistema CRISPR-Cas9. Uno de los factores que influye en la eficiencia de este sistema es la localización subcelular de Cas9 dentro de la célula. Por lo tanto, utilizamos TEM para analizar más a fondo esta aplicación.

**Inmunomarcaje para detectar Cas9 procedente de *Streptococcus pyogenes* en cultivos celulares y tejidos mediante microscopía electrónica**

En este artículo, nuestro objetivo fue desarrollar una estrategia para detectar el sistema CRISPR-Cas9 a nivel intracelular con el propósito de estudiar la dinámica de este sistema en nuestras células de interés, los oligodendrocitos.

El sistema CRISPR-Cas es una herramienta potente y precisa para la edición del genoma. Algunos de los aspectos a considerar al utilizar este sistema incluyen: el método de transfección utilizado para cada tipo de célula, la biosíntesis y disponibilidad de la enzima dentro de la célula, la etapa del ciclo celular en la que se sintetiza la enzima y la capacidad de cada tipo de célula para transportar Cas9 dentro y fuera del núcleo o del orgánulo diana. Por lo tanto, hemos utilizado TEM para evaluar estos puntos en diferentes tipos de células, tanto in vivo como in vitro.

Para ello, inicialmente utilizamos céluls HEK293T, que son el modelo más utilizado para configurar el sistema CRISPR-Cas, antes de implementarlo en otros tipos de células. En las células HEK293T, encontramos un marcaje de Cas9 ampliamente distribuido a través del citoplasma de las células. Con respecto a la localización nuclear de la enzima, se encontraron partículas amplificadas con plata en las porciones no condensadas de la cromatina. Se encontró que el marcaje Cas9 estaba unido a los nucleoporos, lo que indicaba el transporte hacia el núcleo.

A continuación, transfectamos nuestras células de interés, las OPC, que se aislaron de cerebros de ratones en etapas perinatales. En este caso, analizamos cultivos primarios después de 10 h, 24 h, 72 hy 5 días después de la transfección. Después de 10 h, la enzima apenas se encontraba en el citoplasma de una minoría de células. Curiosamente, 24 hy 72 h después de la transfección se observó SpCas9 en vesículas discretas en el citoplasma de las células, excepto en algunas células que presentaban marcaje en sus

núcleos. Finalmente, a los 5 días después de la transfección, las células mostraban la marca de SpCas9 en la membrana de vesículas densas en electrones que identificamos como lisosomas. Esto sugiere que en las OPC transfectadas, SpCas9 se empaqueta y procesa para su degradación.

Además, analizamos la transfección del reportero de GFP 5 días después de la transfección para evaluar la degradación. Este marcador no se observó en vesículas o lisosomas, sino que mostró una localización citoplásmica. Esto indica que el proceso de degradación no ocurre en todas las proteínas transfectadas. Por lo tanto, inferimos que el proceso de degradación es específico para la proteína SpCas9 en células transfectadas.

Adicionalmente, aislamos OPC de ratones Cas9 que expresan constitutivamente (ratones H11-Cas9). En este caso particular, la enzima se observó en el citoplasma de OPC que no se dividían. La expresión de Cas9 no se observó cuando los procesos mitóticos estaban en curso.

También realizamos un análisis de tejido cerebral en ratones Cas9 de expresión constitutiva (ratones H11-Cas9) mediante marcaje de inmunofluorescencia. El inmunomarcaje de SpCas9 proporcionó resultados negativos en este caso. Este conjunto de experimentos reveló que las células Olig2 + mostraban expresión de SpCas9 en su citoplasma. Curiosamente, los astrocitos GFAP + no mostraron expresión de SpCas9 mientras que las neuronas corticales exhibieron expresión de SpCas9 en el citoplasma y nucléolos. Esto sugiere que la enzima Cas9 no se expresa ni se distribuye por igual en todos los tipos de células cerebrales.

Finalmente, realizamos análisis de inmunofluorescencia e inmuno oro para microscopía electrónica en el hígado de ratones H11-Cas9. La

inmunofluorescencia mostró que la expresión de la enzima se distribuye de forma ubicua en el citoplasma de todas las células. Por el contrario, la inmuno oro mostró que solo algunos hepatocitos específicos y células de Kupffer expresaron Cas9 en porciones discretas del citoplasma.

Dado que los sistemas CRISPR requieren ser importados hacia localizaciones subcelulares específicas para realizar su actividad enzimática o de transporte de ADN, las técnicas precisas para la localización subcelular son esenciales. El marcaje para microscopía electrónica es una herramienta válida para este propósito. Además, abre un nuevo espectro de oportunidades para estudiar el sistema CRISPR-Cas9 de una manera más precisa.

# 1. INTRODUCTION

# 1. INTRODUCTION

## 1.1. Oligodendrocytes and oligodendrogenesis in the brain

The cellular composition of the central nervous system (CNS) is classified into five main cell types: 1) neurons, which are the principal executive cells (Gowers 1897); 2) astrocytes, the supporting cells that play their role in physical, metabolic, and repairing function within the CNS (Parpura and Verkhratsky 2012). Furthermore, stem cells in the neurogenic niches (i.e. the ventricular-subventricular zone (V-SVZ) and the hippocampal dentate gyrus) belong to the astroglial lineage (Kriegstein and Alvarez-Buylla 2009); 3) microglia, considered to be the immune phagocytic cells of the CNS (Penfield 1925); 4) ependymal cells, which are ciliated cells that separate the brain parenchyma and the fluid-filled ventricles. Coordinated, whiplike motion of ependymal cilia has been proposed to direct cerebrospinal fluid through the CNS ventricular system in rodents (Sawamoto et al. 2006); and 5) oligodendrocytes are glial cells whose main function is myelination. Myelination leads to the optimization of the saltatory conduction of propagating action potentials (McLaurin and Yong 1995). Moreover, oligodendrocytes perform other supportive activities such as glucose metabolism (Amaral et al. 2016; Saab et al. 2016), calcium influx/efflux towards the axon to impede degeneration (Witte et al. 2019), and pH and ion balance regulation (Inouye and Kirschner 1988).

In the human brain, oligodendrocytes as every other neural lineage-derived cell in the brain, originate from early radial glia cells (Anthony et al. 2004). Recent studies using histological studies combined with transcriptomic profiling in fetal tissues have established that the exact origin of oligodendrocytes and their progenitors is outer radial glia (Huang et al.2020). Moreover, this population has the potential to produce oligodendrocytes *in vitro* (Mo and Zecevic 2009). More. Nonetheless, the regions where oligodendrocyte progenitor cells (OPCs) are generated and their migration pathways are diverse throughout fetal development. Three oligodendrogenic waves with different origin and destination follow each other during brain development (Kessaris et al. 2006). The first massive OPC generation event is thought to originate from

the anterior lateral ganglionic eminences during human gestational weeks 17-22. Cells derived from this first wave are characterized by the expression of cytoplasmic DLX2 together with other OPC-specific markers such as PDGFRa, NG2 and Olig1. These cells are thought to migrate through a discrete stream to the cortical V-SVZ. The second subset of OPCs arises from the medial ganglionic eminence around gestational week 23. Cells in this region are characterized by NKX2.1 expression as a distinctive marker. The third region of OPC generation is thought to be the cortex. These OPCs express specific-lineage markers only (Rakic and Zecevic 2003; Jakovcevski and Zecevic 2005).

In the mouse brain the molecular basis of oligodendrogenesis have been better studied. Developmental oligodendrogenesis begins and depends on the establishment of gradients of sonic hedgehog (SHH), a transcription factor that induces the ventralization of the tissue by inhibiting the action of bone morphogenic protein (Figure 1A-B). SHH is secreted by the notochord and the floor plate of the neural tube, therefore, it has a more robust effect on ventral areas (Takebayashi and Ikenaka, 2015). The ventricular zone of the motor neuron progenitor domain, is one of the areas whose cells suffer specification due to high concentration of SHH. This stimulus induces them to begin expressing Olig2 at E9.5 in this domain (Figure 1C-D). These cells have the potential to differentiate into motor neurons, oligodendrocytes or astrocytes (Masahira et al. 2006). Olig2-positive ($Olig2^{+}$) cells that will differentiate into mature oligodendrocytes pass through a transitional OPC undifferentiated state which can be identified by the expression of PDGFRα. A subset of these progenitors is persistent in a quiescent state in the postnatal and adult brain (Woodruff et al. 2001).

At E12.5, the ventral portion of the motor neuron progenitor domain expresses Nkx 2.2 besides Olig2 and PDGFRα, thereby giving rise to the first migration wave or ventral wave of OPCs (Fu et al. 2002). This cell wave migrates towards dorsal and rostral structures of the early spinal cord, hindbrain and telencephalon (Woodruff et al., 2001). In the telencephalon, by the time all the areas of the ganglionic eminence are entirely differentiated (E14.5), there is a second wave (first telencephalic wave) of progenitor migration. These cells, emerge from the medial area of the ganglionic eminence (Nkx2.1-positive cells)

as a differential marker. Nkx2.1-expressing OPCs migrate and populate most telencephalic areas and the cerebellar cortex (Spassky et al. 1998).

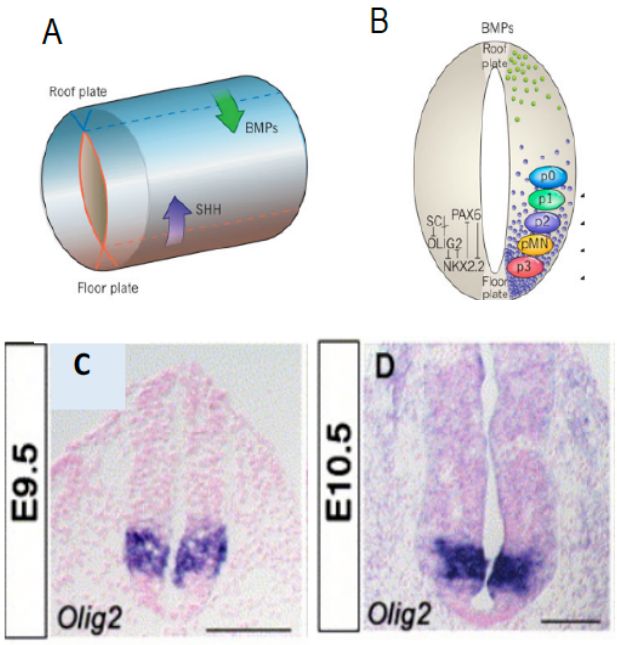


**Figure 1. Establishment of transcription factor gradients in the mouse neural tube.** A) High concentrations of SHH determine the ventralization of the tissue under its influence by inhibiting the action of BMPs that promote the development of dorsal structures. B) SHH gradient induces Olig2 expression at the pMN area of the neural tube, where the first ventral OPC migration wave occurs (Rowitch & Kriegstein, 2010). C) Olig2 expression at mouse developmental stage E9.5. D) Olig2 expression at mouse developmental stage E10.5. Modified from Masahira, et al., 2006.

At E15.5 (second telencephalic wave), other areas of the ganglionic eminence such as the lateral ganglionic eminence and the caudal ganglionic eminence give rise to a new subset of OPCs, which is characterized by the expression of Gsh2. GSH2-positive cells can be found in the cortex at developmental stage E16.5 (Kessaris et al. 2006). The third telencephalic proliferative wave of OPCs takes place at late embryonic phases and perinatally. They are characterized by the expression of Emx1 (Vallstedt et al.

2005) and their role is to replace Nkx2.1$^{+}$ OPCs generated at early developmental stages.

Generation of myelin and new oligodendrocytes plays a critical role in the adult brain, in which remodeling and plasticity are a constant and necessary phenomenon. Once the development of the CNS is complete, there is a population of NG2-glia that remains distributed throughout the adult brain. This population of OPCs has a slow or inactive proliferation capacity and acts as a reservoir, being able to differentiate into myelinating oligodendrocytes during postnatal life (Dimou et al. 2008). In addition to these OPCs distributed throughout the brain parenchyma, neural stem cells located in the V-SVZ can generate new OPCs in the adult brain. Interestingly, these cells are also found in demyelinating lesions such as multiple sclerosis plaques (Wilson et al. 2006).

The dynamics and ultrastructure of oligodendrocytes in the rodent brain is better understood as a result of sample availability and the diversity of transgenic animals. The morphology and the fine structure of oligodendrocytes have been previously characterized in rodents as ramified cells whose soma is small, electron dense, with uneven cytoplasm that adapts to unmyelinated axons and containing short dilated endoplasmic reticulum; they present spherical nucleus and clumps of chromatin attached to the inner nuclear membrane. (Luskin et al. 1993; Olude et al. 2018). Their progenitors on the other hand have been characterized by Olig2 labeling in the V-SVZ of lesioned mice as cells with relatively electron dense cytoplasm, with numerous mitochondria, Golgi apparatus and short endoplasmic reticulum. Their morphology is similar to type C-cells (or transit amplifying progenitors) from the V-SVZ (Menn et al. 2006).

Conversely, in human research there are several issues related to sample preservation, especially for ultrastructural studies, in which fixation is a critical step for subsequent experimental procedures. Considering that the gold standard for myelination/remyelination studies is based on electron microscopy analysis, characterizing oligodendrocytes and their progenitors in human tissue is a milestone for basic and applied oligodendrocyte research.

### 1.2. Oligodendroglial-related pathologies

The importance of studying oligodendrocytes and their generation in the CNS relies on the diversity of pathologies that oligodendrocyte dysfunction can generate. There is a wide variety of causes that result in demyelination and oligodendrocyte impairment, such as genetic, infectious, traumatic, and autoimmune bases.

**Genetic causes** are not the most frequent, but the most severe cases reported. Deficiency or mutations have been reported in different genes such as:

- Mutations in glial fibrillary acidic protein (GFAP), located in 17q21, which cause Alexander disease in the neonatal and infant brain. Signs and symptoms of this leukodystrophy are not homogenous. However, in all patients it results in chronic demyelination leading to physical and cognitive impairment which ultimately leads to death in an average of 10 years after the onset (Messing 2018).

- Mutations in proteolipid protein1 (PLP1), located in Xq22, cause Pelizaeus-Merzbacher disease, a fatal infantile/young leukodystrophy which starts during early infancy and leads to premature death during childhood (Renier et al. 1981).

- Mutations in the aspartoacylase (ASPA), located in chromosome 17p13, are the cause of Canavan disease, whose features are displayed during early infancy and include a wide range of neurological defects from atonia to blindness and ultimately cause death of the infant by 18 months.

- Mutations in the galactosylceramidase gene (*GALC*), located in chromosome 14q31, elicit Krabbe disease. This pathology is mostly manifested in infants with a fatal prognosis at 2 years old. Neurological signs and symptoms are varied, but the outcome is common in all infantile patients. Krabbe disease results in motor and mental deterioration, which leads to decerebration (Tappino et al. 2010).

- Mutations in any of the 5 genes that codify for the subunits of the translation initiation factor *EIF2B*, located either in 1p34, 2p23, 3q27, 12q24 or 14q2, cause leukoencephalopathy with vanishing white matter. Given the variability of the mutations within the genes, the neurological symptoms and prognosis may not coincide among patients (van der Knaap et al. 1998; Biancheri et al. 2003; Labauge et al. 2009). The only common symptom is progressive demyelination.

- Mutations in the modulator of VRAC current 1 (*MLC1*) gene, located in 22q13, causes Van der Knaap disease also known as megalencephalic leukoencephalopathy with subcortical cysts. This leukodystrophy affects mostly infants who die prematurely and comprises neurological features such as megalencephaly, slow progressive ataxia, spasticity and seizures (van der Knaap et al. 1995; Van der Knaap et al. 1996).

- Mutations in arylsulfatase A gene (*ARSA*), located in 22q13, cause metachromatic leukodystrophy. Infantile and juvenile forms exhibit motor symptoms together with mental inability or retardation (Greenfield 1933). Adult forms of the disease debut with psychiatric symptomatology (Propping et al. 1986).

- X-linked adrenoleukodystrophy results from mutations in *ABCD1* gene, located in Xq21. This mutation results in a failure of very long fatty-acid transfer into peroxisomes. One of the forms of the disease results in a cerebral form which includes extensive demyelination (Moser et al. 1991).

**Infectious-related diseases of the CNS** are also a cause of demyelination. The classic infectious agents causing demyelination are viruses. Viruses can induce demyelination in four different manners: 1) By directly infecting oligodendrocytes, which leads to cell death. 2) A persistent response towards viral agents which causes homeostatic and metabolic impairments in the brain and ultimately produces oligodendrocyte death. 3) Cytokine-induced inflammation affecting oligodendroglial environment. 4) Immune response via antigenic mimicry towards oligodendrocyte or myelin specific proteins secondary to a viral infection (Stohlman and Hinton 2001).

Diseases produced by viruses involving one or more mechanisms of the above-described are: subacute-sclerosing panencephalitis, progressive multifocal leukoencephalopathy and post-infectious encephalomyelitis.

Subacute-sclerosing panencephalitis is a rare condition provoked by measles virus or attenuated measles vaccine. It occurs in 1 case per million and causes severe chronic demyelination in children (Modlin et al. 1977). The persistence of this virus within neurons and oligodendrocytes is associated with several mutations that impede the viral assembly and exit from the cells (Stohlman and Hinton 2001).

Progressive multifocal leukoencephalopathy is a fatal disease caused by JC virus. This virus is a ubiquitous virus acquired by humans during infancy and whose reservoir is thought to be the kidney. In immunocompromised patients and patients co-infected with HIV, this virus escapes the immune vigilance and infects oligodendrocytes, thus causing demyelination (Hou and Major 2000).

Finally, post-infectious encephalomyelitis, a subgroup of diseases associated with several different viral infections such as: mumps, varicella and influenza viruses. In this case, the viral agent cannot be directly related to demyelination (Stohlman and Hinton 2001).

**Brain injuries** may also induce demyelination. Various causes can lead to brain injuries, but the common mechanisms are either hemorrhagic or ischemic lesions.

Hemorrhagic lesions are caused either by traumatic injuries or intracerebral strokes. This type of insults results in an inflammatory environment in the damaged area, which impair the homeostatic balance of the cells. In hemorrhagic models, oligodendrocytes and myelin are affected within the hemorrhagic area and, in the periphery, demyelination with poor axonal and oligodendrocyte recovery are classical hallmarks of these type of insults (Wasserman and Schlichter 2008).

On the other hand, ischemic lesions can be caused by an ictus during adulthood or by brain hypoxia leading to hypoxic ischemic encephalopathy or

leukomalacia in infants (Chavali et al. 2020). In adult ischemia models, oligodendrocytes appear to be a selectively affected population at early times after infarction and rapidly die via necrosis (Petito et al. 1998). The same phenomenon is observed in models of leukomalacia, where oligodendrocytes are particularly affected (Back et al. 2002). This has been corroborated in human infant leukomalacia brains, in which the maturation of oligodendrocytes is severely compromised (Volpe 2001).

**Autoimmune diseases** include rare demyelinating syndromes and frequent neurodegenerative impairments such as multiple sclerosis (MS) and optic neuritis.

MS is the leading neurodegenerative cause of disabilities among young adults. The actual world prevalence of MS is estimated to be 1/3,000 people, of which 1.5% account for pediatric MS cases (individuals under 18). On average, 7/10 MS patients are women. The incidence varies among countries; hence, the developed countries present 2-3 times the cases when compared to underdeveloped countries. Given that in underdeveloped countries the access to healthcare is not optimal, it is considered that the epidemiological data (incidence and prevalence) is still underestimated (MS Atlas 2020).

Furthermore, studies suggest the involvement of OPCs and oligodendrocytes in neoplastic pathologies such as diffuse gliomas and glioblastomas (Dufour et al. 2018). Given that OPCs are the most abundant proliferative and cycling population in the brain, it is thought that they may play an important role in the development of gliomas and glioblastomas (Geha et al. 2010). In the same line, state-of-the-art omics studies have pointed out that when OPC-like transcriptional programs are active, oligodendrogliomas tend to be more aggressive and present a worse prognosis (Bielle et al. 2017).

Since the treatments for stopping or at least decreasing the causes of demyelination in infectious, traumatic and autoimmune diseases are available, viable therapies for enhancing remyelination are still the priority in the research field. Strategies for evaluating remyelination are still in development, however, the gold standard for measuring remyelination in tissues is the g-ratio measured

by transmission electron microscopy (TEM). Therefore, studying the ultrastructure of oligodendrocytes, their progenitors and myelin, especially in human tissue, is a relevant aspect in cell biology and neurobiology.

### 1.3 The CRISPR-Cas9 system and oligodendrocyte impairments

Genome engineering has emerged as one of the most prominent fields of study within the last five decades. Particularly, since CRISPR-Cas systems were first demonstrated to work in eukaryotic cells for genomic edition application during the last decade, the possibilities of easy, precise and powerful genomic editions have resulted into an increase in the number of basic biology and clinical studies to successfully treat or ameliorate a wide variety of genetic conditions.

When first discovered, CRISPR-Cas systems were described as an adaptive immune system that allowed bacteria and archaebacteria to defend themselves against plasmids and phages (Barrangou et al. 2007). As of today, CRISPR-Cas systems are used not only to edit the genome and epigenome, but also to target, trace, and regulate gene expression (Sander and Joung 2014), which maximizes the possibilities of modelling and targeting not only genetic conditions.

Regarding oligodendroglial pathologies, the CRISPR-Cas9 system has been used in Alexander's disease to correct the mutations in *GFAP* gene, thus ameliorating the hypomyelination phenotype caused by this condition (Li et al. 2018). Moreover, the use of this novel genomic tool and antisense oligonucleotides have shown to be an effective therapeutic strategy to rescue the short lifespan of PLP1-mutant, also known as *jimpy* mice (model of Pelizaeus-Merzbacher disease) and the resulting hypomyelination phenotype (Elitt et al. 2020).

Nevertheless, both above-mentioned diseases are rare genetic conditions that comprise a minority of the possible demyelinating causes. The effectiveness of treating demyelination as a symptom, especially in adult patients, despite the etiology remains elusive. This is especially important for

the numerous patients that are affected by MS, in whom many brain functions are never recovered after demyelination.

To this purpose, transiently modifying gene expression patterns in oligodendrocyte progenitors in the brain to activate pro-myelinating programs or modifying these progenitors *ex vivo* for subsequent engraftment are some of the alternatives to explore in this field. Taking advantage of CRISPR-Cas genome editing systems for these purposes is yet an underexplored possibility. To trace better strategies, the first step is to characterize and study how this system behaves in this cell lineage both *in vivo* and *ex vivo.*

# 2. HYPOTHESES AND OBJECTIVES

# 2. HYPOTHESES AND OBJECTIVES

## 2.1. Hypotheses

2.1.1. Human oligodendrocytes display a heterogeneous ultrastructural morphology according to their stage of differentiation.

2.1.2. Tyramide signal amplification can be used to enhance specificity of antigen detection in human oligodendrocytes and their progenitors.

2.1.3. Human oligodendrogliomas express markers of oligodendrocyte intermediate differentiation status such as BCAS1.

2.1.4. Immunoelectron microscopy is a valid tool to detect the intracellular localization of the CRISPR-Cas9 system in oligodendrocyte culture and tissue.

## 2.2. Objectives

2.2.1. To determine the fine structure of oligodendrocytes and their progenitors in the human white matter.

2.2.2. To develop a method based on tyramide signal amplification to label human oligodendrocytes in its different stages for electron microscopy analysis.

2.2.3. To analyze cell populations that express the marker BCAS1 in human oligodendroglioma.

2.2.4. To study the subcellular localization of SpCas9 in oligodendrocytes *in vivo and in vitro.*

# 3. SUMMARY OF RESULTS OBTAINED BY ARTICLE

## 3. SUMMARY OF RESULTS OBTAINED BY ARTICLE

### 3.1. Ultrastructural characterization of human oligodendrocytes and their progenitor cells by pre-embedding immunogold

In this article, our main objective was to study and describe the fine structure of oligodendrocytes and their progenitors in human tissue. Ultrastructural analysis studies of these cells are scarce mainly due to the difficult access to human samples with optimal fixation for immunolabeling combined with TEM analysis.

In this study, we analyzed and characterized oligodendrocytes and their progenitors using 10 human pediatric and adult samples of human white matter. These samples were obtained from surgical resections of patients who presented refractory epilepsy and were further diagnosed with focal cortical dysplasia in which the white matter did not present alterations. The patients underwent surgery by craniotomy and lesion scission at Hospital Universitari i Politècnic La Fe. We performed immunofluorescence and immunogold labelling using 9 different markers expressed by oligodendrocyte lineage cells (NG2, PDGFRa, A2B5, Sox10, Olig2, BCAS1, APC [CC1], MAG and MBP) and GFAP as a control for astrocytic labeling.

Our results suggested that oligodendrocytes constitute a very heterogeneous population within the human white matter. According to the molecular markers used, we identified three different stages of differentiation. OPCs comprise the first stage of differentiation and were identified by the expression of Olig2, PDGFRa, NG2 and A2B5. Pre-oligodendrocytes (pre-OLs) were defined as the second stage of differentiation. These cells were characterized by the expression of BCAS1, SOX10 and Olig2. The final stage of differentiation corresponded to fully differentiated myelinating oligodendrocytes (m-OLs) which expressed Olig2 and APC [CC1] as molecular markers for their identification. Myelin was labeled with MAG and MBP, however, because of the low penetration of gold-conjugated secondary antibodies we could not detect the exact location of these proteins.

The ultrastructural analysis of OPCs revealed that the analyzed proteins were located in different subcellular compartments. NG2 labeling was observed in the cytoplasm, endoplasmic reticulum (ER) and intermediate filaments present in OPC processes. PDGFRa was detected forming small clusters in the plasma membrane. A2B5 label was observed in the cytoplasm, proximal to the ER. Finally, Olig2 was observed in the nuclei of OPCs. This subpopulation showed star-shaped morphology with electron lucent nucleus and non-condensed euchromatin. Their cytoplasmic portion exhibited several filamentous processes, abundant short dilated endoplasmic reticulum, mitochondria and ribosomes.

In the case of pre-OLs, we found Sox10 and Olig2 as characteristic nuclear markers. BCAS1 was observed in the plasma membrane of these cells in direct contact with myelin. Our observations pointed out that pre-OLs present scant electron lucent cytoplasm and slightly condensed chromatin. The small cytoplasmic area shows polyribosomes as the most frequent organelle; they also present few mitochondria and short dilated ER.

m-OLs exhibited Olig2 label in the nuclei, as the rest of oligodendroglial maturational stages. The distribution of this transcription factor was associated with non-condensed chromatin within the nucleus. Conversely, the RNA-binding protein quaking7 labelled with APC-[CC1] was found associated both to euchromatin and heterochromatin as well as in the cytoplasm. The nuclear structure of m-OLs presented condensed chromatin bound to the inner nuclear membrane. On the other hand, the cytoplasm showed characteristic short, dilated ER, mitochondria, dense degradation vesicles and polyribosomes.

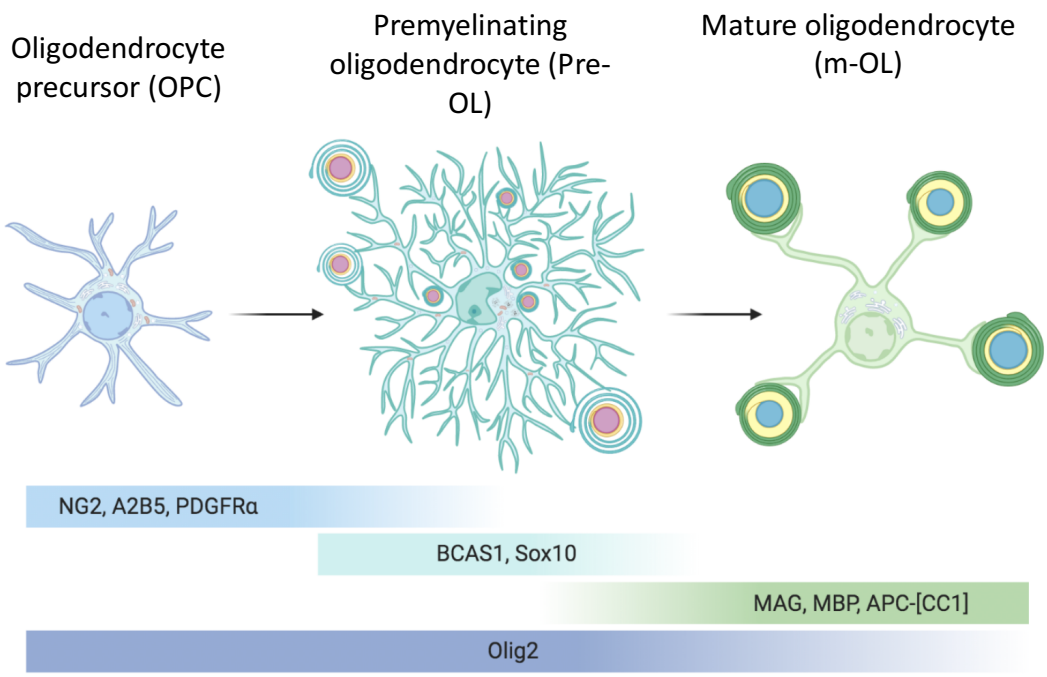


**Figure 2. Diagram representing the oligodendrocyte differentiation process**. The morphology, organelle distribution, and markers to identify each of the three differentiation stages are represented. Oligodendrocyte precursor cells (OPCs) are characterized by NG2, A2B5, PDGFRα and Olig2 expression. Premyelinating oligodendrocytes (pre-OLs) are characterized by the expression of BCAS1, Sox10 and Olig2. Mature oligodendrocytes are characterized by the expression of APC-[CC1] and Olig2 (Ulloa-Navas et al. 2021).

In conclusion, this study shed light on the ultrastructure of the oligodendroglial lineage at different stages of differentiation. These results are a valuable contribution to the field since this characterization can be further used as a tool to identify oligodendrocytes at high-resolution by TEM.

One of the most frequent issues related to immunoelectron microscopy is that some antigens are not well preserved because of the fixation. This causes a low label intensity and thereby the label cannot be distinguished from background noise.

### 3.2. Tyramide signal amplification for immunoelectron microscopy

In this book chapter, our goal was to set up a reliable and robust system that allows us to detect proteins in the human and mouse brain through TEM. Therefore, we took advantage of the tyramide signal amplification (TSA) system

in order to enhance the labeling and optimize processing time and antibody concentration for immunoelectron microscopy. Furthermore, this technique allows the precise visualization of some antigens that were not labelable by standard immunoelectron microscopy.

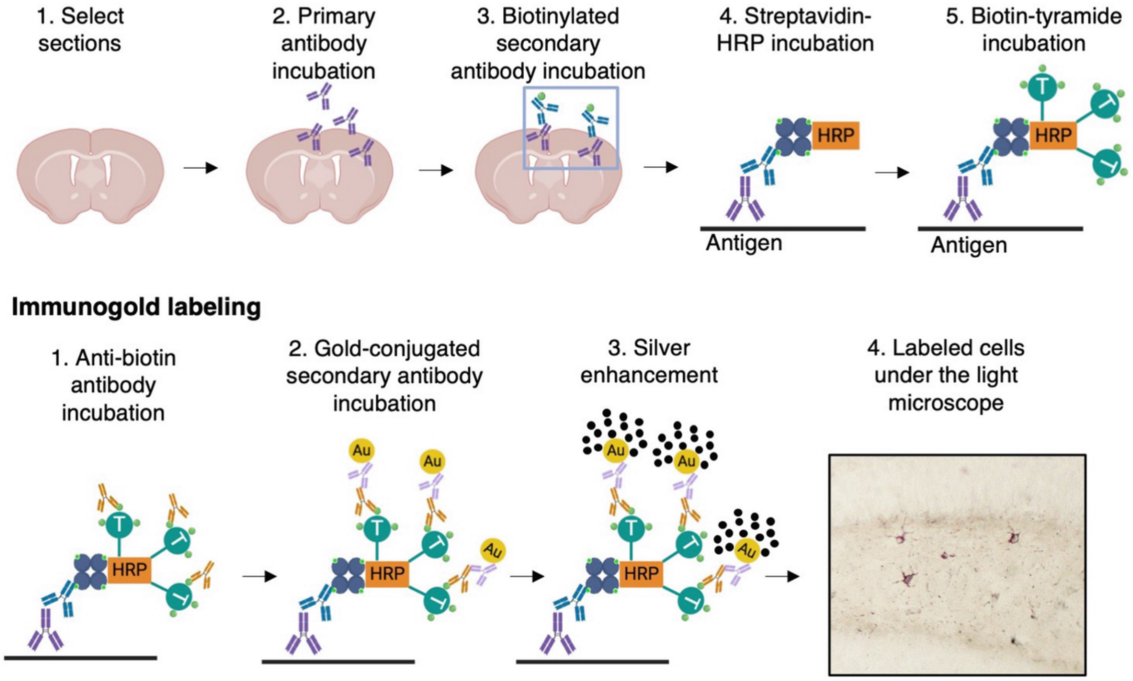


**Figure 3. Step-by-step diagram describing the procedure of TSA labeling for immunoelectron microscopy.** TSA is a method to enhance the precision and intensity of labeling. Tyramide bound to biotin covalently deposits adjacent to the target antigen. An immunogold against biotin is performed thereafter (Ulloa-Navas 2021).

Our method uses TSA, an analyte-dependent reporter enzyme method that enhances the detection sensitivity of any given antigen by catalyzing the deposit of labeled tyramide that is covalently bound near the target molecule, providing high-density signal. Label enhancement is produced after biotinylated secondary antibody incubation which is subsequently incubated with streptavidin-HRP. HRP catalyzes the activation of biotinylated tyramides. Then, we used an antibody that recognizes biotin to perform standard pre-embedding immunogold.

Our results show that by using this approach we were capable of detecting human and mouse oligodendrocytes more precisely. In the case of NG2, there was a remarkable difference between standard immunogold and

TSA enhanced plasma membrane labeling in mouse tissue. The same happened with PDGFRa in human and mouse tissue; without TSA enhancement, this antigen could not be detected. Finally, TSA also improved the quality of the labeling of BCAS1 in human and mouse tissue.

The relevance of our results relies on the improvement of immunogold labeling, which allows a better ultrastructural characterization of CNS cells, especially oligodendrocytes, not only in mouse but also in human tissue.

We utilized TSA to further study the ultrastructure of cells in other human pathological tissues. In particular, we aimed to use TSA immunoelectron microscopy labeling to study markers such as BCAS1 in tumors such as oligodendroglioma.

### 3.3 Heterogeneous pattern of differentiation with BCAS1/NABC1 expression in a case of oligodendroglioma

This work presented the characterization of an example of a human disease which is related to oligodendrocyte impairment, such as oligodendroglioma (ODG), identifying the expression of the novel marker BCAS1. ODGs have been defined as IDH-mutant, 1p/19q-codeleted diffuse gliomas by the 2016 WHO Classification of Tumors of the Central Nervous System (Weller et al. 2017; Wesseling and Capper 2018; Wesseling et al. 2015). The histogenesis underlying gliomas is still elusive, and the cell of origin for gliomas has not been clearly defined.

In this case we studied a brain tumor from a neurologically asymptomatic 65-year-old woman, who underwent MRI examination prior to oral surgery. The patient presented a T2-hyperintense, non-contrast-enhancing mass in her right frontal lobe, measuring 55 mm in greatest dimension, surrounded by edema. A complete *en bloc* surgical resection was performed.

Part of the tumor was embedded in paraffin for pathological analysis and for neuronal and oligodendrocyte marker labeling. The rest of the tumor was conserved in formalin for TEM analysis. We performed immunohistochemical analysis for the neuronal markers: Synaptophysin, NeuN, Tuj1 and

doublecortin. As for the oligodendroglial lineage we performed immunohistochemical analysis for: BCAS1, NG2 and Olig2. The intermediate filaments analyzed were: GFAP and Vimentin. Finally, we studied the growth factors EGFR and PDGFRa.

Our findings show that the tumoral cells within this oligodendroglioma presented three different subsets of cells according to their morphology and organization. The first subset comprised a main component of classical oligodendroglioma, growing diffusely in sheets of tightly packed uniform tumor cells with scant cytoplasm, round nuclei, and perinuclear clear halos. This population also diffusely invaded the adjacent cortex, showing perineuronal and perivascular satellitosis. The second cellular subpopulation corresponded to small, relatively well-defined nodules in the superficial white matter. These nodules were in direct transition with the diffuse, sheet-like cortical tumor growth. They displayed a loosely cohesive tumor cell population, embedded in a micro vacuolated background. These cells showed more abundant and vacuolated cytoplasm, and moderately pleomorphic nuclei with irregular contour and rare mitoses. The third subpopulation of tumoral cells invaded the subcortical white matter forming rows or ill-defined columns, as well as vague rosettes.

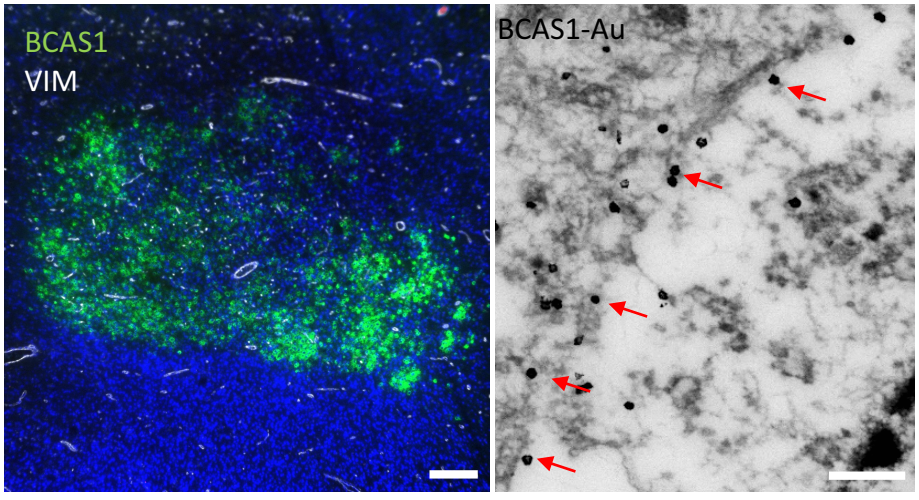


**Figure 4. BCAS1 nodule in a 65-year-old female patient.** BCAS1 is expressed in the cell membrane of a tumor cell (red arrows in right image). Scale bars: left image = 250 µm; right image = 500 nm.

The main finding of this article was the expression of the immature oligodendrocyte marker BCAS1 in the small nodules located in the superficial white matter in an oligodendroglioma. This is the first description of this marker in brain cancer. This discovery has led to further analysis on the expression of BCAS1 in a larger cohort of diffuse gliomas.

An interesting approach to study the function of oligodendrocyte-related molecules by genetic modification is the CRISPR-Cas9 system. One of the factors that influences the efficiency of this system is the subcellular localization of Cas9 within the cell. Thereby, we used TEM to further analyze this application.

### 3.4. Immunogold labeling to detect Streptococcus pyogenes Cas9 in cell culture and tissues by electron microscopy

In this article, our aim was to develop a strategy to detect the CRISPR-Cas9 system at an intracellular level with the purpose of studying the dynamics of this system in our cells of interest, oligodendrocytes.

The CRISPR-Cas system is a powerful and precise tool for genome editing. Some of the aspects to consider when using this system include: the transfection method used for each cell type, the biosynthesis and availability of the enzyme within the cell, the stage of the cell cycle in which the enzyme is synthesized, and the ability of each cell type to transport Cas9 into and out of the nucleus or the target organelle. Therefore, we have used TEM to assess these points in different cell types, both *in vivo* and *in vitro*.

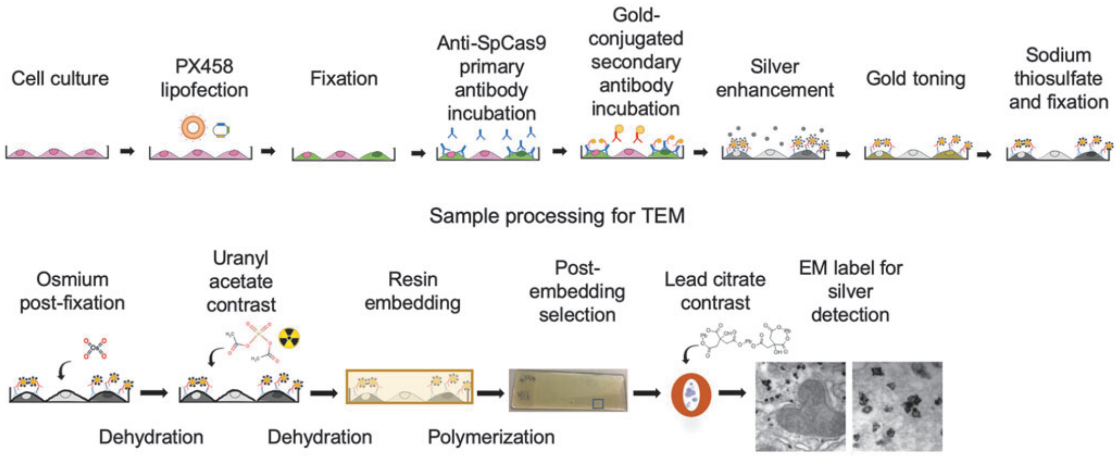


**Figure 5. Diagram showing the processing for SpCas9 detection by TEM.**

To this purpose, we initially used HEK293T cells, which are the most used model to set up the CRISPR-Cas system, prior to implementing it in other cell types. In HEK293T cells, we found Cas9 labeling widely distributed through the cytoplasm of the cells. Regarding the nuclear localization of the enzyme, silver-enhanced particles were found in the uncondensed portions of the chromatin. Cas9 labeling was found bound to nucleopores, thereby indicating transportation towards the nucleus.

We then transfected our cells of interest, OPCs, which were isolated from perinatal mice. In this case, we analyzed primary cultures after 10 h, 24 h, 72 h and 5 days post-transfection. After 10 h, the enzyme was scarcely found in the cytoplasm of a minority of the cells. Interestingly, 24 h and 72 hours after transfection SpCas9 was observed in discrete vesicles in the cytoplasm of the cells, except in some cells which presented labeling in their nuclei. Finally, at 5 days post-transfection cells displayed SpCas9 label in the membrane of electron-dense vesicles which we identified as lysosomes. This suggests that in transfected OPCs, SpCas9 is packaged and processed for degradation.

Additionally, we analyzed the transfection of the GFP reporter 5 days after transfection to assess degradation. This marker was not observed in vesicles or lysosomes, instead it showed a cytoplasmic localization. This indicates that the degradation process does not happen in all the proteins transfected. Thus, we infer that the degradation process is specific for SpCas9 protein in transfected cells.

We further isolated OPCs from constitutively expressing Cas9 mice (H11-Cas9 mice). In this particular case, the enzyme was observed in the cytoplasm of non-dividing OPCs. The expression of Cas9 was not observed when mitotic processes were ongoing.

We also performed a brain tissue analysis in constitutively expressing Cas9 mice (H11-Cas9 mice) by immunofluorescence labeling. SpCas9 immunogold labeling provided negative results in our hands in this case. This set of experiments revealed that $Olig2^{+}$ cells showed SpCas9 expression in their cytoplasm. Interestingly, $GFAP^{+}$ astrocytes did not show SpCas9

expression while cortical neurons exhibited SpCas9 expression in the cytoplasm and nucleoli. This illustrates that the Cas9 enzyme is not equally expressed and distributed in all brain cell types.

Finally, we performed immunofluorescence and immunogold analysis in the liver of H11-Cas9 mice. Immunofluorescence showed that the expression of the enzyme is distributed ubiquitously in the cytoplasm of all the cells. In contrast, immunogold showed that only some specific hepatocytes and Kupffer cells expressed Cas9 in discrete portions of the cytoplasm.

Given that the CRISPR systems require to be imported towards specific subcellular localizations to perform their enzymatic or DNA-transportation activity, precise techniques for subcellular localization are essential. Immunoelectron microscopy is a valid tool for this purpose. Moreover, it opens a new spectrum of opportunities to study the CRISPR-Cas9 system in a more precise manner.

# 4. CONCLUSIONS

## 4. CONCLUSIONS

Based on the results obtained, the conclusions are as follows:

1. The oligodendroglial lineage presents three different morphologies in the human white matter according to their stage of differentiation. OPCs labeled for A2B5, NG2, PDGFRa and Olig2 are electron lucent stellate-shaped filamentous cells intermingled in the white matter. Pre-OLs express Sox10, BCAS1 and Olig2 and are ramified cells that contact myelin, present a scant cytoplasm and scarce organelle diversity. m-OLs are electron dense cells which present condensed chromatin bound to the inner nuclear membrane and whose electron-dense cytoplasm shows characteristic short, dilated ER.

2. Tyramide signal amplification is a valid method to label human oligodendrocytes. This technique can be combined with immunogold for TEM analysis. This method improves the precision and signal-to-background ratio of the labeling, allows a better ultrastructural characterization of CNS cells, especially oligodendrocytes not only in mouse but also in human tissue.

3. The premyelinating oligodendrocyte marker BCAS1 can be found in the small nodules located in the superficial white matter of oligodendrogliomas and can be studied as a marker of a specific population of cells within these tumors.

4. Immunoelectron microscopy shows a higher precision for the detection of the CRISPR-Cas systems at a subcellular level. This technique allows a specific tracking of the tool in hardly transfectable cells such as oligodendrocyte progenitors, as well as in standard cell lines. Interestingly, SpCas9 enzyme is packaged in endosomal vesicles and degraded in cultured OPCs. In vivo oligodendrocytes, also show cytoplasmic restricted localization of the enzyme. SpCas9 tracking via immunoelectron microscopy is achievable with high precision in some tissues such as the liver.

# 5. REFERENCES

## 4. REFERENCES


Amaral, A. I., Tavares, J. M., Sonnewald, U., & Kotter, M. R. N. (2016). Oligodendrocytes: Development, Physiology and Glucose Metabolism. *Advances in Neurobiology*, 13, 275–294. Retrieved from https://doi.org/10.1007/978-3-319-45096-4_10

Anthony, T. E., Klein, C., Fishell, G., & Heintz, N. (2004). Radial glia serve as neuronal progenitors in all regions of the central nervous system. Neuron, 41(6), 881–890. Retrieved from https://doi.org/10.1016/s0896-6273(04)00140-0

Back, S. A., Han, B. H., Luo, N. L., Chricton, C. A., Xanthoudakis, S., Tam, J., … Holtzman, D. M. (2002). Selective Vulnerability of Late Oligodendrocyte Progenitors to Hypoxia–Ischemia. *The Journal of Neuroscience: The Official Journal of the Society for Neuroscience*, 22(2), 455–463. Retrieved 9 February 2021 from https://doi.org/10.1523/JNEUROSCI.22-02-00455.2002

Barrangou, R., Fremaux, C., Deveau, H., Richards, M., Boyaval, P., Moineau, S., … Horvath, P. (2007). CRISPR provides acquired resistance against viruses in prokaryotes. *Science*, 315(5819), 1709–1712. Retrieved from https://doi.org/10.1126/science.1138140

Biancheri, R., Rossi, A., Di Rocco, M., Filocamo, M., Pronk, J. C., van der Knaap, M. S., & Tortori-Donati, P. (2003). Leukoencephalopathy with vanishing white matter: an adult onset case. *Neurology*, 61(12), 1818–1819. Retrieved from https://doi.org/10.1212/01.wnl.0000098994.35677.3c

Bielle, F., Ducray, F., Mokhtari, K., Dehais, C., Adle-Biassette, H., Carpentier, C., … Pola Network. (2017). Tumor cells with neuronal intermediate progenitor features define a subgroup of 1p/19q co-deleted anaplastic gliomas. *Brain Pathology*, 27(5), 567–579. Retrieved from https://doi.org/10.1111/bpa.12434

Chavali, M., Ulloa-Navas, M. J., Pérez-Borredá, P., Garcia-Verdugo, J. M., McQuillen, P. S., Huang, E. J., & Rowitch, D. H. (2020). Wnt-Dependent Oligodendroglial-Endothelial Interactions Regulate White Matter Vascularization and Attenuate Injury. *Neuron*. Retrieved from https://doi.org/10.1016/j.neuron.2020.09.033

Dimou, L., Simon, C., Kirchhoff, F., Takebayashi, H., & Götz, M. (2008). Progeny of Olig2-expressing progenitors in the gray and white matter of the adult mouse cerebral cortex. *The Journal of Neuroscience: The Official Journal of the Society for Neuroscience*, 28(41), 10434–10442. Retrieved from https://doi.org/10.1523/JNEUROSCI.2831-08.2008

Dufour, A., Gontran, E., Deroulers, C., Varlet, P., Pallud, J., Grammaticos, B., & Badoual, M. (2018). Modeling the dynamics of oligodendrocyte precursor cells and the genesis of gliomas. *PLoS Computational Biology*, 14(3), e1005977. Retrieved from https://doi.org/10.1371/journal.pcbi.1005977

Elitt, M. S., Barbar, L., Shick, H. E., Powers, B. E., Maeno-Hikichi, Y.,

Madhavan, M., … Tesar, P. J. (2020). Suppression of proteolipid protein rescues Pelizaeus-Merzbacher disease. *Nature*, 585(7825), 397–403. Retrieved from https://doi.org/10.1038/s41586-020-2494-3
Fu, H., Qi, Y., Tan, M., Cai, J., Takebayashi, H., Nakafuku, M., … Qiu, M. (2002). Dual origin of spinal oligodendrocyte progenitors and evidence for the cooperative role of Olig2 and Nkx2.2 in the control of oligodendrocyte differentiation. Development , 129(3), 681–693. Retrieved from https://www.ncbi.nlm.nih.gov/pubmed/11830569

Geha, S., Pallud, J., Junier, M.-P., Devaux, B., Leonard, N., Chassoux, F., … Varlet, P. (2010). NG2+/Olig2+ cells are the major cycle-related cell population of the adult human normal brain. *Brain Pathology* , 20(2), 399–411. Retrieved from https://doi.org/10.1111/j.1750-3639.2009.00295.x

Gowers, W. R. (1897). The Neuron and Disease. *The Hospital*, 23(579), 78. Retrieved from https://www.ncbi.nlm.nih.gov/pubmed/29833089

Greenfield, J. G. (1933). A Form of Progressive Cerebral Sclerosis in Infants associated with Primary Degeneration of the Interfascicular Glia. *Proceedings of the Royal Society of Medicine*, 26(6), 690–697. Retrieved from https://www.ncbi.nlm.nih.gov/pubmed/19989245

Hou, J., & Major, E. O. (2000). Progressive multifocal leukoencephalopathy: JC virus induced demyelination in the immune compromised host. *Journal of Neurovirology*, 6 Suppl 2, S98–S100. Retrieved from https://www.ncbi.nlm.nih.gov/pubmed/10871795

Huang, W., Bhaduri, A., Velmeshev, D., Wang, S., Wang, L., Rottkamp, C. A., … Kriegstein, A. R. (2020). Origins and Proliferative States of Human Oligodendrocyte Precursor Cells. *Cell*, 182(3), 594–608.e11. Retrieved from https://doi.org/10.1016/j.cell.2020.06.027

Inouye, H., & Kirschner, D. A. (1988). Membrane interactions in nerve myelin. I. Determination of surface charge from effects of pH and ionic strength on period. *Biophysical Journal*, 53(2), 235–245. Retrieved from https://doi.org/10.1016/S0006-3495(88)83085-6

Jakovcevski, I., & Zecevic, N. (2005). Sequence of oligodendrocyte development in the human fetal telencephalon. *Glia*, 49(4), 480–491. Retrieved from https://doi.org/10.1002/glia.20134

Kessaris, N., Fogarty, M., Iannarelli, P., Grist, M., Wegner, M., & Richardson, W. D. (2006). Competing waves of oligodendrocytes in the forebrain and postnatal elimination of an embryonic lineage. *Nature Neuroscience*, 9(2), 173–179. Retrieved from https://doi.org/10.1038/nn1620

Kriegstein, A., & Alvarez-Buylla, A. (2009). The glial nature of embryonic and adult neural stem cells. *Annual Review of Neuroscience*, 32, 149–184. Retrieved from https://doi.org/10.1146/annurev.neuro.051508.135600

Labauge, P., Horzinski, L., Ayrignac, X., Blanc, P., Vukusic, S., Rodriguez, D., … Boespflug-Tanguy, O. (2009). Natural history of adult-onset eIF2B-related disorders: a multi-centric survey of 16 cases. *Brain: A Journal of Neurology*, 132(Pt 8), 2161–2169. Retrieved from https://doi.org/10.1093/brain/awp171

Li, L., Tian, E., Chen, X., Chao, J., Klein, J., Qu, Q., … Shi, Y. (2018). GFAP Mutations in Astrocytes Impair Oligodendrocyte Progenitor Proliferation and Myelination in an hiPSC Model of Alexander Disease. *Cell Stem Cell*, 23(2), 239–251.e6. Retrieved from https://doi.org/10.1016/j.stem.2018.07.009

Luskin, M. B., Parnavelas, J. G., & Barfield, J. A. (1993). Neurons, astrocytes, and oligodendrocytes of the rat cerebral cortex originate from separate progenitor cells: an ultrastructural analysis of clonally related cells. The Journal of Neuroscience: The Official Journal of the Society for Neuroscience, 13(4), 1730–1750. Retrieved from https://www.ncbi.nlm.nih.gov/pubmed/8463848

Masahira, N., Takebayashi, H., Ono, K., Watanabe, K., Ding, L., Furusho, M., … Ikenaka, K. (2006). Olig2-positive progenitors in the embryonic spinal cord give rise not only to motoneurons and oligodendrocytes, but also to a subset of astrocytes and ependymal cells. *Developmental Biology*, 293(2), 358–369. Retrieved from https://doi.org/10.1016/j.ydbio.2006.02.029

Matalon, R., Michals, K., Sebesta, D., Deanching, M., Gashkoff, P., & Casanova, J. (1988). Aspartoacylase deficiency and N-acetylaspartic aciduria in patients with Canavan disease. *American Journal of Medical Genetics*, 29(2), 463–471. Retrieved from https://doi.org/10.1002/ajmg.1320290234

McLaurin, J. A., & Yong, V. W. (1995). Oligodendrocytes and myelin. *Neurologic Clinics*, 13(1), 23–49. Retrieved from https://www.ncbi.nlm.nih.gov/pubmed/7739504

Menn, B., Garcia-Verdugo, J. M., Yaschine, C., Gonzalez-Perez, O., Rowitch, D., & Alvarez-Buylla, A. (2006). Origin of oligodendrocytes in the subventricular zone of the adult brain. The Journal of Neuroscience: The Official Journal of the Society for Neuroscience, 26(30), 7907–7918. Retrieved from https://doi.org/10.1523/JNEUROSCI.1299-06.2006

Messing, A. (2018). Alexander disease. *Handbook of Clinical Neurology*, 148, 693–700. Retrieved from https://doi.org/10.1016/B978-0-444-64076-5.00044-2

Mo, Z., & Zecevic, N. (2009). Human fetal radial glia cells generate oligodendrocytes in vitro. *Glia*, 57(5), 490–498. Retrieved from https://doi.org/10.1002/glia.20775

Modlin, J. F., Jabbour, J. T., Witte, J. J., & Halsey, N. A. (1977). Epidemiologic studies of measles, measles vaccine, and subacute sclerosing panencephalitis. *Pediatrics*, 59(4), 505–512. Retrieved from https://www.ncbi.nlm.nih.gov/pubmed/850592

Moser, H. W., Moser, A. B., Naidu, S., & Bergin, A. (1991). Clinical aspects of

adrenoleukodystrophy and adrenomyeloneuropathy. *Developmental Neuroscience*, 13(4-5), 254–261. Retrieved from https://doi.org/10.1159/000112170

Olude, M. A., Bello, S. T., Mustapha, O. A., Olopade, F. E., Plendl, J., Ihunwo, A. O., & Olopade, J. O. (2018). Oligodendrocyte morphology in the developing brain of the African giant rat (Cricetomys gambianus, Waterhouse): Histology, immunohistochemistry and electron microscopy. Anatomia, Histologia, Embryologia, 47(3), 231–238. Retrieved from https://doi.org/10.1111/ahe.12348
Parpura, V., & Verkhratsky, A. (2012). Astrocytes revisited: concise historic outlook on glutamate homeostasis and signaling. *Croatian Medical Journal*, 53(6), 518–528. Retrieved from https://doi.org/10.3325/cmj.2012.53.518

Penfield, W. (1925). Microglia and the Process of Phagocytosis in Gliomas. *The American Journal of Pathology*, 1(1), 77–90.15. Retrieved from https://www.ncbi.nlm.nih.gov/pubmed/19969634

Petito, C. K., Olarte, J. P., Roberts, B., Nowak, T. S., Jr, & Pulsinelli, W. A. (1998). Selective glial vulnerability following transient global ischemia in rat brain. *Journal of Neuropathology and Experimental Neurology*, 57(3), 231–238. Retrieved from https://doi.org/10.1097/00005072-199803000-00004

Propping, P., Friedl, W., Huschka, M., Schlör, K. H., Reimer, F., Lee-Vaupel, M., … Sandhoff, K. (1986). The influence of low arylsulfatase A activity on neuropsychiatric morbidity: a large-scale screening in patients. *Human Genetics*, 74(3), 244–248. Retrieved from https://doi.org/10.1007/BF00282542

Rakic, S., & Zecevic, N. (2003). Early oligodendrocyte progenitor cells in the human fetal telencephalon. *Glia*, 41(2), 117–127. Retrieved from https://doi.org/10.1002/glia.10140

Renier, W. O., Gabreëls, F. J., Hustinx, T. W., Jaspar, H. H., Geelen, J. A., Van Haelst, U. J., … Ter Haar, B. G. (1981). Connatal Pelizaeus-Merzbacher disease with congenital stridor in two maternal cousins. *Acta Neuropathologica*, 54(1), 11–17. Retrieved from https://doi.org/10.1007/BF00691328

Rowitch, D. H., & Kriegstein, A. R. (2010). Developmental genetics of vertebrate glial-cell specification. Nature, 468(7321), 214–222. Retrieved from https://doi.org/10.1038/nature09611

Saab, A. S., Tzvetavona, I. D., Trevisiol, A., Baltan, S., Dibaj, P., Kusch, K., … Nave, K.-A. (2016). Oligodendroglial NMDA Receptors Regulate Glucose Import and Axonal Energy Metabolism. *Neuron*, 91(1), 119–132. Retrieved from https://doi.org/10.1016/j.neuron.2016.05.016

Sander, J. D., & Joung, J. K. (2014). CRISPR-Cas systems for editing, regulating and targeting genomes. *Nature Biotechnology*, 32(4), 347–355. Retrieved from https://doi.org/10.1038/nbt.2842

Sawamoto, K., Wichterle, H., Gonzalez-Perez, O., Cholfin, J. A., Yamada, M.,

Spassky, N., … Alvarez-Buylla, A. (2006). New neurons follow the flow of cerebrospinal fluid in the adult brain. *Science*, 311(5761), 629–632. Retrieved from https://doi.org/10.1126/science.1119133

Spassky, N., Goujet-Zalc, C., Parmantier, E., Olivier, C., Martinez, S., Ivanova, A., … Thomas, J. L. (1998). Multiple restricted origin of oligodendrocytes. The Journal of Neuroscience: The Official Journal of the Society for Neuroscience, 18(20), 8331–8343. Retrieved from https://www.ncbi.nlm.nih.gov/pubmed/9763477

Stohlman, S. A., & Hinton, D. R. (2001). Viral induced demyelination. *Brain Pathology*, 11(1), 92–106. Retrieved from https://doi.org/10.1111/j.1750-3639.2001.tb00384.x

Takebayashi, H., & Ikenaka, K. (2015). Oligodendrocyte generation during mouse development. Glia, 63(8), 1350–1356. Retrieved from https://doi.org/10.1002/glia.22863

Tappino, B., Biancheri, R., Mort, M., Regis, S., Corsolini, F., Rossi, A., … Filocamo, M. (2010). Identification and characterization of 15 novel GALC gene mutations causing Krabbe disease. *Human Mutation*, 31(12), E1894–914. Retrieved from https://doi.org/10.1002/humu.21367

Vallstedt, A., Klos, J. M., & Ericson, J. (2005). Multiple dorsoventral origins of oligodendrocyte generation in the spinal cord and hindbrain. Neuron, 45(1), 55–67. Retrieved from https://doi.org/10.1016/j.neuron.2004.12.026

van der Knaap, M. S., Barth, P. G., Stroink, H., van Nieuwenhuizen, O., Arts, W. F., Hoogenraad, F., & Valk, J. (1995). Leukoencephalopathy with swelling and a discrepantly mild clinical course in eight children. *Annals of Neurology*, 37(3), 324–334. Retrieved from https://doi.org/10.1002/ana.410370308

van der Knaap, M. S., Barth, P. G., Vrensen, G. F., & Valk, J. (1996). Histopathology of an infantile-onset spongiform leukoencephalopathy with a discrepantly mild clinical course. *Acta Neuropathologica*, 92(2), 206–212. Retrieved from https://doi.org/10.1007/s004010050510

van der Knaap, M. S., Kamphorst, W., Barth, P. G., Kraaijeveld, C. L., Gut, E., & Valk, J. (1998). Phenotypic variation in leukoencephalopathy with vanishing white matter. *Neurology*, 51(2), 540–547. Retrieved from https://doi.org/10.1212/wnl.51.2.540

Volpe, J. J. (2001). Neurobiology of periventricular leukomalacia in the premature infant. *Pediatric Research*, 50(5), 553–562. Retrieved from https://doi.org/10.1203/00006450-200111000-00003

Wasserman, J. K., & Schlichter, L. C. (2008). White matter injury in young and aged rats after intracerebral hemorrhage. *Experimental Neurology*, 214(2), 266–275. Retrieved from https://doi.org/10.1016/j.expneurol.2008.08.010

Weller, M., van den Bent, M., Tonn, J. C., Stupp, R., Preusser, M., Cohen-Jonathan-Moyal, E., … European Association for Neuro-Oncology (EANO) Task Force on Gliomas. (2017). European Association for Neuro-Oncology (EANO) guideline on the diagnosis and treatment of adult astrocytic and oligodendroglial gliomas. The Lancet Oncology, 18(6), e315–e329. Retrieved from https://doi.org/10.1016/S1470-2045(17)30194-8
Wesseling, P., & Capper, D. (2018). WHO 2016 Classification of gliomas. Neuropathology and Applied Neurobiology, 44(2), 139–150. Retrieved from https://doi.org/10.1111/nan.12432

Wesseling, P., van den Bent, M., & Perry, A. (2015). Oligodendroglioma: pathology, molecular mechanisms and markers. Acta Neuropathologica, 129(6), 809–827. Retrieved from https://doi.org/10.1007/s00401-015-1424-1

Wilson, H. C., Scolding, N. J., & Raine, C. S. (2006). Co-expression of PDGF alpha receptor and NG2 by oligodendrocyte precursors in human CNS and multiple sclerosis lesions. *Journal of Neuroimmunology*, 176(1-2), 162–173. Retrieved from https://doi.org/10.1016/j.jneuroim.2006.04.014

Witte, M. E., Schumacher, A.-M., Mahler, C. F., Bewersdorf, J. P., Lehmitz, J., Scheiter, A., … Kerschensteiner, M. (2019). Calcium Influx through Plasma-Membrane Nanoruptures Drives Axon Degeneration in a Model of Multiple Sclerosis. *Neuron*, 101(4), 615–624.e5. Retrieved from https://doi.org/10.1016/j.neuron.2018.12.023

Woodruff, R. H., Tekki-Kessaris, N., Stiles, C. D., Rowitch, D. H., & Richardson, W. D. (2001). Oligodendrocyte development in the spinal cord and telencephalon: common themes and new perspectives. *International Journal of Developmental Neuroscience: The Official Journal of the International Society for Developmental Neuroscience*, 19(4), 379–385. Retrieved from https://doi.org/10.1016/s0736-5748(00)00083-6

# 6. ANNEX

frontiers in Neuroanatomy

ORIGINAL RESEARCH
published: 23 June 2021
doi: 10.3389/fnana.2021.696376

# Ultrastructural Characterization of Human Oligodendrocytes and Their Progenitor Cells by Pre-embedding Immunogold

*María J. Ulloa-Navas[1], Pedro Pérez-Borredá[1,2], Raquel Morales-Gallel[1], Ana Saurí-Tamarit[1], Patricia García-Tárraga[1], Antonio J. Gutiérrez-Martín[3], Vicente Herranz-Pérez[1,4]* and José M. García-Verdugo[1]**

[1]Laboratory of Compared Neurobiology, University of Valencia-CIBERNED, Paterna, Spain, [2]Neurosurgery Department, Consorcio Hospital General Universitario de Valencia, Valencia, Spain, [3]Neurosurgery Department, Hospital Universitari i Politècnic La Fe, Valencia, Spain, [4]Predepartmental Unit of Medicine, Faculty of Health Sciences, Universitat Jaume I, Castelló de la Plana, Spain

Oligodendrocytes are the myelinating cells of the central nervous system. They provide trophic, metabolic, and structural support to neurons. In several pathologies such as multiple sclerosis (MS), these cells are severely affected and fail to remyelinate, thereby leading to neuronal death. The gold standard for studying remyelination is the g-ratio, which is measured by means of transmission electron microscopy (TEM). Therefore, studying the fine structure of the oligodendrocyte population in the human brain at different stages through TEM is a key feature in this field of study. Here we study the ultrastructure of oligodendrocytes, its progenitors, and myelin in 10 samples of human white matter using nine different markers of the oligodendrocyte lineage (NG2, PDGFRα, A2B5, Sox10, Olig2, BCAS1, APC-(CC1), MAG, and MBP). Our findings show that human oligodendrocytes constitute a very heterogeneous population within the human white matter and that its stages of differentiation present characteristic features that can be used to identify them by TEM. This study sheds light on how these cells interact with other cells within the human brain and clarify their fine characteristics from other glial cell types.

**Keywords: oligodendrocytes, OPCs, human oligodendrocytes, transmission electron microscopy, immunogold, BCAS1**

OPEN ACCESS

***Edited by:***
*Rafael Luján, Instituto de Investigación en Discapacidades Neurológicas (IDINE), Spain*

***Reviewed by:***
*Rosa M. Villalba, Emory University, United States*
*Jose Martinez-Hernandez, University of Castilla La Mancha, Spain*
*Fernando de Castro, Cajal Institute (CSIC), Spain*

****Correspondence:***
*José M. García-Verdugo*
*j.manuel.garcia@uv.es*
*Vicente Herranz-Pérez*
*vicente.herranz@uv.es*

***Received:*** *16 April 2021*
***Accepted:*** *02 June 2021*
***Published:*** *23 June 2021*

***Citation:***
*Ulloa-Navas MJ, Pérez-Borredá P, Morales-Gallel R, Saurí-Tamarit A, García-Tárraga P, Gutiérrez-Martín AJ, Herranz-Pérez V and García-Verdugo JM (2021) Ultrastructural Characterization of Human Oligodendrocytes and Their Progenitor Cells by Pre-embedding Immunogold. Front. Neuroanat. 15:696376. doi: 10.3389/fnana.2021.696376*

## INTRODUCTION

Oligodendrocytes are glial cells whose main function is myelination. Myelination leads to the optimization of the saltatory conduction along neuronal axons (McLaurin and Yong, 1995). Moreover, oligodendrocytes perform other supportive activities such as glucose metabolism (Amaral et al., 2016; Saab et al., 2016), calcium influx/efflux towards the axon to impede

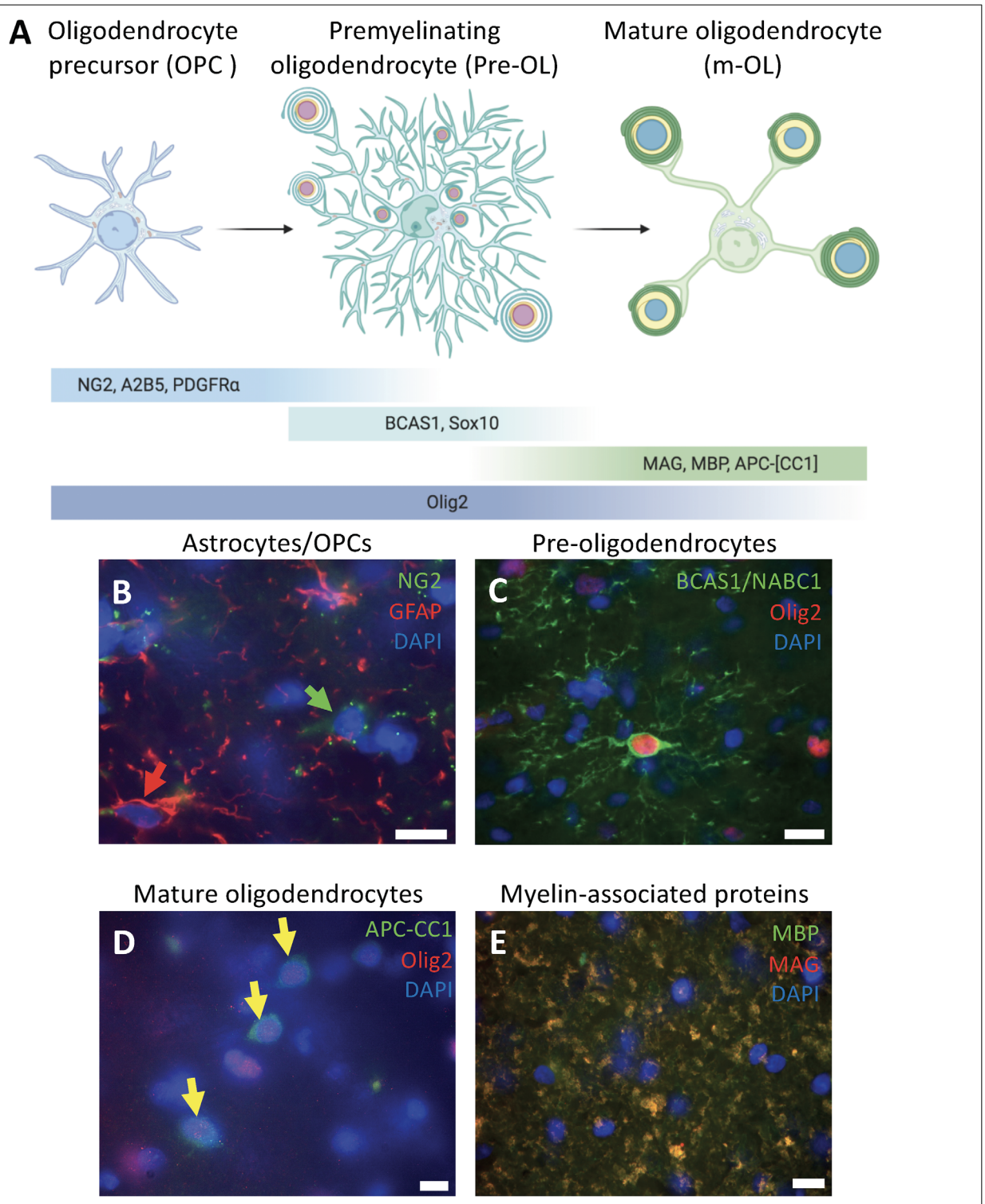


**FIGURE 1 |** Differentiation stages of oligodendrocytes in human white matter. **(A)** Schematic diagram of the oligodendrocyte differentiation process representing the morphology, organelle distribution, and markers to identify each of the three stages: oligodendrocyte precursor cells (OPCs), premyelinating oligodendrocytes (pre-OLs), and mature oligodendrocytes. **(B)** Human white matter labeled for the astrocytic marker GFAP (red arrow) and the OPC marker NG2 (green arrow) showing that these are two different populations within the white matter of a 39-year-old male (PB4). **(C)** Human white matter labeled for pre-myelinating oligodendrocyte markers BCAS1/NABC1 and Olig2 co-expressed in highly ramified cells from a 5-year-old female (PB19). **(D)** Mature oligodendrocytes labeled for Olig2 and APC-(CC1; yellow arrows) from a white matter sample of a 5-year-old female (PB19). **(E)** Myelin wrapped axons co-expressing MAG and MBP from a white matter sample of a 39-year-old male (PB4). Scale bars: 50 μm.

degeneration (Witte et al., 2019), and pH and ion balance regulation (Inouye and Kirschner, 1988). Given that oligodendroglial or myelin degeneration can produce quite severe pathologies such as in genetic conditions in children (Greenfield, 1933; Renier et al., 1981; Matalon et al., 1988; van der Knaap et al., 1995; Tappino et al., 2010) or neurodegenerative conditions with a very high incidence in adults such as multiple sclerosis (MS; Howard et al., 2016) and that the causes that may trigger oligodendroglial damage can be quite diverse e.g., genetic (Greenfield, 1933; Renier et al., 1981; Matalon et al., 1988; Tappino et al., 2010; van der Knaap et al., 1995), autoimmune (Howard et al., 2016), infectious (Stohlman and Hinton, 2001), and vascular (Volpe, 2001; Chavali et al., 2020)—studying the biology underlying this cell population and its progenitors is a relevant aspect in central nervous system research.

After numerous studies in animal models, evidence suggests that in the postnatal brain oligodendrocytes arise from NG2/PDGFRa/Olig2-positive progenitors in different regions of the brain and spinal cord (Rivers et al., 2008; Zhu et al., 2008; Kang et al., 2010; Sánchez-González et al., 2020). The processes of oligodendrocyte replacement, maturation, and myelin regeneration play a critical role in the adult brain, where remodeling and plasticity are a constant phenomenon. Correspondingly, when there is an insult in the brain, especially in the white matter such as in MS, $NG2^{+}$-cells are recruited towards the lesions, and thus, studies demonstrate their presence in MS plaques (Wilson et al., 2006).

In rodents, the stages of differentiation of the oligodendroglial lineage have been largely studied and have shed light on the expression of different markers of oligodendrocyte maturation (Barateiro and Fernandes, 2014; Marques et al., 2016; Domingues et al., 2018; Schoor et al., 2019). These studies have described that there are at least three oligodendrocyte stages according to the morphology and protein markers expressed by each population. The first population corresponds to oligodendrocyte precursor cells (OPCs), which express markers such as: NG2, PDGFRα, A2B5, CD9, CNP, GPR17, NKX 2.2, Olig1, Olig2, Sox9, and Sox10. The second population is pre-oligodendrocytes or premyelinating oligodendrocytes (pre-OLs) which can be labeled for CD9, O4, BCAS1, CNP; NKX 2.2, Sox17, Sox10, and Olig2. The last population is myelinating oligodendrocytes (m-OLs) which express: O1, CD9, CNP, MAG, MBP, MOG, PLP1, Sox17, APC1-(CC1), and Olig2 (Goldman and Kuypers, 2015). Furthermore, single-cell transcriptional analysis has described 12 different populations of oligodendrocytes and their progenitors along with the juvenile and adult postnatal brain, thereby describing the great heterogeneity among these cells (Marques et al., 2016; van Bruggen et al., 2017). However, the fine morphology of oligodendrocytes is still elusive.

In contrast to mice, the number of human oligodendrogenesis studies is not as high. This can be explained because of the scarce availability of human brain tissue and poor fixation conditions. This is more evident in ultrastructural studies, which require an outstanding fixation and tissue preservation. Considering that the gold standard for understanding remyelination is the g-ratio measured by transmission electron microscopy (TEM), analyzing human tissue using TEM is fundamental.

Here we present a detailed study of the fine structure of oligodendrocytes in different stages in human white matter. This analysis includes samples from patients at different ages with exceptional preservation of the tissue combined with pre-embedding immunogold for nine different markers. Our results suggest that oligodendrocytes present three marked ultrastructural stages (**Figure 1A**): OPCs labeled for NG2, A2B5 and PDGFRα; pre-OLs labeled for BCAS1/NABC1, Sox10 and Olig2; and m-OLs labeled with APC-(CC1) and Olig2. Furthermore, we studied the presence of myelin-associated proteins and myelin ultrastructure labeling for MAG and MBP combined with standard TEM.

## MATERIALS AND METHODS

All reagents were purchased from Sigma Aldrich unless otherwise specified.

### Human Sample Collection

Samples were obtained from surgical resections from focal cortical dysplasia patients operated at Hospital Universitarii Politècnic La Fe at Valencia, Spain. Samples included in this study ($n$ = 10) comprehend the non-affected white matter of female and male patients ages 2–44-year-old (**Table 1**). Sample collection was approved by the Research Ethics committee from the Hospital Universitari i Politècnic La Fe. Patients or their representatives signed an informed consent prior to donating the samples for the study.

**TABLE 1** | Human samples and brain areas included in this study.

| Sample code | Age (years) | Sex | Diagnosis | Area |
|---|---|---|---|---|
| PB2 | 9 | Male | Type IA FCD | Left temporal lobe |
| PB3 | 6 | Male | Type IA FCD | Left temporal lobe |
| PB4 | 39 | Male | Type IIB FCD | Left frontal lobe |
| PB8 | 27 | Male | Type IIA FCD | Right anterior insular cortex |
| PB9 | 2 | Female | Type IIB FCD | Right temporal lobe |
| PB11 | 13 | Female | Type IC FCD | Left frontal lobe |
| PB12 | 44 | Male | Type IIB FCD | Right frontal lobe |
| PB16 | 32 | Male | Type IB FCD | Right frontal lobe |
| PB19 | 5 | Female | No lesion | Right frontal lobe |
| PB20 | 2 | Female | Type IIA FCD | Right frontal lobe |

*Note: FCD, focal cortical displasia.*

## Sample Processing

After surgical resection samples were immediately fixed with 4% paraformaldehyde in 0.1 M phosphate buffer (pH 7.4, PB) for 7 days. Samples were then washed with 0.1 M PB and kept in 0.1 M PB-0.05% sodium azide at 4°C until subsequent use. Brain tissue was sectioned at 50 μm using a Leica VT1000S vibratome (Leica Biosystems, Wetzlar, Germany). We performed the same procedures in a P21 4% PFA perfused mouse as a control for the following experiments, except for A2B5 and PDGFRa immunogold labeling, since the antibodies worked for human tissue only (**Table 2**).

## Immunofluorescence

Sections were washed with 0.1 M PB, incubated in 1:200 Immunosaver (Electron Microscopy Sciences, Hatfield, PA) in water at 60°C for 30 min. Peroxidase blocking was performed using a solution containing 10% methanol and 10% $H_2O_2$ in 0.1 M PB. For permeabilization, the samples were washed three times for 5 min in PTA solution: 0.1% Triton X-100, 1 mg/ml bovine serum albumin (BSA) in 0.1 M phosphate buffer saline (PBS). The samples were then incubated in blocking solution (5% normal goat serum in PTA) for 1 h at room temperature. Subsequently, the samples were incubated overnight in primary antibodies diluted in blocking solution [1:300 rabbit anti-Olig2, Merck-Millipore Burlington, MA; 1:200 rabbit anti-NG2, Abcam, Cambridge, United Kingdom; 1:200 mouse anti-GFAP, Merck-Millipore Burlington, MA; 1:200 mouse anti-NABC1, Santa Cruz Biotechnology, Dallas, TX; 1:100 mouse anti-MAG, Merck-Millipore Burlington, MA; 1:100 rat anti MBP, Abcam, Cambridge, United Kingdom, 1:100 mouse anti-APC (CC1), Abcam, Cambridge, United Kingdom; see **Table 3**]. The following day, samples were thoroughly washed in PTA and incubated in a secondary antibody solution (1:500 AlexaFluor 488 goat anti-mouse, Invitrogen; or 1:500 AlexaFluor 555 goat anti-rabbit, Invitrogen). Samples were then washed in 0.1 M PB and incubated in 1:1,000 DAPI in water for 5 min. Finally, the samples were mounted with FluorSave [Merck Millipore (Calbiochem), Burlington, MA].

## Immunogold Labeling

Tissue sections were cryoprotected in a solution containing 25% saccharose in 0.1 M PB-0.05% azide for 30 min. Immediately after cryoprotection, sections were permeabilized by repeated freeze–thaw cycles by immersion in −60°C 2-methylbutane and rapidly transfer to a room temperature saccharose solution. These steps were repeated three or four times. Subsequently, tissue sections were left in 0.1 M PB and then incubated in primary antibody blocking solution [0.3% BSAc (Aurion, Wageningen, The Netherlands), 0.05% sodium azide in 0.1 M PB] for 1 h. Next, the samples were incubated in primary antibody [1:150 rabbit anti-Olig2, Merck-Millipore Burlington, MA; 1:100 mouse anti-GFAP, Merck-Millipore Burlington, MA; 1:100 mouse anti-MAG, Merck-Millipore Burlington, MA; 1:100 rat anti MBP, Abcam, Cambridge, United Kingdom, 1:50 mouse anti-APC (CC1), Abcam, Cambridge, United Kingdom; 1:50 mouse anti-A2B5 Merck-Millipore Burlington, MA, 1:150 rabbit anti-Sox10 Abcam, Cambridge, United Kingdom; see **Table 3**] in primary antibody blocking solution for 72 h at 4°C. The samples were rinsed in 0.1 M PB and then

**TABLE 2** | Antibody and concentrations used.

| Antigen | Host species | Antibody | IF concentration | IG concentration | Cell type labeling |
|---|---|---|---|---|---|
| NG2 | Rabbit | ab5320 (Abcam) | 1:200 | 1:100 | OPCS |
| PDGFRα | Mouse | 556001 (BD Biosciences) | 1:50 | 1:50 | OPCs |
| A2B5 | Mouse | MAB312 (Millipore) | 1:100 | 1:50 | OPCS |
| Olig2 | Rabbit | AB9610 (Millipore) | 1:300 | 1:150 | OPCs, pre-OLs, m-OLs |
| BCAS1 | Mouse | sc-136342 (Santa Cruz) | 1:200 | 1:150 | pre-OLs |
| Sox10 | Rabbit | ab155279 (Abcam) | 1:300 | 1:150 | pre-OLs |
| APC (CC1) | Mouse | ab16794 Abcam | 1:100 | 1:50 | m-OLs |
| MAG | Mouse | Mab15667 (Millipore) | 1:100 | 1:100 | myelin |
| MBP | Rat | ab7349 (Abcam) | 1:100 | 1:100 | myelin |
| GFAP | Mouse | Millipore | 1:200 | 1:100 | Astrocytes |

**TABLE 3** | Antibody tested per sample.

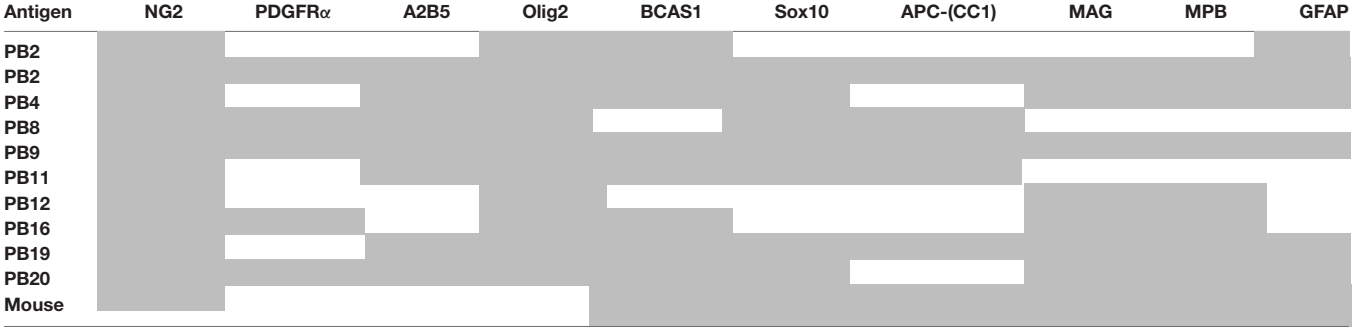


*Shaded areas correspond to antibodies tested in the samples indicated.*

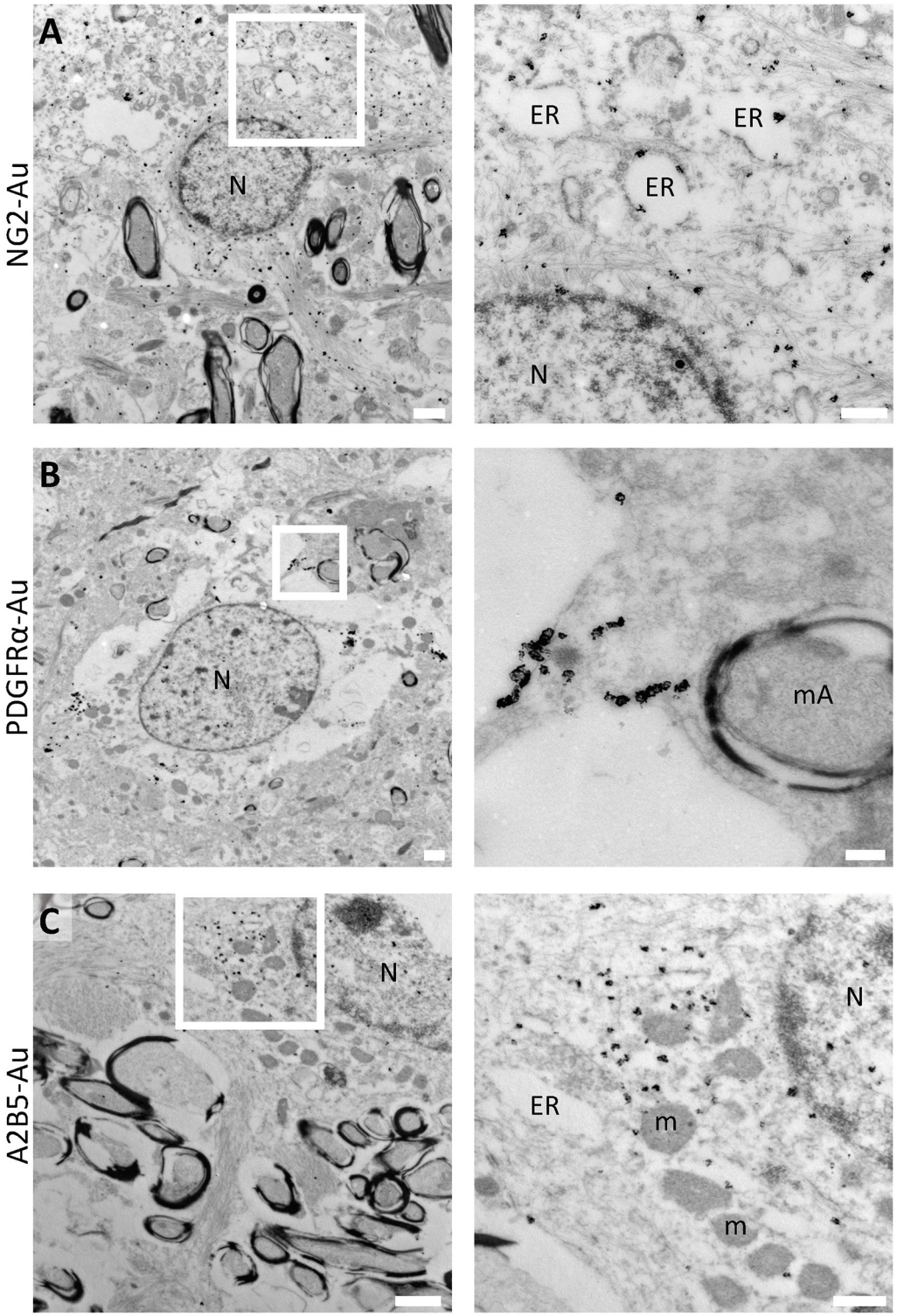


**FIGURE 2 |** Immunoelectron microscopy for human OPC molecular markers. **(A)** NG2 label in large electron-lucent cells in the white matter. Inset shows NG2 subcellular distribution in cytoplasmic intermediate filaments and in short dilated endoplasmic reticulum cisternae in a sample of a 2-year-old male sample (PB20). **(B)** PDGFRα is expressed in discrete clusters in the plasma membrane of OPCs in the white matter of a 6-year-old male (PB3). **(C)** OPCs in the white matter labeled with A2B5. Immunogold shows the subcellular localization of this marker in the cytoplasmic portion of the cells and is also associated with the endoplasmic reticulum in the white matter of a 5-year-old female (PB19). N, Nucleus; ER, endoplasmic reticulum; mA, myelinated axon; m, mitochondria. Scale bars: panoramic micrographs, 1 μm; insets: 250 nm.

incubated in secondary antibody blocking solution consisting of 0.5% BSAc (Aurion), 0.025% CWFS gelatin (Aurion), 0.05% sodium azide in 0.1 M PB for 1 h, followed by incubation in secondary antibody [1:50 goat anti-mouse IgG gold ultrasmall (Aurion); 1:50 goat anti-rabbit IgG gold ultrasmall (Aurion); 1:50 goat-anti-rat IgG gold ultrasmall (Aurion)] diluted in the same secondary antibody blocking solution overnight at 4°C. To enhance gold labeling, we performed silver enhancement (R-GENT SE-LM, Aurion) for 15–25 min in the dark, followed by gentle washing in 2% sodium acetate and incubation in gold toning solution (0.05% gold chloride in water) for 10 min. The samples were then washed twice with 0.3% sodium thiosulfate in water. Finally, we post-fixed with 2% glutaraldehyde (Electron Microscopy Sciences) in 0.1 M PB for 30 min. Samples were rinsed and kept in 0.1 M PB containing 0.05% sodium azide at 4°C until processing them for resin embedding.

For PDGFRa, NABC1, and NG2, we performed Tyramide Signal Amplification. Sections were washed in 0.05% Triton X-100 in PBS (PBS-Tx) at room temperature for 15 min. To quench endogenous peroxidases, we incubated the sections in peroxidase blocking solution (1% $H_2O_2$ in PBS-Tx) for 45 min in the dark at room temperature. Samples were washed and incubated in blocking solution [0.87% NaCl, 5% normal goat serum (Gibco), 0.05% sodium azide in 0.1 M Tris-HCl at pH 7.5] for 1 h. Then, the sections were incubated in primary antibody overnight (1:50 mouse anti-PDGFRa, BD Biosciences, Franklin Lakes, NJ; 1:100 rabbit anti-NG2 Abcam, Cambridge, United Kingdom, 1:150 mouse anti-NABC1 Santa Cruz Biotechnology, Dallas, TX; see **Table 3**) under mild agitation at 4°C. Samples were subsequently washed in PBS-Tx and incubated in secondary antibody solution for 2 h at room temperature. After washing with PBS-Tx, an incubation in Streptavidin-HRP (Vector Labs, San Francisco, CA) solution was performed for 30 min. Then, we incubated the samples in 1:50 biotin-tyramide solution (Akoya Biosciences, Marlborough, MA) for 5 min at room temperature. Subsequently, the sections were blocked in 0.3% BSAc (Aurion, The Netherlands) in 0.1 M PB-0.05% sodium azide for 1 h at room temperature in the dark. Then we incubated the samples in immunogold primary antibody (1:300 mouse anti-Biotin antibody; Jackson Immunoresearch) diluted in blocking solution overnight at 4°C with gentle shaking. The following day, samples were washed and incubated in a blocking solution consisting of 0.5% BSAc and 0.1% fish skin gelatin (Aurion) in 0.1 M PB-0.05% sodium azide. Next, we incubated the samples in 1:50 goat anti-mouse gold-conjugated antibody (Ultra Small; Aurion) in blocking solution for 2 h, in the dark at and under mild agitation. Finally, we proceeded with the silver enhancement process as in the standard immunogold labeling as described above.

## Tissue Processing for TEM Analysis

For TEM analysis, sections were embedded in epoxy resin. First, samples were post-fixed with 1% osmium tetroxide (Electron Microscopy Sciences), 7% glucose in 0.1 M PB for 30 min at room temperature, washed in deionized water, and partially dehydrated in 70% ethanol. Afterward, the samples were contrasted in 2% uranyl acetate (Electron Microscopy Sciences) in 70% ethanol for 2 h at 4°C. The samples were further dehydrated and embedded in Durcupan ACM epoxy resin at room temperature overnight, and then at 70°C for 72 h. Once the resin was polymerized, immunolabeled sections were selected and cut into semithin (1.5 μm) and then into ultrathin sections (60–80 nm) using an Ultracut UC7 ultramicrotome (Leica). Ultrathin sections were placed on formvar-coated single-slot copper grids (Electron Microscopy Sciences) stained with lead citrate and examined at 80 kV on a FEI Tecnai $G^2$ Spirit (FEI Company, Hillsboro, OR) transmission electron microscope equipped with a Morada CCD digital camera (Olympus, Tokyo, Japan).

## Criteria Used for Immunogold Analysis

Our general criteria to differentiate label and background is 5:1 ratio of silver-enhanced gold nanoparticles. And depending on the labeled structure and marker (plasma membrane or organelle) we consider a minimum number of silver-enhanced nanoparticles within an ultrathin section as follows:

For NG2: seven silver-enhanced gold nanoparticles/$\mu m^2$.

PDGFRα: seven silver-enhanced gold nanoparticles/cluster in at least three clusters per cell.

A2B5: seven silver-enhanced gold nanoparticles/$\mu m^2$ when there is a proximal ER.

BCAS1: 10 silver-enhanced gold nanoparticles within the extent of the plasma membrane.

Olig2: at least 15 silver-enhanced gold nanoparticles within the nucleus.

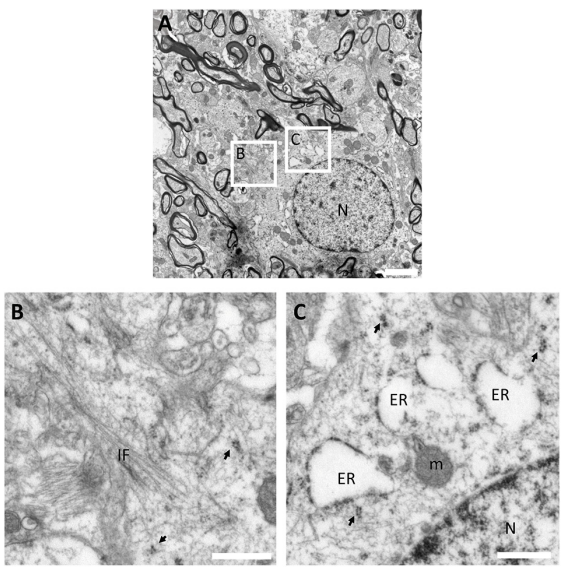


**FIGURE 3 |** Ultrastructural characterization of OPCs in the human white matter. **(A)** Panoramic micrograph of an OPC showing a large electron-lucent star-shaped cell with electron-lucent nucleus (with abundant euchromatin) intermingled between myelinated axons in the white matter. **(B)** OPCs present abundant filamentous processes, and **(C)** an electron-lucent cytoplasm with abundant short dilated endoplasmic reticulum cisternae, mitochondria and ribosomes. The micrograph proceeds from the white matter of a 27-year-old male (PB8) fixed with 2% PFA-2.5% Glutaraldehyde. N, Nucleus; ER, endoplasmic reticulum; m, mitochondria; IF, intermediate filaments; arrows, polyribosomes. Scale bars: (**A**), 2 μm; **(B,C)**, 500 nm.

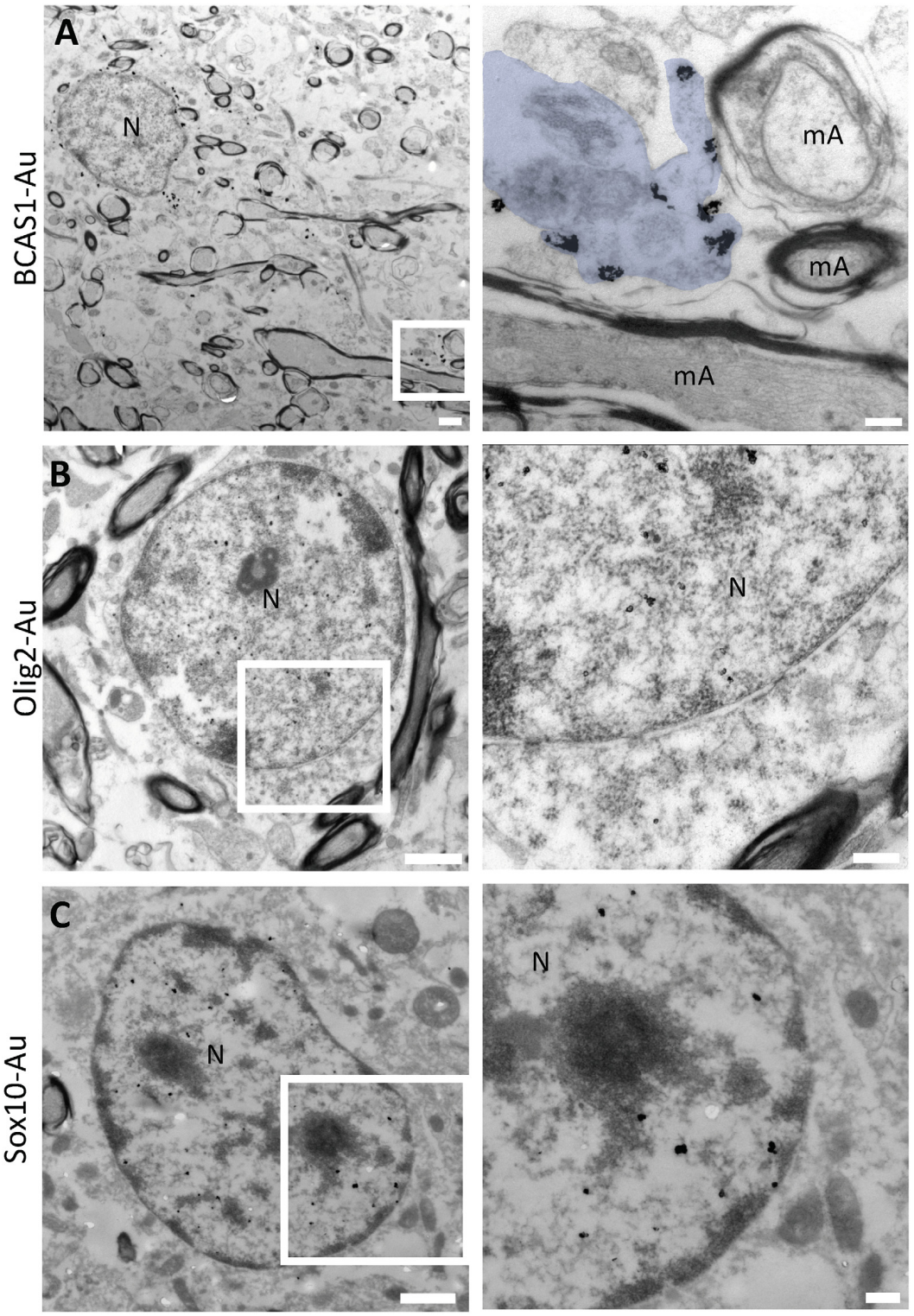


**FIGURE 4 |** Pre-embedding immunogold labeling for pre-myelinating oligodendrocytes. **(A)** BCAS1/NABC1 labeled pre-myelinating oligodendrocyte. BCAS1 is observed in the plasma membrane of the cell and in processes in direct contact with thin myelin sheets (blue pseudocolor) in the white matter of a 2-year-old female (PB9). **(B)** Olig2 labels the uncondensed chromatin of electron-lucent cells with scant cytoplasm in the white matter of a 32-year-old male (PB16). **(C)** The transcription factor SOX10 labels the nucleus of pre-myelinating oligodendrocytes in the white matter of a 13-year-old female (PB11). N, Nucleus; mA, myelinated axon. Scale bars: panoramic micrographs: 1 μm; insets: 250 nm.

Sox10: at least 15 silver-enhanced gold nanoparticles within the nucleus.

APC: at least 15 silver-enhanced gold nanoparticles within the cell.

MAG/MBP: at least 15 silver-enhanced gold nanoparticles in the myelin proximity.

GFAP: 15 silver-enhanced gold nanoparticles/$\mu m^2$.

# RESULTS

## Human Oligodendrocytes Go Through Three Sequential Morphological Stages of Differentiation

Previous studies indicate that human oligodendrocytes acquire three sequential phenotypes through their maturation (Goldman and Kuypers, 2015). The identification of these maturational stages is typically based on the expression of different molecular markers. In order to establish a connection between the molecular and ultrastructural changes which characteristically follow each maturational stage, we first performed immunofluorescence detection for a group of markers described for oligodendrocytes, their progenitors, and myelin proteins. This analysis was performed in human intraoperatively obtained brain tissue containing white matter from donors of different ages. Our results suggest that oligodendrocytes in the human white matter display three distinctive morphologies and can be labeled with distinctive molecular markers (**Figure 1A**). The first stage is characterized by star-shaped cells, negative for astrocyte marker GFAP, in which NG2-labeling is distributed as cytoplasmic/plasma membrane dots in cells evenly distributed through the white matter (**Figure 1B**). NG2 expression defines a population which has been widely described as OPCs with a broad distribution through the white matter. The second stage of differentiation was identified with the oligodendrocyte lineage markers BCAS1/NABC1 and Olig2, corresponding to pre-OLs. Pre-OLs expand their processes and become highly ramified cells with a small soma (**Figure 1C**). The subcellular localization of Olig2 is limited to the cell nucleus, while in the case of BCAS1/NABC1 it is cytoplasmic. The third and final stage of differentiation comprises m-OLs, which are small cells with scant cytoplasm distributed throughout the white matter and label profusely for the nuclear transcription factor Olig2 and the RNA binding protein quaking7, which binds to APC-(CC1) antibody. This protein appears to be in a cytoplasmic/nuclear localization when detected by immunofluorescence (**Figure 1D**). Finally, we have observed myelin-associated proteins such as MAG and MBP broadly scattered through the white matter (**Figure 1E**). Our results confirm that at least three maturational stages can be defined in the oligodendroglial lineage based on molecular marker expression and gross morphology.

## OPCs in the Human White Matter Display an Astrocytic-like Morphology and Ultrastructure

To better characterize the ultrastructure of human OPCs, we have analyzed cells labeled for NG2, PDGFRα, A2B5, and Olig2 using immunoelectron microscopy and described their fine features through conventional TEM. Our results show that NG2 is expressed in the cytoplasm, endoplasmic reticulum, and intermediate filaments present in the processes of star-shaped electron-lucent cells (**Figure 2A**). PDGFRα, on the other hand, is expressed in small clusters in discrete regions of the plasma membrane of OPCs (**Figure 2B**). A2B5 is observed to be expressed in a cytoplasmic portion of OPCs which includes the endoplasmic reticulum (ER; **Figure 2C**). Finally, Olig2 labels the nuclei of these populations (**Supplementary Figure 2**).

The fine structure of OPCs is very similar to that of astrocytes present in the human white matter (**Supplementary Figure 1**). TEM analysis shows that human OPCs can be identified as star-shaped cells with electron-lucent nucleus and non-condensed euchromatin (**Figure 3A**). Their soma exhibits several filamentous processes (**Figure 3B**) and their electron-lucent cytoplasm presents abundant short dilated endoplasmic reticulum, similar to that of classic oligodendrocytes, being also rich in mitochondria and ribosomes (**Figure 3C**).

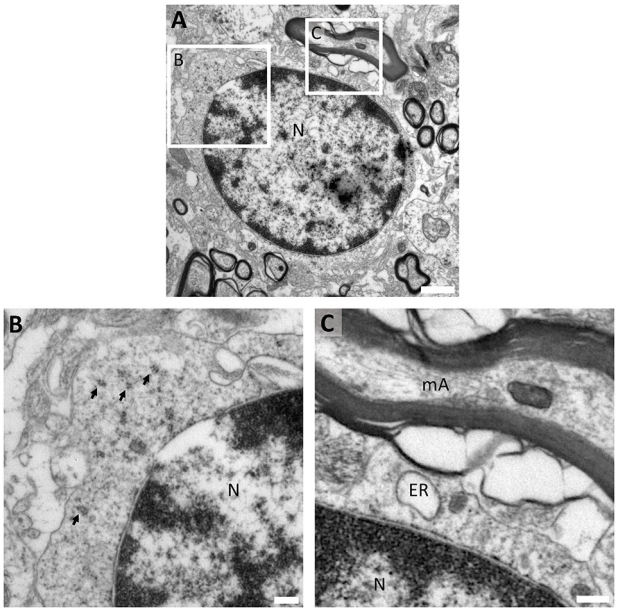


**FIGURE 5 |** Fine structure of human pre-myelinating oligodendrocytes. **(A)** Pre-myelinating oligodendrocytes are highly ramified cells with scant electron-lucent cytoplasm and slightly condensed chromatin. **(B)** Their cytoplasm contains abundant polyribosomes, **(C)** a few small mitochondria and short dilated endoplasmic reticulum. These cells are in direct contact with myelin sheets The micrograph proceeds from the white matter of a 9-year-old male (PB2) fixed with 2% PFA–2.5% Glutaraldehyde. N, Nucleus; ER, endoplasmic reticulum; arrows, polyribosomes. T Scale bars: **(A)**, 1 μm; **(B,C)**, 250 nm.

## Pre-oligodendrocytes in the Human White Matter Show Scarce Organelle Variety

Since pre-myelinating oligodendrocytes presented a distinctive morphology in our immunofluorescence studies, we performed immunogold and conventional TEM analyses to study whether these morphological changes can be correlated

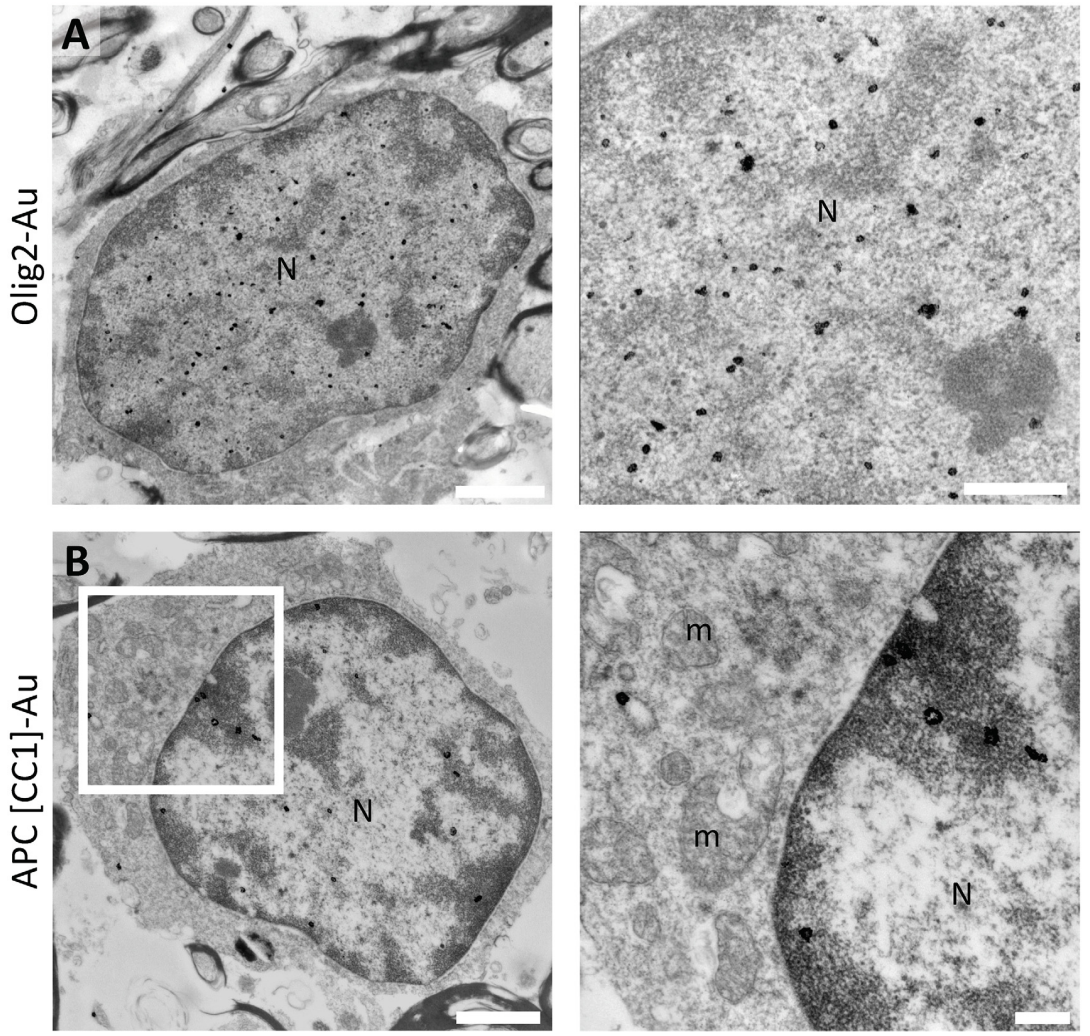


**FIGURE 6 |** Fully differentiated oligodendrocytes display Olig2 and APC-(CC1) labeling. **(A)** Olig2 expression in mature oligodendrocytes is restricted to the uncondensed chromatin within the nucleus in the white matter of a 44-year-old male (PB12). **(B)** The RNA-binding protein quaking7 labeled with APC-(CC1) was found in the condensed chromatin portion as well as in non-condensed chromatin; faint labeling was also observed in the plasma membrane in the white matter of a 13-year-old female (PB11). N, Nucleus; m, mitochondria. Scale bars: panoramic micrographs, 1 μm; insets: 250 nm.

with characteristic ultrastructural features. Our TEM data corroborate that the soma of pre-OLs is small, with the vast majority of its volume occupied by the nucleus. We found that the expression of BCAS1/NABC1, a novel marker of intermediate oligodendroglial maturational stages (Fard et al., 2017), is tightly associated with the plasma membrane of this population and allows the identification of cellular processes which contact thin myelin sheets (**Figure 4A**). On the other hand, the transcription factors Olig2 and Sox 10 are expressed in the nuclei of pre-OLs (**Figures 4B,C**). The distribution of both markers is similar to that of loosely condensed euchromatin within the nuclear space.

Prior immunogold characterization of pre-OLs allowed us to further study this cell population in better-preserved conventional TEM samples. As a result, we observed that pre-OLs are highly ramified cells with scant electron-lucent cytoplasm and slightly condensed chromatin (**Figure 5A**). Since the cytoplasmic area is rather small, this population does not present a great organelle abundance. Polyribosomes are the most frequent organelle in pre-OLs (**Figure 5B**), while they also present few mitochondria and short dilated ER. Interestingly, this subset of cells displays a stretch contact with myelin sheets (**Figure 5C**).

## Mature Oligodendrocytes Are Electron-Dense Cells Distributed Through the White Matter

To gain insight into the fine structure of fully differentiated oligodendrocytes in the human white matter, we performed immunogold labeling using Olig2 and APC-(CC1) antibodies combined with standard TEM analysis. As observed in the

previous stages of differentiation, Olig2 is also expressed in m-OLs. The distribution of this transcription factor is associated with non-condensed chromatin within the nucleus (**Figure 6A**). Conversely, the RNA-binding protein quaking7 labeled with APC-(CC1) was found associated both to euchromatin and heterochromatin as well as in the cytoplasm (**Figure 6B**).

Conventional ultrastructural characterization allowed us to describe that m-OLs are small electron-dense cells with a broad distribution in the human white matter. These cells are intermingled between myelin-wrapped axons (**Figure 7A**). Their chromatin is more condensed than that observed in earlier stages of oligodendroglial differentiation. Frequently, highly condensed chromatin is bound to the inner nuclear membrane (**Figure 7B**). m-OLs display characteristic short dilated ER, mitochondria, dense degradation vesicles, and polyribosomes (**Figure 7C**).

## Human Myelin-Associated Proteins Are Observed in Different Portions of the Wrapping Sheets in Pre-embedding Immunogold

To further investigate into the structure of human myelin structure, we sought to study the expression and localization of two well-studied myelin-associated proteins (MBP and MAG) by pre-embedding immunogold detection. Our analysis shows that MBP localizes to the outermost layer of the myelinated axon in the cerebral white matter (**Figure 8A**), while MAG is observed in the most internal layer of the myelinated axon in direct contact with the axon (**Figure 8B**). However, to study the fine structure of myelin sheets in different stages of the myelination process, conventional TEM is necessary. Our analysis unveiled that for the study of different myelin features, such as thickness (**Figure 8C**) or the number of myelin sheets wrapping a particular axon (**Figure 8D**) high-quality fixation with glutaraldehyde is required. The drawback of this fixation protocol is that it is, in many cases, non-compatible with immunogold labeling. Nevertheless, the combination of immunogold detection and conventional TEM allowed us to observe that while tightly packed, human white matter myelin presents variable periaxonal space as well as myelin thickness, which could be related to the particular type or function for each axon.

# DISCUSSION

Oligodendrocytes and their progenitors are cells of great interest because of the several diseases related to their malfunction and the potential that this population represents in the regeneration of the central nervous system. On the other hand, ultrastructural studies in human brain tissue are scarce since most of the studies are based on post-mortem samples, in which the quality of the tissue is not optimal neither for TEM analysis nor for immunogold labeling and processing. TEM studies are highly valuable in oligodendrocyte analysis given that the gold standard to determine the remyelination rate in white matter regeneration is measured by the *g-ratio*.

The identification of different stages of morphological transformation in the oligodendroglial lineage from

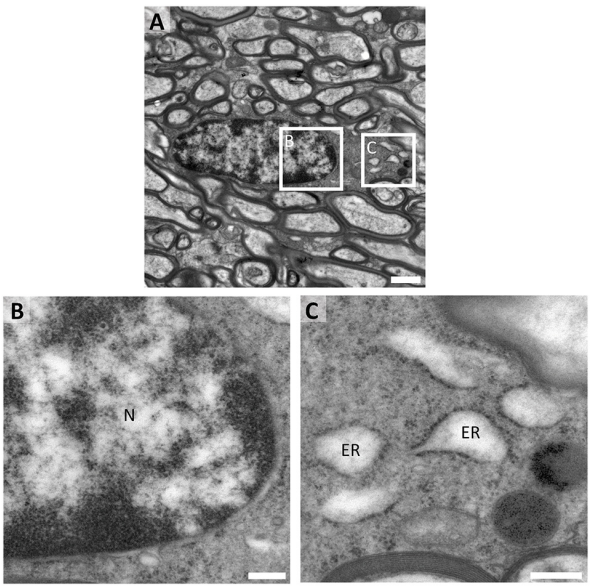


**FIGURE 7 |** Mature oligodendrocytes are electron-dense cells in the human white matter. **(A)** Mature oligodendrocytes are small electron-dense cells with a broad distribution in the white matter. These cells are intermingled between myelin-wrapped axons. **(B)** Chromatin condensation occurs bound to the inner nuclear membrane in mature oligodendrocytes. **(C)** Cytoplasmic organization in this population displays characteristic short dilated endoplasmic reticulum, few mitochondria, dense degradation vesicles, and polyribosomes. The micrograph proceeds from the white matter of a 6-year-old male (PB3) fixed with 2% PFA-2.5% Glutaraldehyde. N, Nucleus; ER, endoplasmic reticulum. Scale bars: **(A)**, 1 μm; **(B–C)**, 250 nm.

NG2-positive cells has been described in mouse control tissue (Sánchez-González et al., 2020). Furthermore, the generation of oligodendrocytes from OPCs has also been studied in mouse models of focal demyelination in the white matter (Menn et al., 2006). However, because of the above-mentioned technical limitations in the obtention of well-preserved human tissue, these studies are scarce.

Here we have studied the human *pre-mortem* white matter, which displays a great status of preservation, to shed light on the variation of the ultrastructural morphology of the oligodendroglial lineage combined with pre-embedding immunogold labeling for nine well-known oligodendroglial markers. Our results suggest that, in the human white matter, there are three markedly different stages of differentiation in oligodendrocyte progenitors according to their ultrastructural features and molecular markers.

The first stage of differentiation can be recognized by the expression of PDGFRα, NG2, and A2B5 (Berg and Schachner, 1982; Schnitzer and Schachner, 1982; Richardson et al., 1988; Chang et al., 2000; Rivers et al., 2008). This subset of progenitors presents ultrastructural and morphological characteristics that are very similar to astrocytes such as an electron-lucent filamentous cytoplasm, an electron-lucent nuclear content with scarcely condensed chromatin, dilated ER, mitochondria, and ribosomes. Therefore, when analyzing OPCs through TEM we recommend performing immunogold to avoid misclassification between this population and astrocytes.

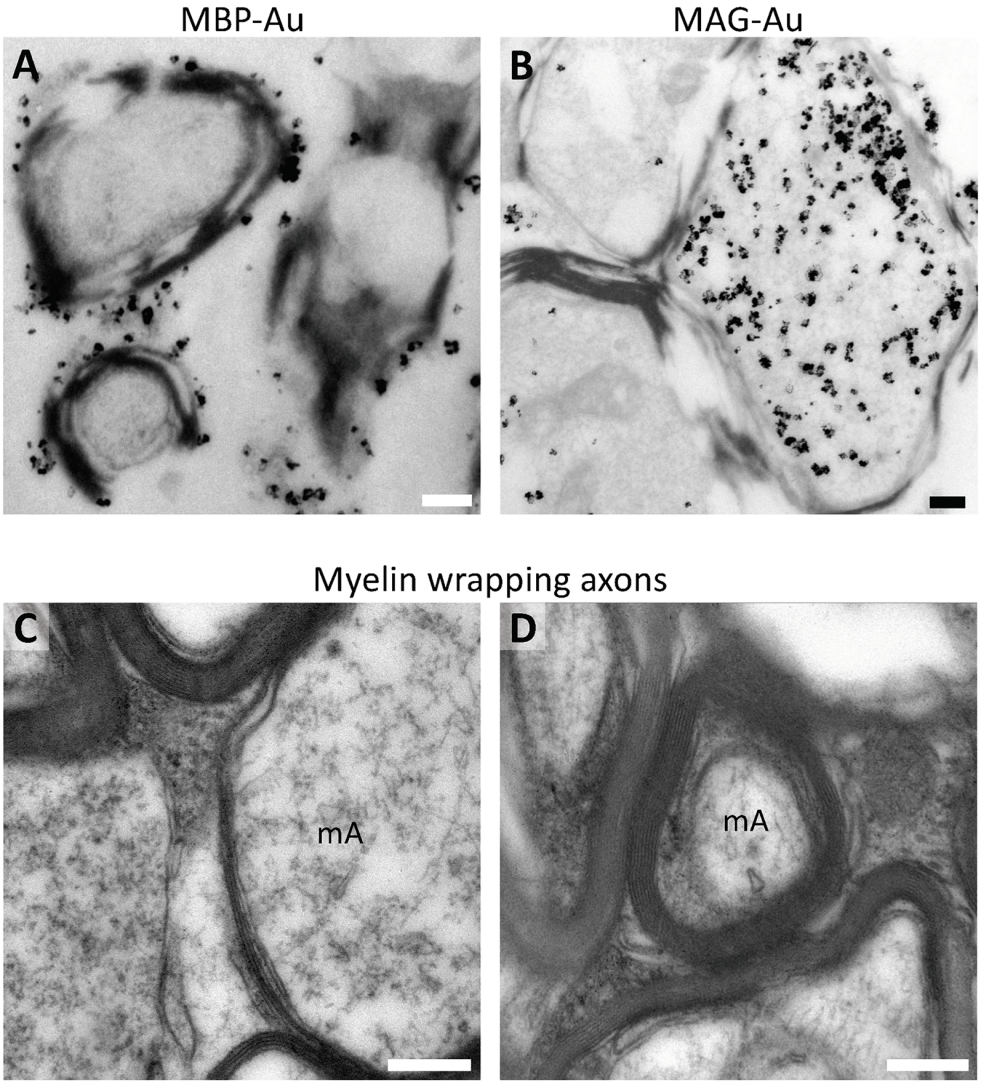


**FIGURE 8 |** Ultrastructural analysis of myelin in the human *pre-mortem* white matter. **(A)** Pre-embedding immunogold labeling shows that MBP is located in the outermost layer of the myelinated axon in the cerebral white matter of a 5-year-old female (PB19). **(B)** MAG is observed in the internal layer of the myelinated axon in direct contact with the axon in the white matter of a 5-year-old female (PB19). **(C)** Glutaraldehyde fixation allows a better analysis of the fine structure of myelin sheets in different stages of the myelination process, allowing to discern different myelin thickness. **(D)** Furthermore, it allows the visualization of the number of myelin layers. Ultrastructural analysis reveals that myelin is tightly packed, and exhibits variable periaxonal space. **(C,D)** Micrographs proceed from the white matter of a 2-year-old female (PB9) fixed with 2% PFA-2.5% Glutaraldehyde. mA, myelinated axon. Scale bars: 250 nm.

The second stage of differentiation (pre-OLs) has been described as a transitory stage of maturation of oligodendrocytes. This phase is characterized by the expression of the molecular marker BCAS1/NABC1, Sox10, and Olig2 (Fard et al., 2017; Ishimoto et al., 2017). Interestingly, this population is more prominently represented in pediatric patients than in adult patients (data not shown; Fard et al., 2017). By immunofluorescence, these cells appear to be highly ramified and present scarce cytoplasmic content. TEM analysis reveals that pre-OLs present scant cytoplasmic content in which the most abundant organelle are polyribosomes and short dilated ER. The chromatin in this population is more condensed than in OPCs. The most interesting feature of pre-OLs is their contact with myelin sheaths, which conforms with the previous studies that indicate that these cells are actively synthesizing myelin (Fard et al., 2017).

The last stage of differentiation in the oligodendroglial lineage are m-OLs, which have been typically labeled with Olig2 and APC-(CC1) (Bin et al., 2016). These cells show a remarkable electron density in their cytoplasm and nucleus. The cytoplasmic portion contains short dilated endoplasmic reticulum, mitochondria, dense degradation vesicles, and polyribosomes, while the nucleus contains abundant heterochromatin associated with the inner nuclear membrane. This indicates that, as oligodendrocytes mature, their chromatin becomes more condensed and attaches to the nuclear membrane. Another

remarkable feature shared by all the oligodendroglial lineage populations is that they maintain short, dilated ER through their maturation process.

Moreover, state-of–the-art studies (Bribián et al., 2020; Perlman et al., 2020) depict RNA or protein expression differences between age, sex, and status of activation or differentiation in the oligodendroglial lineage. By immunofluorescence, we observed more ramified BCAS1-positive cells. and an apparently larger number of immature oligodendrocytes in pediatric patients (data not shown). However, our results suggest that these shifts do not translate into ultrastructural differences, thus, allowing the characterization of oligodendrocytes despite the demographic differences.

Regarding the myelin that OLs synthesize, we used MBP and MAG for labeling. The first is found in the outermost portion of the myelinated axon, while the latter is found in direct contact with the axon. However, the conservation of myelin and thereby the labeling are not as precise. We suggest that myelin studies in the human brain require exquisite fixation, which implies the addition of glutaraldehyde in high concentrations (2.5%), which is a barrier to overcome for immunolabeling.

Hereby, studying the differences between the stages of differentiation in human oligodendrocytes has been of great interest because of the neuropathological implications especially in frequent disabling neurodegenerative conditions such as MS (Marques et al., 2016; Fard et al., 2017; Jäkel et al., 2019). In this pathology, the presence of immature oligodendrocytes in lesioned areas can indicate remyelination (Lucchinetti et al., 2000). Nonetheless, the cellular composition combined with the myelination/remyelination status has never been studied at an ultrastructural level, which could enhance the current knowledge and could give clues of intracellular processes within the cells in a lesion. Therefore, the fine characterization of the oligodendroglial lineage in the human brain can lead to future studies that include tissue fixed for TEM studies (i.e., glutaralehyde), that allow the combination of both myelination analysis and subcellular organelle composition for each cell type.

## DATA AVAILABILITY STATEMENT

The original contributions presented in the study are included in the article/**Supplementary Material**, further inquiries can be directed to the corresponding author/s.

## ETHICS STATEMENT

The studies involving human participants were reviewed and approved by Research Ethics committee from the Hospital Universitari i Politècnic La Fe. Written informed consent to participate in this study was provided by the participants' legal guardian/next of kin.

## AUTHOR CONTRIBUTIONS

MU-N, VH-P, and JG-V conceived the original idea and supervised the experimental procedures. PP-B and AG-M performed surgical resections. PP-B selected the non-affected areas of the white matter for analysis. MU-N, RM-G, AS-T, and PG-T performed immunofluorescence, immunogold, and TEM processing. MU-N, VH-P, and JG-V wrote the manuscript. All authors contributed to the article and approved the submitted version.

## FUNDING

This study was funded by the Nano-scaffolding for neuronal migration and generation project (PCI2018-093062) granted by the Spanish Ministry of Science, Innovation and Universities to VH-P through CIBERNED. JG-V was funded by Red deTerapia Celular (TerCel-RD16/0011/0026) and the Valencian Council for Innovation, Universities Science and Digital Society (PROMETEO/2019/075).

## ACKNOWLEDGMENTS

We acknowledge the support of Susana González-Granero at the Laboratory of Comparative Neurobiology of the University of Valencia and the electron microscopy service at the Centro de Investigación Príncipe Felipe (Mario Soriano-Navarro) for their valuable help. **Figure 1A** was created using Biorender.com.

## SUPPLEMENTARY MATERIALS

The Supplementary Material for this article can be found online at: https://www.frontiersin.org/articles/10.3389/fnana.2021.696376/full#supplementary-material.

**SUPPLEMENTARY FIGURE 1 |** The ultrastructural characteristics of GFAP-positive astrocytes are similar to OPCS. **(A)** A GFAP-labeled astrocyte appears as a large electron-lucent cell (black asterisk) compared to an unlabeled oligodendrocyte (white asterisk) in the white matter. The inset shows that the GFAP silver enhanced label marks intermediate filaments in this cell. **(B)** GFAP-labeled expansions (arrows) surrounding an unlabeled OPC (white asterisk) showing the similarity of the morphology between these two populations. **(A,B)** Micrographs were obtained from the white matter of a 6-year-old male (PB3). Scale bars: panoramic micrographs, 1 μm; insets: 250 nm.

**SUPPLEMENTARY FIGURE 2 |** OPCs express Olig2 in the nucleus. An electron-lucent cell displaying Olig2 label in the nuclear compartment in the white matter of a 27-year-old male (PB8). Scale bar: 1 μm.

## REFERENCES

Amaral, A. I., Tavares, J. M., Sonnewald, U., and Kotter, M. R. N. (2016). Oligodendrocytes: development, physiology and glucose metabolism. *Adv. Neurobiol.* 13, 275–294. doi: 10.1007/978-3-319-45096-4_10

Barateiro, A., and Fernandes, A. (2014). Temporal oligodendrocyte lineage progression: *In vitro* models of proliferation, differentiation and myelination. *Biochim. Biophys. Acta* 1843, 1917–1929. doi: 10.1016/j.bbamcr.2014.04.018

Berg, G. J., and Schachner, M. (1982). Electron-microscopic localization of A2B5 cell surface antigen in monolayer cultures of murine cerebellum and retina. *Cell Tissue Res.* 224, 637–645. doi: 10.1007/BF00213758

Bribián, A., Medina-Rodríguez, E. M., Josa-Prado, F., García-Álvarez, I., Machín-Díaz, I., Esteban, P. F., et al. (2020). Functional heterogeneity of mouse and

human brain OPCs: relevance for preclinical studies in multiple sclerosis. *J. Clin. Med. Res.* 9:1681. doi: 10.3390/jcm9061681

Bin, J. M., Harris, S. N., and Kennedy, T. E. (2016). The oligodendrocyte-specific antibody "CC1" binds quaking 7. *J. Neurochem.* 139, 181–186. doi: 10.1111/jnc.13745

Chang, A., Nishiyama, A., Peterson, J., Prineas, J., and Trapp, B. D. (2000). NG2-positive oligodendrocyte progenitor cells in adult human brain and multiple sclerosis lesions. *J. Neurosci.* 20, 6404–6412. doi: 10.1523/JNEUROSCI.20-17-06404.2000

Chavali, M., Ulloa-Navas, M. J., Pérez-Borredá, P., Garcia-Verdugo, J. M., McQuillen, P. S., Huang, E. J., et al. (2020). Wnt-dependent oligodendroglial-endothelial interactions regulate white matter vascularization and attenuate injury. *Neuron* 108, e5.1130–e5.1145. doi: 10.1016/j.neuron.2020.09.033

Domingues, H. S., Cruz, A., Chan, J. R., Relvas, J. B., Rubinstein, B., and Pinto, I. M. (2018). Mechanical plasticity during oligodendrocyte differentiation and myelination. *Glia* 66, 5–14. doi: 10.1002/glia.23206

Fard, M. K., van der Meer, F., Sánchez, P., Cantuti-Castelvetri, L., Mandad, S., Jäkel, S., et al. (2017). BCAS1 expression defines a population of early myelinating oligodendrocytes in multiple sclerosis lesions. *Sci. Transl. Med.* 9:eaam7816. doi: 10.1126/scitranslmed.aam7816

Goldman, S. A., and Kuypers, N. J. (2015). How to make an oligodendrocyte. *Development* 142, 3983–3995. doi: 10.1242/dev.126409

Greenfield, J. G. (1933). A form of progressive cerebral sclerosis in infants associated with primary degeneration of the interfascicular glia. *Proc. R. Soc. Med.* 26, 690–697. Available online at: https://www.ncbi.nlm.nih.gov/pubmed/19989245.

Howard, J., Trevick, S., and Younger, D. S. (2016). Epidemiology of multiple sclerosis. *Neurol. Clin.* 34, 919–939. doi: 10.1016/j.ncl.2016.06.016

Inouye, H., and Kirschner, D. A. (1988). Membrane interactions in nerve myelin. I. Determination of surface charge from effects of pH and ionic strength on period. *Biophys. J.* 53, 235–245. doi: 10.1016/S0006-3495(88)83085-6

Ishimoto, T., Ninomiya, K., Inoue, R., Koike, M., Uchiyama, Y., and Mori, H. (2017). Mice lacking BCAS1, a novel myelin-associated protein, display hypomyelination, schizophrenia-like abnormal behaviors and upregulation of inflammatory genes in the brain. *Glia* 65, 727–739. doi: 10.1002/glia.23129

Jäkel, S., Agirre, E., Mendanha Falcão, A., van Bruggen, D., Lee, K. W., Knuesel, I., et al. (2019). Altered human oligodendrocyte heterogeneity in multiple sclerosis. *Nature* 566, 543–547. doi: 10.1038/s41586-019-0903-2

Kang, S. H., Fukaya, M., Yang, J. K., Rothstein, J. D., and Bergles, D. E. (2010). NG2+ CNS glial progenitors remain committed to the oligodendrocyte lineage in postnatal life and following neurodegeneration. *Neuron* 68, 668–681. doi: 10.1016/j.neuron.2010.09.009

Lucchinetti, C., Brück, W., Parisi, J., Scheithauer, B., Rodriguez, M., and Lassmann, H. (2000). Heterogeneity of multiple sclerosis lesions: implications for the pathogenesis of demyelination. *Ann. Neurol.* 47, 707–717. doi: 10.1002/1531-8249(200006)47:6<707::aid-ana3>3.0.co;2-q

Marques, S., Zeisel, A., Codeluppi, S., van Bruggen, D., Mendanha Falcão, A., Xiao, L., et al. (2016). Oligodendrocyte heterogeneity in the mouse juvenile and adult central nervous system. *Science* 352, 1326–1329. doi: 10.1126/science.aaf6463

Matalon, R., Michals, K., Sebesta, D., Deanching, M., Gashkoff, P., and Casanova, J. (1988). Aspartoacylase deficiency and N-acetylaspartic aciduria in patients with Canavan disease. *Am. J. Med. Genet.* 29, 463–471. doi: 10.1002/ajmg.1320290234

McLaurin, J. A., and Yong, V. W. (1995). Oligodendrocytes and myelin. *Neurol. Clin.* 13, 23–49. Available online at: https://www.ncbi.nlm.nih.gov/pubmed/7739504.

Menn, B., Garcia-Verdugo, J. M., Yaschine, C., Gonzalez-Perez, O., Rowitch, D., and Alvarez-Buylla, A. (2006). Origin of oligodendrocytes in the subventricular zone of the adult brain. *J. Neurosci.* 26, 7907–7918. doi: 10.1523/JNEUROSCI.1299-06.2006

Perlman, K., Couturier, C. P., Yaqubi, M., Tanti, A., Cui, Q.-L., Pernin, F., et al. (2020). Developmental trajectory of oligodendrocyte progenitor cells in the human brain revealed by single cell RNA sequencing. *Glia* 68, 1291–1303. doi: 10.1002/glia.23777

Renier, W. O., Gabreëls, F. J., Hustinx, T. W., Jaspar, H. H., Geelen, J. A., Van Haelst, U. J., et al. (1981). Connatal pelizaeus-merzbacher disease with congenital stridor in two maternal cousins. *Acta Neuropathol.* 54, 11–17. doi: 10.1007/BF00691328

Richardson, W. D., Pringle, N., Mosley, M. J., Westermark, B., and Dubois-Dalcq, M. (1988). A role for platelet-derived growth factor in normal gliogenesis in the central nervous system. *Cell* 53, 309–319. doi: 10.1016/0092-8674(88)90392-3

Rivers, L. E., Young, K. M., Rizzi, M., Jamen, F., Psachoulia, K., Wade, A., et al. (2008). PDGFRA/NG2 glia generate myelinating oligodendrocytes and piriform projection neurons in adult mice. *Nat. Neurosci.* 11, 1392–1401. doi: 10.1038/nn.2220

Saab, A. S., Tzvetavona, I. D., Trevisiol, A., Baltan, S., Dibaj, P., Kusch, K., et al. (2016). Oligodendroglial NMDA receptors regulate glucose import and axonal energy metabolism. *Neuron* 91, 119–132. doi: 10.1016/j.neuron.2016.05.016

Sánchez-González, R., Bribián, A., and López-Mascaraque, L. (2020). Cell Fate Potential of NG2 Progenitors. *Sci. Rep.* 10:9876. doi: 10.1038/s41598-020-66753-9

Schnitzer, J., and Schachner, M. (1982). Cell type specificity of a neural cell surface antigen recognized by the monoclonal antibody A2B5. *Cell Tissue Res.* 224, 625–636. doi: 10.1007/BF00213757

Schoor, C., Brocke-Ahmadinejad, N., Gieselmann, V., and Winter, D. (2019). Investigation of oligodendrocyte precursor cell differentiation by quantitative proteomics. *Proteomics* 19:e1900057. doi: 10.1002/pmic.201900057

Stohlman, S. A., and Hinton, D. R. (2001). Viral induced demyelination. *Brain Pathol.* 11, 92–106. doi: 10.1111/j.1750-3639.2001.tb00384.x

Tappino, B., Biancheri, R., Mort, M., Regis, S., Corsolini, F., Rossi, A., et al. (2010). Identification and characterization of 15 novel GALC gene mutations causing Krabbe disease. *Hum. Mutat.* 31, E1894–E1914. doi: 10.1002/humu.21367

van Bruggen, D., Agirre, E., and Castelo-Branco, G. (2017). Single-cell transcriptomic analysis of oligodendrocyte lineage cells. *Curr. Opin. Neurobiol.* 47, 168–175. doi: 10.1016/j.conb.2017.10.005

van der Knaap, M. S., Barth, P. G., Stroink, H., van Nieuwenhuizen, O., Arts, W. F., Hoogenraad, F., et al. (1995). Leukoencephalopathy with swelling and a discrepantly mild clinical course in eight children. *Ann. Neurol.* 37, 324–334. doi: 10.1002/ana.410370308

Volpe, J. J. (2001). Neurobiology of periventricular leukomalacia in the premature infant. *Pediatr. Res.* 50, 553–562. doi: 10.1203/00006450-200111000-00003

Wilson, H. C., Scolding, N. J., and Raine, C. S. (2006). Co-expression of PDGF alpha receptor and NG2 by oligodendrocyte precursors in human CNS and multiple sclerosis lesions. *J. Neuroimmunol.* 176, 162–173. doi: 10.1016/j.jneuroim.2006.04.014

Witte, M. E., Schumacher, A.-M., Mahler, C. F., Bewersdorf, J. P., Lehmitz, J., Scheiter, A., et al. (2019). Calcium influx through plasma-membrane nanoruptures drives axon degeneration in a model of multiple sclerosis. *Neuron* 101, e5.615–e5.624. doi: 10.1016/j.neuron.2018.12.023

Zhu, X., Bergles, D. E., and Nishiyama, A. (2008). NG2 cells generate both oligodendrocytes and gray matter astrocytes. *Development* 135, 145–157. doi: 10.1242/dev.004895

**Conflict of Interest**: The authors declare that the research was conducted in the absence of any commercial or financial relationships that could be construed as a potential conflict of interest.

# Chapter 16

# Tyramide Signal Amplification for Immunoelectron Microscopy

**María José Ulloa-Navas, Patricia García-Tárraga, Susana González-Granero, Pedro Pérez-Borreda, Vicente Herranz-Pérez, and José Manuel García-Verdugo**

## Abstract

Tyramide signal amplification (or catalyzed-reporter deposition) is an analyte-dependent reporter enzyme method that enhances the detection sensitivity of any given antigen by catalyzing the deposit of labeled tyramide that is covalently bound near the target molecule, providing high-density signal. Current methods allow identification of any protein or RNA using antibodies or probes, respectively. This technique has also been validated for electron microscopy detection by either DAB or for gold-conjugated streptavidin staining. Both techniques present several limitations, DAB staining hampers the ultrastructure of the sample since it precipitates all over the cell. Streptavidin, on the other hand, requires a strong permeabilization protocol which also compromises sample integrity. Hereby, we present a methodology which uses TSA in combination with immunogold labeling to improve the detection sensitivity for antigens that cannot be detected by conventional immunogold methods, or whose label is weak compared to background noise. As a proof of concept, we show the effectiveness of this technique for detecting difficult antigens expressed in the central nervous system such as NG2, PDGFRa, or BCAS1.

**Key words** Tyramide signal amplification, Catalyzed reporter deposition, Immunoelectron microscopy, Transmission electron microscopy, BCAS1, PDGFRa, TSA, CARD

## 1 Introduction

The brain is an organ that controls all functions of the body in all vertebrate and most invertebrate animals and thereby, it requires the harmonious expression of a wide variety of proteins by a broad heterogeneity of cell types. Hence, protein labeling and cell type identification is one of the most commonly used techniques in the field of neurosciences. To identify cell types and detect specific protein expression, we routinely rely on immunolabeling either by immunofluorescence or immunohistochemistry. On the other hand, electron microscopy is one of the most useful tools to

Rafael Lujan and Francisco Ciruela (eds.), *Receptor and Ion Channel Detection in the Brain*, Neuromethods, vol. 169, https://doi.org/10.1007/978-1-0716-1522-5_16,

describe the fine morphology, ultrastructure, and contacts formed by any cell in the brain. The combination of both techniques allows the subcellular localization of proteins and the description of the morphology of specific cells.

The precision of immunolabeling detection depends on many factors such as the expression levels of a given protein and the structural artefacts provoked by the fixation and histological processing of the sample. This is particularly critical in the very delicate nervous tissue of the brain. To enhance the sensitivity and the signal intensity of immunolabeling, some methods such as tyramide signal amplification (TSA) or catalyzed reporter deposition (CARD) have been developed [1]. TSA is an analyte-dependent reporter enzyme method which uses horseradish peroxidase (HRP) to catalyze the activation of a fluorescent or biotinylated substrate which is deposited near the target molecule for its visualization by immunofluorescence [2], immunohistochemistry for light or electron microscopy [3, 4], and in situ hybridization [5]. TSA enhances the signal produced by other imaging techniques such as traditional immunofluorescence, not only in animal but also in human tissues. This is especially relevant for the detection of membrane receptors which are hard to bring to light in human tissues due to suboptimal fixation methods (Fig. 1).

Protein detection with TSA is based on the use of biotinylated secondary antibodies which are subsequently incubated with streptavidin-HRP. HRP catalyzes the activation of fluorescent/biotinylated tyramides. Current ultrastructural TSA studies use either 3,3′-diaminobenzidine (DAB) staining [3] or gold-conjugated streptavidin [6]. DAB staining for electron microscopy studies are based on the photooxidation of DAB, which precipitates as electron-dense particles which scatter the electron beam [7]. However, DAB precipitates all over the cell and thereby it does not permit the analysis of the fine ultrastructure of the cell. On the other hand, gold-conjugated streptavidin requires 10–25 nm gold particles which hardly penetrate into the tissue due to the particle size.

To take advantage of the signal amplification provided by TSA and to overcome the above-mentioned issues, we have developed a methodology that significantly reduces the time needed for primary antibody incubation in standard immunogold protocols, and only needs ~25% of the antibody concentration that is normally used (Fig. 2). Furthermore, this technique allows the precise visualization of some antigens that were not labelable by standard immunoelectron microscopy such as mouse NG2; human and mouse PDGFRa; or antigens whose label is not strong enough to be distinguished from background noise, such as BCAS1 (Fig. 3). Our approach also reduces the background nonspecific label, not only by using the tyramide blocking protocol but also by performing the immunogold detection against biotin instead of

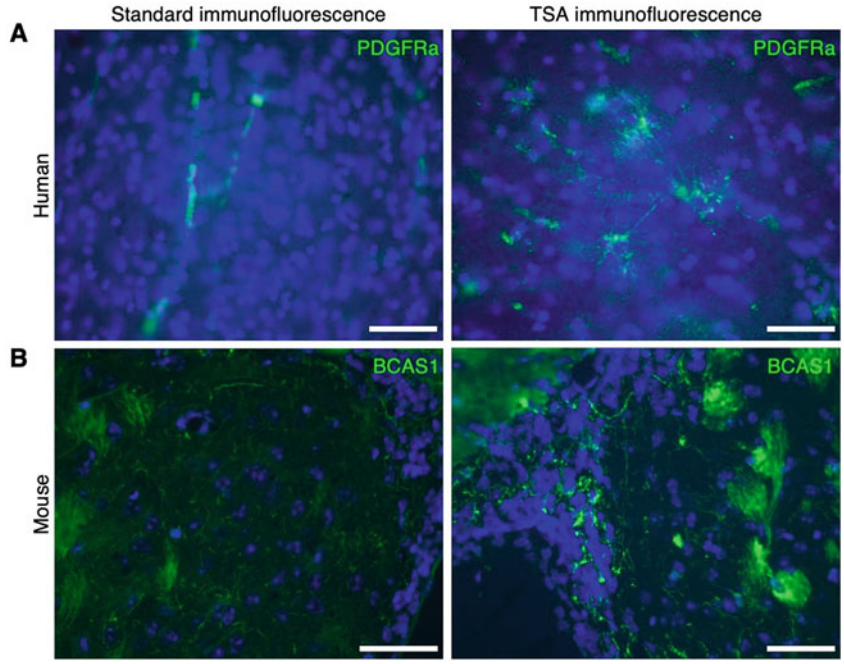


**Fig. 1** Standard immunofluorescence versus TSA immunofluorescence. (**a**) Human PDGFRa label in human white matter. By standard immunofluorescence, PDGFRa signal cannot be detected, while TSA labeling shows cells with abundant labeled expansions. (**b**) Mouse BCAS1 cells in the lateral wall of the lateral ventricle and in the striatum. By TSA, the signal is enhanced. Scale bars: 50 μm

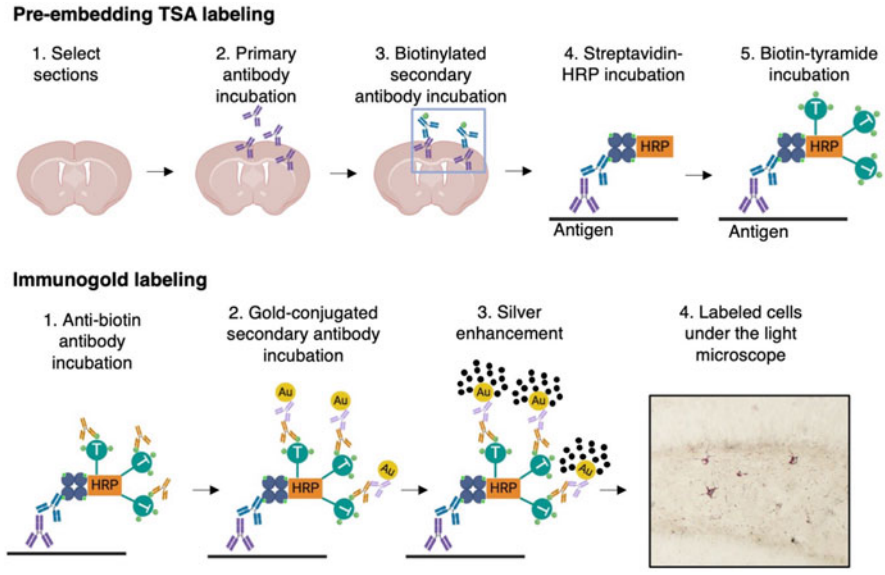


**Fig. 2** Step-by-step diagram describing the procedure of TSA labeling for immunoelectron microscopy

the primary antigen (Fig. 2). Finally, aggressive permeabilization steps that are commonly used in immunoelectron microscopy—

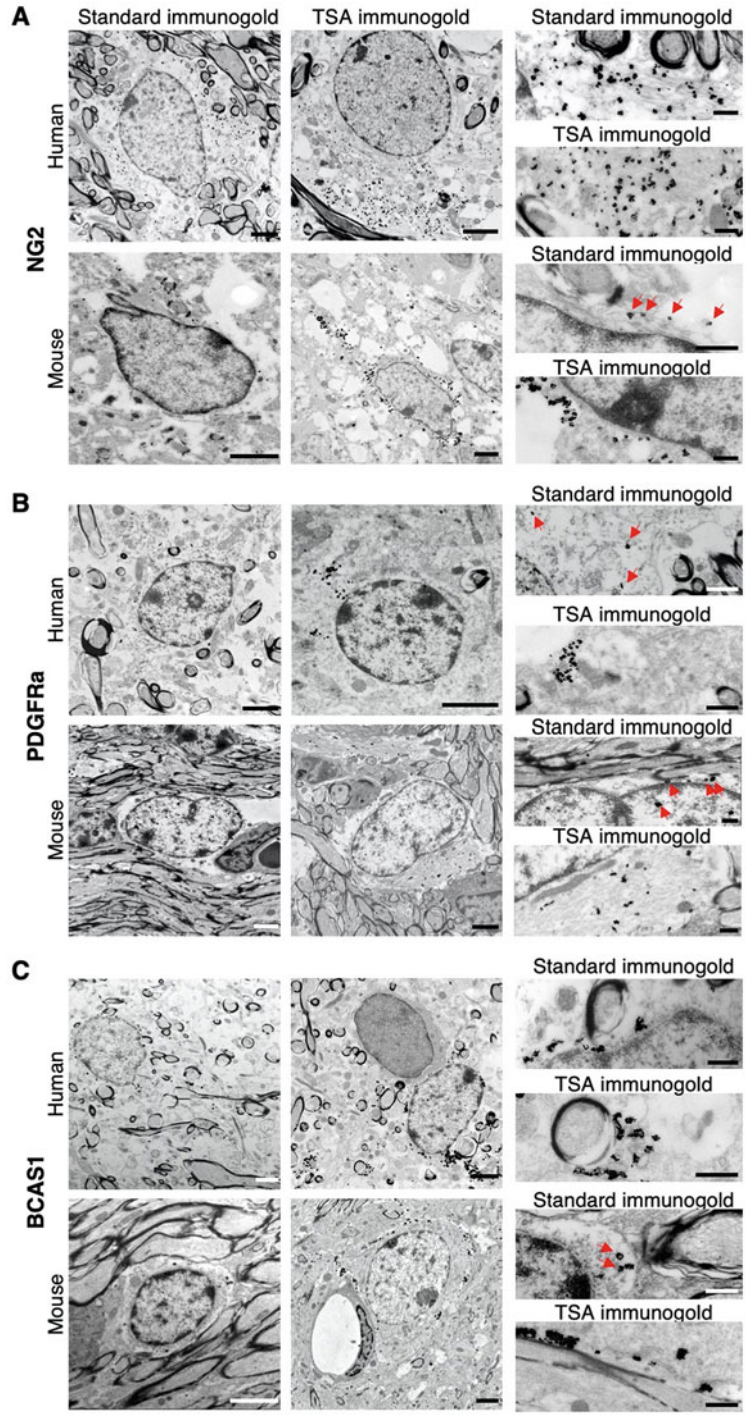


**Fig. 3** Standard immunogold vs. TSA immunoelectron microscopy. (**a**) NG2 in human tissue displaying the label at the intermediate filaments. Mouse tissue displaying the label at the plasma membrane. In mouse tissue, the signal is weak by standard immunogold detection compared to TSA labeling. (**b**) PDGFRa

such as multiple freezing and thawing cycles—are not required in this modified method. Therefore, the ultrastructure especially that of cell membranes is preserved much better than using conventional methods.

## 2 Materials

All reagents were purchased from Sigma-Aldrich unless it is otherwise specified.

### 2.1 Buffers and Solutions

1. Phosphate buffer (PB): 0.1 M at pH 7.4. This buffer is made of monobasic sodium phosphate ($NaH_2PO_4$) and dibasic sodium phosphate ($Na_2HPO_4$), both at a final concentration of 0.1 M.
2. Phosphate buffer-azide (PB-Az): 0.1 M PB, 0.05% sodium azide at pH 7.4. This buffer is made of monobasic sodium phosphate ($NaH_2PO_4$) and dibasic sodium phosphate ($Na_2HPO_4$), both at a final concentration of 0.1 M and sodium azide at 0.05%.
3. Phosphate buffer saline-Triton (PBS-Tx): 1× PBS (Gibco) containing 0.05% Triton X-100.
4. Phosphate buffer saline-Triton-Azide (PBS-Tx-Az): 1× PBS (Gibco) containing 0.05% Triton X-100 and 0.05% sodium azide.
5. Saline solution: 0.9% NaCl and 0.1% heparin in double-distilled water.
6. Fixative solution for animal tissue: 4% paraformaldehyde (PFA) and 0.5% glutaraldehyde (GA) (from a 25% aqueous stock solution; Electron Microscopy Sciences, EMS, Hatfield, PA, USA) in 0.1 M PB (*see* **Note 1**).
7. Fixative solution for human tissue: 4% paraformaldehyde (PFA) in 0.1 M PB.
8. Agar solution: 4% agar in 0.1 M PB.
9. Peroxidase blocking solution: 1% $H_2O_2$ in PBS-Tx.
10. Blocking solution I: 0.87% NaCl, 10% Casein (Vector, Burlingame, CA, USA), 5% normal goat serum (Gibco), 0.05% sodium azide in 0.1 M Tris–HCl at pH 7.5.

**Fig. 3** (continued) signal in human and mouse tissue. In human tissue, the signal is only detectable by using TSA labeling in specific membrane domains. In mouse tissue, the label is at the cytoplasm. By standard immunogold, the signal is weak compared to TSA labeling. (**c**) BCAS1 in human and mouse tissues present the label at the plasma membrane. Immunogold detection renders a weak signal compared to TSA labeling. Red arrows pinpoint the location of gold particles (signal). Scale bars: 2 nm, magnifications: 500 nm

11. Primary antibody solution: 1:400 rabbit-anti-NG2 (ab5320, Millipore), 1:200 Mouse-anti-PDGFRa (556001, BD Biosciences), 1:300 Mouse-anti-NaBC1 (sc-136342, Santa Cruz) in blocking solution I.
12. Secondary antibody solution: 1:400 biotinylated goat anti-rabbit (BA-5000, Vector), 1:400 biotinylated goat anti-mouse (BA-9200, Vector) in PBS-Tx-Az.
13. Streptavidin-HRP solution: 1:200 horseradish peroxidase-conjugated streptavidin (SA-5004, Vector) in blocking solution I.
14. Biotin-Tyramide solution: 1:50 Biotin-Tyramine solution in Assay diluent (SAT700001EA, Perkin Elmer).
15. Blocking solution II: 0.3% BSAc (900.022, Aurion, The Netherlands) in 0.1 M PB-Az.
16. Immunogold primary antibody: 1:300 mouse anti-Biotin antibody (200-002-211, Jackson Immunoresearch) in blocking solution II.
17. Blocking solution III: 0.5% BSAc and 0.1% fish skin gelatin (900.033, Aurion) in 0.1 M PB-Az.
18. Immunogold secondary antibody: 1:50 goat anti-mouse gold-conjugated antibody (Ultra Small; Aurion) in blocking solution III.
19. Sodium acetate solution: 2% sodium acetate ($C_2H_3O_2Na{\cdot}3H_2O$) in double-distilled water.
20. Silver enhancement solution: mix equal parts of developer and enhancer reagents in a dark chamber immediately before use (Silver enhancement kit, R-Gent SE-LM, Aurion).
21. Gold toning solution: 0.05% gold chloride (AuCl) in double-distilled water.
22. Sodium thiosulfate solution: sodium thiosulfate 0.3% ($Na_2S_2O_3{\cdot}5H_2O$) in double-distilled water.
23. Fixative solution II: 2% GA (from an aqueous 25% stock solution, Electron Microscopy Sciences) in 0.1 M PB.
24. Osmium tetroxide solution: 1% osmium tetroxide (Electron Microscopy Sciences), 7% glucose in 0.1 M PB.

### 2.2 Labware and Other Equipment

1. Vibratome (VT1000S; Leica Microsystems Inc., Germany).
2. Ultramicrotome (UC7 Ultracut, Leica).
3. Transmission electron microscope (Tecnai $G^2$ Spirit; FEI, The Netherlands).
4. Fume hood.
5. Orbital shaker.
6. Refrigerator.

## 3 Methods

### 3.1 Pre-embedding TSA Labeling

1. *Option 1A:* For animal tissue: intracardially perfuse the animal at a rate of 4.5 mL/min with room-temperature (RT) saline solution for 5 min, followed by fixative solution for 15 min. Postfix the tissue overnight in the same fixative solution at 4 °C.

   *Option 1B:* For human tissue: fix the sample in 4% PFA by immersion for 3–7 days at 4 °C according to the size of the piece.
2. Wash the fixed tissue three times for 10 min each with 0.1 M PB. If not used immediately, the tissue can be stored in a glass vial containing PB-Az at 4 °C.
3. Embed the tissue in 4% agar and use the vibratome to cut 50–100 μm sections. Keep the sections in PB-Az at 4 °C if not for immediate use.
4. Select and wash the sections three times for 5 min in PBS-Tx at RT (*see* **Note 2**).
5. To quench endogenous peroxidases, incubate the sections in peroxidase blocking solution for 45 min in the dark on an orbital shaker at RT.
6. Wash the samples three times for 5 min in PBS-Tx at RT.
7. Block the samples in blocking solution I for 1 h at RT on an orbital shaker.
8. Incubate the samples in primary antibody solution overnight under mild agitation at 4 °C. If assaying other antibodies, use the same concentration as for immunohistochemistry or immunofluorescence.
9. Wash the sections three times for 5 min in PBS-Tx at RT.
10. Incubate the sections in secondary antibody solution for 2 h at RT.
11. Wash the sections three times for 5 min in PBS-Tx at RT.
12. Incubate the samples in Streptavidin-HRP solution for 30 min* at RT.

    *Do not exceed 30 min of incubation (*see* **Note 3**).
13. Wash the sections three times for 5 min in PBS-Tx at RT.
14. Incubate the samples in biotin-tyramide solution for 5 min* at RT.

    *Do not exceed 5 min of incubation (*see* **Note 3**).
15. Wash the sections in PBS-Tx-Az five times for 5 min at RT.

### 3.2 Immunogold Labeling

1. Block the sections in blocking solution II for 1 h at RT in the dark.
2. Incubate the samples in immunogold primary antibody overnight at 4 °C with gentle shaking.
3. Wash the sections three times for 5 min in PB at RT.
4. Block the sections in blocking solution III for 1 h at RT in the dark.
5. Incubate the samples in immunogold secondary antibody solution III for 2 h at RT in the dark under mild agitation.
6. Rinse three times for 5 min with PB at RT.
7. Wash three times for 15 min in 2% sodium acetate solution in the dark with gentle shaking.
8. Incubate in silver enhancement solution for 10–30 min* at RT in the dark.

   *Check every 5 min and stop the reaction once you observe a dark label under a light microscope. Do not exceed 30 min of incubation (*see* **Note 3**).
9. Wash three times for 5 min in 2% sodium acetate in the dark at RT.
10. Incubate for 10 min in gold toning solution for 10 min in the dark at RT.
11. Wash the samples twice in 0.3% sodium thiosulfate solution for 10 min at RT.
12. Rinse three times for 5 min with PB at RT.
13. Fix for 30 min with fixative solution II at RT.
14. Rinse five times for 5 min with PB at RT.
15. Keep the samples in PB-Az until embedding at 4 °C.
16. For embedding, postfix the samples in Osmium tetroxide solution for 30 min at RT (*see* **Note 4**).
17. Wash and prepare the samples for Durcupan epoxy resin embedding following standard electron microscopy methods.

## 4 Notes

1. Considerations for tissue and fixation.

   Using 0.5% glutaraldehyde (GA) improves the ultrastructural characteristics of the cell, in fact increasing the GA concentration enhances the preservation of the tissue. However, GA interferes with the immunodetection of some antibodies. If the label is weak or if the protocol does not work with 4% PFA–0.5% GA, lower concentrations of GA, such as 4% PFA–0.1% GA, or 4% PFA only can be used. On the other hand, if the label is strong, a fixative solution of 4% PFA–1% GA can be used.

2. Considerations for permeabilization.

   Some antigens, such as proteins which are only present inside organelles or even intravesicular antigens, may require a more thorough permeabilization such as freezing and thawing after selecting the sections (**step 4**). To perform this permeabilization, a cryoprotection protocol with 25% saccharose in 0.1 M PB for 30 min at RT should be previously performed. Subsequently, sections should be immersed in −60 °C methylbutane for 5 s, then in RT 25% saccharose solution for the same time. Repeat this freezing and thawing cycle 4–5 times.

3. Considerations for avoiding nonspecific labeling.

   Avoid longer periods of incubation in the following steps: streptavidin-HRP incubation, tyramide-biotin incubation, and silver enhancement.

4. Safety.
   (a) Use a fume hood, gloves, and glasses.
   (b) For embedding you will require a specialized facility for radioactive reagents.

## Acknowledgments

We acknowledge the electron microscopy service at the Centro de Investigación Príncipe Felipe (Mario Soriano-Navarro) for their valuable help. This study was funded by the Nano-scaffolding for neuronal migration and generation project (PCI2018-093062) granted by the Spanish Ministry of Science, Innovation and Universities to VHP, Red de Terapia Celular (TerCel-RD16/0011/0026) to JMGV, and the Valencian Council for Innovation, Universities Science and Digital Society (PROMETEO/2019/075) granted to JMGV. MJUN was supported by a McDonald Fellowship from the Multiple Sclerosis International Federation. The authors declare that they have no conflict of interest.

### References

1. Bobrow MN, Harris TD, Shaughnessy KJ, Litt GJ (1989) Catalyzed reporter deposition, a novel method of signal amplification application to immunoassays. J Immunol Methods 125 (1):279–285
2. Chao J, DeBiasio R, Zhu Z, Giuliano KA, Schmidt BF (1996 Jan) Immunofluorescence signal amplification by the enzyme-catalyzed deposition of a fluorescent reporter substrate (CARD). Cytometry 23(1):48–53
3. Stanarius A, Töpel I, Schulz S, Noack H (1997) Wolf G. immunocytochemistry of endothelial nitric oxide synthase in the rat brain: a light and electron microscopical study using the tyramide signal amplification technique. Acta Histochem 99(4):411–429
4. Low KL, Ma C, Soma KK (2017) Tyramide signal amplification permits Immunohistochemical analyses of androgen receptors in the rat prefrontal cortex. J Histochem Cytochem 65 (5):295–308
5. Adler K, Erickson T, Bobrow M (1997) High sensitivity detection of HPV-16 in SiHa and CaSki cells utilizing FISH enhanced by TSA. Histochemistry 108(4):321–324

6. Lee S, Lee SE, Ko SH, Hong EK, Nam KI, Nakamura K et al (2005) Introduction of Tyramide signal amplification (TSA) to pre-embedding Nanogold-silver staining at the electron microscopic level. J Histochem Cytochem 53(2):249–252

7. Röhrl C, Meisslitzer-Ruppitsch C, Bittman R, Li Z, Pabst G, Prassl R et al (2012) Combined light and electron microscopy using diaminobenzidine photooxidation to monitor trafficking of lipids derived from lipoprotein particles. Curr Pharm Biotechnol 13(2):331–340

*J Neuropathol Exp Neurol*
Vol. 80, No. 4, April 2021, pp. 379–383
doi: 10.1093/jnen/nlaa144

LETTER TO THE EDITOR

# *Heterogeneous Pattern of Differentiation With BCAS1/NABC1 Expression in a Case of Oligodendroglioma*

María José Ulloa-Navas, MSc[1], Luis Rubio, PhD[2], Anna Teruel-Sanchis, MSc[1], Jorge Peña-Peña, BSc[1], José Manuel García-Verdugo, PhD[1], Vicente Herranz-Pérez, PhD[1,3], and Jaime Ferrer-Lozano, MD

Laboratory of Comparative Neurobiology, Cavanilles Institute of Biodiversity and Evolutionary Biology, Universitat de València, CIBERNED, Valencia, Spain
Department of Pathology, Hospital Universitari i Politècnic La Fe, Valencia, Spain
Predepartamental Unit of Medicine, Faculty of Health Sciences, Universitat Jaume I, Castelló de la Plana, Spain

Correspondence to: Vicente Herranz-Pérez, Institute Cavanilles of Biodiversity and Evolutionary Biology, Laboratory of Comparative Neurobiology, C/ Catedrático José Beltrán Martínez, 2, 46980 Paterna, Valencia, Spain; E-mail: vicente.herranz@uv.es

To the Editor:

Oligodendrogliomas (ODGs) have been defined as *IDH*-mutant, 1p/19q-codeleted diffuse gliomas by the 2016 WHO Classification of Tumours of the Central Nervous System (1–3). The histogenesis underlying gliomas is still elusive, and the cell of origin for gliomas has not been clearly defined. However, glial progenitors have been suggested as possible candidates for malignant glioma generation (4). Moreover, NG2-glia and PDGFRα-expressing oligodendrocyte progenitors (OPCs) have been identified in some astrocytomas and ODGs as a direct evidence of tumorigenesis originating from these cell types (5, 6). More recent research based on genetic evidence indicates that ODGs may not have a unique cell of origin, but that they can arise from ventricular-subventricular zone-like stem cells, oligodendrocyte or astrocyte progenitor cells (7).

The study of ODG cellular heterogeneity may offer further insight into the complexity of tumor constituents and how they might influence the malignant behavior. To better understand this aspect, state-of-the-art multi-omics studies (8, 9) have subclassified 1p/19q-codeleted diffuse gliomas into different inter and intratumoral populations, according to the genomic features they display, or the common markers that tumor cells share with immature ventricular-subventricular zone cells (i.e. oligodendrocytes, OPCs, neuronal precursors, or stem cells). These analyses show that in anaplastic ODGs there is a subpopulation of cells that express OPC markers and exhibit more aggressive behavior due to *MYC* upregulation (8).

Therefore, to improve our current understanding of the histogenesis and diversity of ODG biology, new markers of differentiation should be studied. Herein, we describe a remarkable case of an ODG presenting diverse histologic features and phenotypic heterogeneity labeled with the novel marker BCAS1/NABC1 (brain enriched myelin associated protein 1, encoded by *BCAS1* gene located on 20q13.2). BCAS1 expression has been recently proposed as a marker that defines a discrete maturation stage of oligodendrocytes in the human brain (10). BCAS1-positive cells or premyelinating oligodendrocytes have been studied in the white matter of nonpathologic brains and in the brain of multiple sclerosis patients, but not as a marker of a specific population within an ODG. Therefore, to our knowledge, this is the first report of discrete, clustered BCAS1-positive nodules in a glioma.

A casual finding was made in a neurologically asymptomatic 65-year-old woman, who underwent MRI examination prior to oral surgery. Clinical history revealed a thalamic stroke. The patient presented a T2-hyperintense, noncontrast-enhancing mass in her right frontal lobe, measuring 55 mm in greatest dimension, surrounded by edema. A complete en bloc surgical resection was performed. The patient has been free of disease for 2 years following adjuvant chemoradiotherapy.

Histopathologic analysis disclosed a heterogeneous picture (Fig. 1A), with a main component of classical ODG, growing diffusely in sheets of tightly packed uniform tumor cells with scant cytoplasm, round nuclei, and perinuclear clear halos. The tumor harbored very few mitotic figures. Rounded microcalcifications were seen within the tumor sheets. These cells diffusely invaded the adjacent cortex, showing perineuronal and perivascular satellitosis. On the other hand, small, relatively well-defined nodules were seen in the superficial white matter. These nodules were in direct transition with the diffuse, sheet-like cortical tumor growth. They displayed a loosely cohesive tumor cell population, embedded in a microvacuolated background. These cells showed more abundant and vacuolated cytoplasm, and moderately pleomorphic nuclei with irregular contour and rare mitoses. Together with the previous patterns, tumor cells invaded the subcortical white matter forming rows or ill-defined columns, as well as vague rosettes.

Immunohistochemical assessment showed expression of mutant IDH1 (R132H) protein in all tumor areas (Fig. 1B),

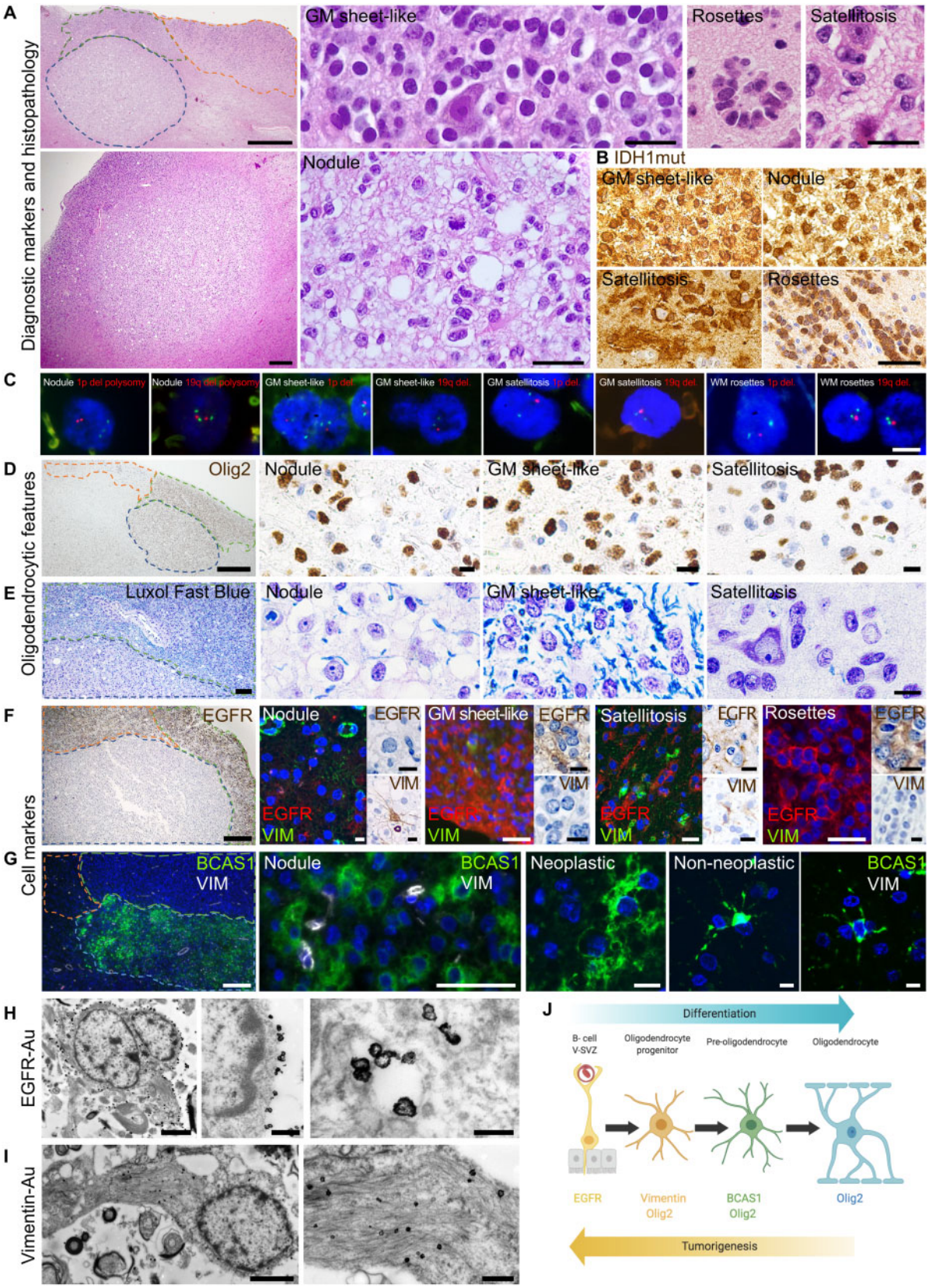


**FIGURE 1.** Histological and molecular characterization of the different cell types within the tumor. **(A)** Hematoxylin and eosin staining of the tumor. The area surrounded by a blue dotted line corresponds to the nodule, the area surrounded by a green

indicating the *IDH*-mutant status, together with preservation of ATRX staining (not shown). All neoplastic populations disclosed 1p/19q-codeletion by FISH analysis, with a fraction of tumor cells showing polysomy (Fig. 1C). Olig-2 positivity was also uniformly detected throughout the tumor (Fig. 1D). A final diagnosis of ODG, *IDH*-mutated, 1p/19q-codeleted, WHO grade II was rendered. Molecular analysis revealed a mutation in *TERT* promoter region, c.-146C > T (C250T), and an *MGMT*-methylated status. In order to better characterize the different tumor cell populations, further immunohistochemistry, immunofluorescence, and transmission electron microscopy studies were performed (Table).

The diffuse, main sheet-like tumor component showed a highly aberrant myelination pattern. The myelination observed through Luxol fast blue staining displayed hypermyelination in the whole area (Fig. 1E). A strong expression of EGFR (Fig. 1F), with a negative staining against vimentin, PDGFRa, and NG2 was observed. Neuronal markers (NeuN, synaptophysin) were also negative. Immunofluorescence study proved the absence of BCAS1 expression in this fraction of tumor cells (Fig. 1G). Immunoelectron microscopy for EGFR showed cells with abundant intermediate filaments, rough endoplasmic reticulum and mitochondria. EGFR expression was associated with the plasma membrane and endocytic vesicles (Fig. 1H).

The small nodules located in the superficial white matter, on the other hand, showed hypomyelination (Fig. 1E). A rather different protein expression profile was noted, with absence of EGFR and PDGFRa staining and a strong reactivity against BCAS1, displaying small nuclei and a cytoplasmic pattern that was very different from that observed in the nonneoplastic cells in the white matter (Fig. 1F, G). Neuronal and other OPC markers (Table) proved negative. Ultrastructural examination showed vimentin-positive cells with long processes contacting blood vessels (Fig. 1I).

The area composed of perivascular and perineuronal satellitosis in the cortex, adjacent to the diffuse gray matter infiltration, exhibited scaffolding ramified vimentin-positive cells contacting the blood vessels, and invasive EGFR-positive cells (Fig. 1F). Moreover, this subset of the lesion was GFAP-negative and its cellular composition was different from those seen in the cortical sheet-like and white matter nodular components. The rosettes scattered through the white matter, on the other hand, were also EGFR-positive but did not exhibit vimentin expression. Other evaluated markers are shown in the Table.

Altogether, this tumor can be considered a remarkable entity of cellular heterogeneity, combined with an example of differentiation mimicry performed by neoplasias. Specifically, the complex heterogeneity that recapitulates the natural differentiation of oligodendrocytes (Fig. 1J) is demonstrated. The intermingled vimentin-positive cells present between BCAS- or EGFR-positive cells have been described as more immature glial progenitors linked to gliomas (11, 12). The difference in cellular size and morphology of the different vimentin-positive cells in our case could be related to the different tumor cell density of the various growth patterns. On the other hand, the presence of internal vesicles labeled with EGFR could demonstrate the activation of the receptor. In the diffuse area of the tumor, EGFR expression and its associated myelination replicate the phenotype observed in human progenitors (13, 14). Although the patterns of myelination and BCAS1 expression, together with the cellular morphology of neoplastic cells, were very different from what has been previously described (10) and from those of the cells observed in the neighboring nonneoplastic white matter, we consider that the expression of this marker imitates the myelinating pre-oligodendrocyte stage. As such, the presence of a BCAS1-positive tumor cell subpopulation might be relevant to exploring the ways that could promote differentiation in OPC-derived gliomas (15).

## FUNDING

This study was supported by the Valencian Council for Innovation, Universities, Science and Digital Society

**FIGURE 1.** Continued
dotted line corresponds to the diffuse sheet-like tumor component, the area surrounded by an orange dotted line corresponds to the satellitosis present in the cortex. This shows the cellular heterogeneity in this oligodendroglioma. **(B)** Oligodendroglioma IDH1 (R132H) mutation labels all the tumoral populations. **(C)** 1p/19q-codeletion in all the areas corroborates the diagnosis of oligodendroglioma. A fraction of neoplastic cells in the nodule exhibits polysomy. **(D)** Olig2 immunohistochemistry reveals an intense staining in all the areas, showing the oligodendroglial nature of this tumor. **(E)** Luxol fast blue staining showing the abnormal pattern of myelination in this tumor. The nodular area exhibits a pattern of hypomyelination while the spreading sheet-like zone shows a pattern of hypermyelination. **(F)** EGFR and vimentin immunofluorescence staining. EGFR labels the diffuse sheet-like cellular component and the satellitosis, but not the cells within the nodule. Vimentin marks large ramified cells in the nodule and small ramified cells in the gray matter satellitosis. **(G)** BCAS1 and vimentin immunofluorescence staining showing the differential expression of these markers within the tumor. The diffuse area of the tumor (green dotted line) shows absence of BCAS1 staining, while the nodule (blue dotted line) presents BCAS1-expressing cells. Neoplastic nodular cells are larger and morphologically aberrant compared with those in the nonneoplastic areas. **(H)** EGFR immunoelectron microscopy showing EGFR label in the plasma membrane and in internal vesicles. EGFR-positive cells show abundant intermediate filaments, rough endoplasmic reticulum and mitochondria. **(I)** Vimentin immunogold labelling in the nodule area shows large cells with abundant processes and intermediate filaments. **(J)** Scheme of oligodendrocyte differentiation from immature EGFR progenitors in the ventricular-subventricular zone, vimentin positive oligodendrocyte progenitors, BCAS1-positive oligodendrocytes to Olig2 differentiated oligodendrocytes. Scale bars: **A**, Panoramics: 500 μm, GM Sheet-like, satellitosis, rosettes: 50 μm; **B**, 50 μm; **C**, 5 μm; **D**, Panoramic: 250 μm, magnifications: 50 μm; **E**, Panoramic: 250 μm, magnification: 100 μm; **F**, Panoramic: 250 μm, Nodule: 10 μm, GM sheet-like, Satellitosis, Rosettes: 50 μm, EGFR and VIM immunohistochemistry: 5 μm; **G**, Panoramic: 100 μm, Nodule: 25 μm, Neoplastic, Nonneoplastic: 10 μm; **H**, Panoramic: 2 μm, membrane detail: 500 nm, vesicle detail: 200 nm; **I**, Panoramic: 2 μm, magnification: 500 nm.

**TABLE** List of Markers Used in Diagnostic Experiments and Tumoral Characterization

| Marker Type | Marker | Method | Source | Reference (Clone) | Dilution | Sheet-like | Nodules | GM Satellitosis | WM Rosettes |
|---|---|---|---|---|---|---|---|---|---|
| Diagnostic | 1p | FISH | ZytoVision (Bremerhaven, Germany) | SPEC 1p36/1q25 | N/A | Deletion | Deletion | Deletion | Deletion |
| | 19q | FISH | ZytoVision | SPEC 19q13/19p13 | N/A | Deletion | Deletion | Deletion | Deletion |
| | IDH1 | IHC | Dianova (Hamburg, Germany) | DIAH09 (H09) | 1:20 | Mutant | Mutant | Mutant | Mutant |
| | ATRX | IHC | Dianova | DIAAX1 (AX1) | 1:100 | Not-mutated | Not-mutated | Not-mutated | Not-mutated |
| Neuronal lineage | NeuN | IHC | Merck (Darmstadt, Germany) | MAB377 (A60) | 1:1000 | Negative | Negative | Negative | Negative |
| | DCX | IHC | Cell Signaling (Danvers, MI) | 4604 (Polyclonal) | 1:400 | Negative | Negative | Negative | Negative |
| | Synaptophysin | IHC | DAKO (Glostrup, Denmark) | IR660 (DAK-SYNAP) | Prediluted | Negative | Negative | Negative | Negative |
| | TUJ1 | IHC | Covance (Princeton, MA) | MMS-435P (TUJ1) | 1:100 | Negative | Negative | Negative | Negative |
| Intermediate filaments | GFAP | IHC | DAKO | IR524 (Polyclonal) | Prediluted | Positive | Negative | Negative | Negative |
| | GFAP | IF | Millipore (Burlington, MA) | MAB360 (GA5) | 1:1000 | Positive | Negative | Negative | Negative |
| | Vimentin | IHC | DAKO | IR630 (V9) | Prediluted | Positive | Negative | Negative | Negative |
| | Vimentin | IF/IG-TEM | Abcam (Cambridge, UK) | ab73159 (Polyclonal) | 1:300/1:150 | Negative | Positive | Positive | Negative |
| Oligodendroglial lineage | NaBC1(BCAS1) | IF | Santa Cruz (Dallas, TX) | sc-136342 (NaBC1 (5)) | 1:200 | Negative | Positive | Negative | Negative |
| | NG2 | IF/IHC | Millipore | ab5320 (Polyclonal) | 1:200 | Negative | Negative | Negative | Negative |
| | Olig2 | IHC | Gennova Scientific (Seville, Spain) | AP10616 (211F1.1) | 1:50 | Positive | Positive | Positive | Positive |
| Proliferation markers | Ki67 | IHC | DAKO | IR626 (MIB-1) | Prediluted | Negative | Positive | Negative | Positive |
| | c-MYC | IHC | Biocare Medical (Pacheco, CA) | 415 (EP121) | 1:50 | Negative | Positive | Negative | Positive |
| | MYC | FISH | Agilent (Princeton, MA) | G-11623-2 | N/A | Negative | Positive | Negative | Positive |
| | MYCN | FISH | Kreatech (Wetzlar, Germany) | KI-10706 | N/A | Negative | Negative | Negative | Negative |
| Growth factors | EGFR | IHC | DAKO | M7239 (E-30) | 1:50 | Positive | Negative | Positive | Positive |
| | EGFR | IF/IG-TEM | Millipore | 06-847 (Polyclonal) | 1:200/1:100 | Negative | Negative | Negative | Negative |
| | PDGFRa | IHC | BD Biosciences (San Diego, CA) | 556001 (aR1) | 1:50 | Negative | Negative | Negative | Negative |

Marker expression in the different tumor areas is shown.
Abbreviations: FISH, fluorescent in situ hybridization; IF, immunofluorescence; IG-TEM, immuno-gold electron microscopy; IHC, immunohistochemistry.

(PROMETEO/2019/075) to J.M.G.V. and by the Spanish Ministry of Science, Innovation and Universities (PCI2018-093062) to V.H.P.

## COMPETING INTERESTS

The authors have no duality or conflicts of interest to declare.

## ACKNOWLEDGMENTS

*All procedures followed were in accordance with the ethical standards of the responsible committee on human experimentation (institutional and national) and with the Helsinki Declaration of 1964 and its later amendments. Informed consent was obtained from all patients for being included in the study. The authors acknowledge the support of Patricia García-Tárraga at the Laboratory of Comparative Neurobiology of the University of Valencia.*

## REFERENCES

1. Reifenberger G, Collins VP, Hartmann C, et al. Oligodendroglioma, IDH-mutant and 1p/19q-codeleted. In: Louis DN, Ohgaki H, Wiestler OD, Cavenee WK, ed. WHO Classification of Tumours of the Central Nervous System. Lyon, France: International Agency for Research on Cancer 2016:60–9
2. Wesseling P, van den Bent M, Perry A. Oligodendroglioma: Pathology, molecular mechanisms and markers. Acta Neuropathol 2015;129:809–27
3. Wesseling P, Capper D. WHO 2016 Classification of gliomas. Neuropathol Appl Neurobiol 2018;44:139–50
4. Canoll P, Goldman JE. The interface between glial progenitors and gliomas. Acta Neuropathol 2008;116:465–77
5. Shoshan Y, Nishiyama A, Chang A, et al. Expression of oligodendrocyte progenitor cell antigens by gliomas: Implications for the histogenesis of brain tumors. Proc Natl Acad Sci USA 1999;96:10361–6
6. Persson AI, Petritsch C, Swartling FJ, et al. Non-stem cell origin for oligodendroglioma. Cancer Cell 2010;18:669–82
7. Zong H, Verhaak RGW, Canoll P. The cellular origin for malignant glioma and prospects for clinical advancements. Expert Rev Mol Diagn 2012;12:383–94
8. Kamoun A, Idbaih A, Dehais C, et al. Integrated multi-omics analysis of oligodendroglial tumours identifies three subgroups of 1p/19q co-deleted gliomas. Nat Commun 2016;7:11263.
9. Bielle F, Ducray F, Mokhtari K, et al. Tumor cells with neuronal intermediate progenitor features define a subgroup of 1p/19q co-deleted anaplastic gliomas. Brain Pathol 2017;27:567–79.
10. Fard MK, van der Meer F, Sánchez P, et al. BCAS1 expression defines a population of early myelinating oligodendrocytes in multiple sclerosis lesions. Sci Transl Med 2017;9:eaam7816
11. Lindberg N, Kastemar M, Olofsson T, et al. Oligodendrocyte progenitor cells can act as cell of origin for experimental glioma. Oncogene 2009; 28:2266–75
12. Gorris R, Fischer J, Erwes KL, et al. Pluripotent stem cell-derived radial glia-like cells as stable intermediate for efficient generation of human oligodendrocytes. Glia 2015;63:2152–67
13. Aguirre A, Dupree JL, Mangin JM, et al. A functional role for EGFR signaling in myelination and remyelination. Nat Neurosci 2007;10: 990–1002
14. Doetsch F, Petreanu L, Caille I, et al. EGF converts transit-amplifying neurogenic precursors in the adult brain into multipotent stem cells. Neuron 2002;36:1021–34
15. Dougherty JD, Fomchenko EI, Akuffo AA, et al. Candidate pathways for promoting differentiation or quiescence of oligodendrocyte progenitor-like cells in glioma. Cancer Res 2012;72:4856–68

The CRISPR Journal
Volume 2, Number 6, 2019

DOI: 10.1089/crispr.2019.0032

The CRISPR Journal

RESEARCH ARTICLE

# Immunogold Labeling to Detect *Streptococcus pyogenes* Cas9 in Cell Culture and Tissues by Electron Microscopy

María José Ulloa-Navas,[1] Patricia García-Tárraga,[1] José Manuel García-Verdugo,[1] and Vicente Herranz-Pérez[1,2,*]

## Abstract

The CRISPR-Cas9 system is a powerful and yet precise DNA-editing tool in rapid development. By combining immunogold labeling and electron microscopy with the novel CRISPR-Cas9 system, we propose a new method to gain insight into the biology of this tool. In this study, we analyzed different Cas9-induced systems such as HEK293T cell line, murine oligodendrocyte progenitor cells, brain and liver to detect Cas9 expression by immunoelectron microscopy. Our results show that while Cas9 expression could be found in the nuclei and nucleopores of transfected HEK293T cells, in transfected oligodendrocyte precursor cells, Cas9 was found in cytoplasmic vesicles. In Cas9 constitutively expressing oligodendrocyte precursors, the enzyme was located in the cytoplasm of nondividing cells. Finally, while in the liver Cas9 was detected in different cell types, in the brain we found no specifically labeled cells. In conclusion, immunoelectron microscopy opens a new spectrum of opportunities to study the CRISPR-Cas9 system in a more precise manner.



## Introduction

Genome editing has become one of the most studied fields among the biomedical sciences in the last five decades. The number of applications in genome engineering have skyrocketed because of CRISPR-Cas systems.[1] First and foremost, CRISPR-Cas systems were described as an adaptive immune system in bacteria and archaebacteria against viruses and plasmids.[2,3] As an application for eukaryotic cells, CRISPR-Cas9 was originally described as a powerful tool to modify specific genome loci.[4] Nonetheless, today CRISPR-Cas systems are used not only to edit the genome and epigenome, but also to target, trace, and regulate its expression.[5]

The effectiveness of CRISPR-Cas systems to perform any activity in eukaryotic cells resides in different factors, such as the metabolic state of each cell type, which determines the biosynthesis and availability of the enzyme within the cell, and the stage of the cell cycle in which the enzyme is synthesized.[6–8] Another aspect to take into consideration is the ability of each cell type to transport Cas9 into and out of the nucleus or the target organelle. Finally, the ability of each cell type to degrade Cas9 after a time remains to be elucidated.

Another current topic usually debated in this field is the optimization of the transfection method, and how the CRISPR system *per se* can modify the characteristics of any cell type, especially in the case of stem cells or primary cultures, implying one of the most studied issues among the field.[9–11] Although high transfection efficiencies have been achieved in a wide variety of stem cells,[12–16] a gold standard to analyze not only transfection efficiency as a molecular parameter, but also the fitness status of cells in culture, has not been yet established.

Recently, some CRISPR-Cas applications to target extranuclear DNA in different organelles, such as the mitochondria, have been developed.[17] Furthermore, state-of-the-art technology nowadays allows this system to be directed to different compartments within the nucleus.[18] Therefore, it is important to develop a high-resolution tool to track Cas9 at a subcellular localization level with high precision.

In this study, we present transmission electron microscopy (TEM) and immunogold (IG) labeling, as a method to analyze the above-mentioned criteria. TEM is a classic technique that presents advantages such as a high-definition resolution at a single-cell level. When combined

[1]*Laboratory of Comparative Neurobiology, Cavanilles Institute of Biodiversity and Evolutionary Biology, University of Valencia, CIBERNED, Paterna, Spain; and* [2]*Predepartamental Unit of Medicine, Faculty of Health Sciences, University Jaume I, Castelló de la Plana, Spain.*

*Address correspondence to: *Vicente Herranz-Pérez, PhD, Laboratory of Comparative Neurobiology, Cavanilles Institute of Biodiversity and Evolutionary Biology, University of Valencia, CIBERNED, C/ Catedrático José Beltrán Martínez 2, 46980 Paterna (Valencia), Spain,* E-mail: vicente.herranz@uv.es

with IG labeling, it permits the subcellular location and distribution of a protein of interest to be observed.[19,20] Since IG-TEM can be used to study both tissues and cell cultures, it can be considered as a valid tool to detect Cas9 at a single-cell or single-organelle level and to evaluate the ultrastructural characteristics of modified cells. Therefore, here we extensively describe a method to detect *Streptococcus pyogenes* Cas9 (SpCas9) by IG labeling and TEM detection, both in Cas9-expressing cell cultures (HEK293T cell line and oligodendrocyte precursor cells [OPCs]) and in mouse tissues (liver and brain), comparing different approaches to deliver the enzyme, such as lipofection and transgenic tools.

## Materials and Methods

Unless otherwise stated, all reagents were purchased from Sigma–Aldrich (St. Louis, MO).

### HEK293T culture

HEK293T cells (ATCC® CRL-3216™) were seeded at a density of $4.2 \times 10^4$ cells/cm$^2$ in 13 mm glass coverslips on 24-well plates or 8-well Nunc Lab-Tek permanox chamber slides coated with 10 $\mu$g/mL laminin. Cells were grown in Dulbecco's modified Eagle's medium (DMEM) containing 2 mM L-glutamine, 1 × antibiotic–antimycotic solution, 5% fetal bovine serum (FBS; all from Gibco, New York, NY) at 37°C, 5% $CO_2$.

### OPC isolation

OPCs were isolated from P0 C57BL6/J (Charles River Laboratories, Wilmington, MA) or P0 B6J.129(Cg)-Igs2tm1.1(CAG-cas9*)Mmw/J, also known as H11-Cas9 (The Jackson Laboratory, Bar Harbor, ME) mouse brains in order to isolate wild-type or Cas9 endogenously expressing OPCs, respectively. The H11-Cas9 mouse line has been previously used for pre- and post-mitotic brain-cell editing by Nishiyama *et al.*[21] The telencephalon was dissected in ice-cold Hank's Balanced Salt Solution (HBSS) with $Ca^{2+}$ and $Mg^{2+}$ (Gibco). Brains were transferred to 50 mL Falcon tubes (Thermo Fisher Scientific, Waltham, MA) in 10 mL ice-cold HBSS with $Ca^{2+}$ and $Mg^{2+}$ and subsequently incubated at 37°C for 5 min in papain solution, consisting of 0.09 mg/mL papain (Worthington Biochemical, Lakewood, NJ) and 0.02 mg/mL EDTA (Gibco) in 1× HBSS without $Ca^{2+}$ and $Mg^{2+}$ (Gibco). Tissue was dissociated with sterile scissors and repeated pipetting through 1,000 $\mu$L pipette tips. The papain was neutralized using a media consisting of 5% FBS and 1× antibiotic-antimycotic solution in DMEM (all from Gibco). The resulting cell suspension was filtered through a 70 $\mu$m mesh (BD Biosciences, Franklin Lakes, NJ) and centrifuged at 300 *g* for 10 min. Then, we isolated the OPC fraction using PDGFRα-MACS (Miltenyi Biotech, Bergisch Gladbach, Germany), as recommended by the manufacturer. Following this, cells were seeded at a density of $5.25 \times 10^5$ cells/cm$^2$ in laminin-coated 13 mm glass coverslips or on 8-well permanox chamber slides and cultured in DMEM medium containing 1× N-2 and B-27 supplements (Gibco), 10 ng/$\mu$L bFGF, and 20 ng/$\mu$L PDGF-AA (PeproTech, Rocky Hill, NJ). Medium was replaced the next day and then every other day until cells were subcultured for transfection. This process was reviewed and approved by the Animal Welfare Ethical Review Board of the University of Valencia (2017/VSC/PEA/0017).

### Cell-culture transfection

For Cas9 expression, we used pSpCas9(BB)-2A-GFP plasmid (PX458), a kind gift from Dr. Feng Zhang (Addgene plasmid #48138). For green fluorescent protein (GFP) expression, we used pmaxGFP (Lonza, Basel, Switzerland). Plasmids were purified using a GenJet MiniPrep Kit (Thermo Fisher Scientific).

OPCs were transfected after 13 days *in vitro* using 750 ng of plasmid with Lipofectamine LTX with Plus reagent (Invitrogen, Carlsbad, CA), as recommended by the manufacturer, in each well of 24-well plates or with 375 ng in each well of 8-well chamber slides. HEK293T cells were transfected using 500 ng of plasmid in each well of 24-well plates or 250 ng of plasmid in each well of 8-well chamber slides, as described by Ran *et al.*,[22] with Lipofectamine 2000 (Invitrogen), as recommended by the manufacturer.

### Sample processing for immunofluorescence and IG labeling

**Cell-culture fixation.** Cells were rinsed with 0.1 M phosphate buffer (PB) at 37°C and fixed with 4% paraformaldehyde (PFA) in 0.1 M PB at 37°C for 10 min. Then, the cells were further incubated at 4°C for 50 min. Finally, fixative solution was removed, and cells were gently washed with 0.1 M PB.

**Tissue fixation and processing.** P60 H11-Cas9 mice ($n = 6$) and P60 C57BL6/J ($n = 3$) mice were perfused using 0.9% saline solution at 37°C for 5 min using a flow rate of 4.5 mL/min. Then, the animals were fixed by transcardial perfusion with 4% PFA in 0.1 M PB at 37°C for 15 min. The liver and the brain were extracted and post fixed in the same solution overnight. This process was reviewed and approved by the Animal Welfare Ethical Review Board of the University of Valencia (2017/VSC/PEA/0017). For immunofluorescence (IF) detection, the organs were dehydrated and embedded in

paraffin. Following this, 5 $\mu$m sections were obtained with an HM 340E microtome (Microm International GmbH, Walldorf, Germany). For immunoelectron detection, 50 $\mu$m sections were obtained using a Leica VT1000S vibratome (Leica Biosystems, Wetzlar, Germany).

### IF detection

Cells and sections were incubated in 1:200 Immunosaver (Electron Microscopy Sciences, Hatfield, PA) in water at 60°C for 30 min. Peroxidase blocking was performed using a solution of 10% methanol and 10% $H_2O_2$ in 0.1 M PB. For permeabilization, the samples were washed three times for 5 min in PTA solution: 0.1% Triton X-100, 1 mg/mL bovine serum albumin (BSA) in 0.1 M phosphate buffer saline (PBS). The samples were then incubated in blocking solution (10% casein, 5% normal goat serum in PTA) for 1 h at room temperature. Subsequently, the samples were incubated overnight in primary antibodies diluted in blocking solution (1:300 rabbit-anti-Olig2, Chemicon, Temecula, CA; 1:100 mouse-anti-SpCas9, Abcam, Cambridge, United Kingdom; or 1:1000 rabbit-anti-GFAP for cell culture, DAKO, Jena, Germany). The following day, samples were thoroughly washed in PTA, and incubated in secondary antibody solution (1:500 AlexaFluor 488 goat-anti-mouse, Invitrogen; or 1:500 AlexaFluor 555 goat-anti-rabbit, Invitrogen). Samples were then washed in 0.1 M PB and incubated in 1:1,000 DAPI in water for 5 min. Finally, the samples were mounted with FluorSave™ (Merck Millipore [Calbiochem], Burlington, MA).

### IG labeling for cell culture

Cell cultures cultured on 8-well permanox chamber slides were permeabilized with 0.1% Triton X-100 in 0.1 M PB for 10 min. Following this, the cells were incubated in a blocking solution consisting of 0.3% BSAc (Aurion, Wageningen, the Netherlands), 0.05% sodium azide in 0.1 M PB for 1 h. Subsequently, the cells were incubated in primary antibody (1:50 mouse-anti-SpCas9, Abcam; 1:150 rabbit-anti-Olig2, Millipore; or 1:200 chicken-anti-Olig2, Aves Labs, Tigard, OR) in blocking solution overnight at 4°C. The samples were rinsed in 0.1 M PB and then incubated in secondary antibody blocking solution consisting of 0.5% BSAc (Aurion), 0.025% CWFS gelatin (Aurion), 0.05% sodium azide in 0.1 M PB for 1 h, followed by incubation in secondary antibody (1:50 goat-anti-mouse IgG gold ultrasmall; Aurion) diluted in the same solution overnight at 4°C. To enhance gold labeling, we performed silver enhancement (R-GENT SE-LM, Aurion) for 15–25 min in the dark, followed by gentle washing in 2% sodium acetate and incubation in gold toning solution (0.05% gold chloride in water) for 10 min. The samples were then washed twice with 0.3% sodium thiosulfate in water. Finally we post fixed with 2% glutaraldehyde (Electron Microscopy Sciences) in 0.1 M PB for 30 min. Samples were rinsed and kept in 0.1 M PB containing 0.05% sodium azide at 4°C until resin embedding.

### IG labeling for tissues

Processing for tissue was performed in a similar manner as for cell cultures, with a few changes. Briefly, the permeabilization step was performed by repeated freeze–thaw cycles. Before performing this process, the sections were cryoprotected in a solution containing 25% saccharose in 0.1 M PB for 30 min, after which the sections were immersed in −60°C 2-methylbutane and rapidly transferred to a room temperature saccharose solution. This cycle was repeated three or four times. Subsequently, tissues were left in 0.1 M PB and then incubated in primary antibody blocking solution for 1 h, followed by primary antibody in blocking solution (1:100 mouse-anti-SpCas9; Cell Signaling Technology, Danvers, MA) for 72 h at 4°C. The rest of the process was identical to that described for cell cultures.

### Sample processing for TEM

Samples were embedded in resin, as previously described.[20] Briefly, samples were post fixed with 1% osmium tetroxide (Electron Microscopy Sciences), 7% glucose in 0.1 M PB for 30 min at room temperature, washed in deionized water, and partially dehydrated in 70% ethanol. Afterwards, the samples were contrasted in 2% uranyl acetate (Electron Microscopy Sciences) in 70% ethanol for 2 h at 4°C. The samples were further dehydrated and infiltrated in Durcupan ACM epoxy resin at room temperature overnight, and then at 60°C for 72 h. Once the resin was cured, immunolabeled sections were selected and cut into ultrathin sections (60–80 nm) using an Ultracut UC6 ultramicrotome (Leica Biosystems). These sections were placed on Formvar-coated single-slot copper grids (Electron Microscopy Sciences) stained with lead citrate and examined at 80 kV on a FEI Tecnai $G^2$ Spirit (FEI Company, Hillsboro, OR) transmission electron microscope equipped with a Morada CCD digital camera (Olympus, Tokyo, Japan).

### Statistical analysis

Quantitation of transfected OPCs and HEK293T cells was performed in triplicate experiments by counting the number of IF-positive cells relative to the total number of cells in three different fields (Supplementary Fig. S1A–E). Statistical analyses were performed using GraphPad Prism v8 (GraphPad, San Diego, CA).

Differences among different time points were assessed by one-way analysis of variance followed by Tukey's *post hoc* test. All numerical data are expressed as the mean ± standard error of the mean. All statistical tests were two-sided, and a $p$-value of $<0.05$ was considered to be statistically significant.

## Results

We evaluated immunoelectron microscopy as a useful technique to detect Cas9 precisely in different biological systems, including cell cultures and tissue sections (Fig. 1). First, to standardize our method in cell lines, we used transfected human embryonic kidney 293 cell line (HEK293T). In addition, we explored the expression and immunodetection of Cas9 in OPC primary cultures from the mouse brain. Finally, we used a similar strategy to analyze the liver and brain of transgenic mice that constitutively express SpCas9.

### Immunoelectron microscopy improves the visualization of the subcellular distribution of SpCas9 in HEK293T cell line

To identify the strengths and flaws of our method, we first transfected HEK293T cells in order to assess the differences between Cas9 IF and IG detection (Fig. 1). In every case, IF was used as a control to evaluate Cas9 expression at the subcellular level. First, we transfected the cells with PX458 plasmid containing SpCas9 and GFP sequences. Subsequent IF detection 24 h after transfection showed that both SpCas9 and GFP were present within the nucleus and in the cytoplasm of the cells (Fig. 2A and Supplementary Fig. S1A; 43.94 ± 2.75% $GFP^+$ cells; 40.58 ± 2.99% $SpCas9^+$ cells; $n = 1{,}650$ cells). However, IG labeling displayed a finer localization of the enzyme (Fig. 2B–F). By using this method, we observed that cells expressed SpCas9 protein in the cytoplasm, although we could not detect it inside any particular organelle (Fig. 2C). A small fraction of cells expressed SpCas9 exclusively in the nucleus but not in the nucleolus (Fig. 2D), and interestingly enough, IG labeling allowed us to detect Cas9 clearly in the boundary of many nuclear pores, suggesting a potential nuclear translocation of this protein (Fig. 2E and F).

Together, these results indicate that immunoelectron microscopy is a valuable tool for gaining insight into the subcellular dynamics of Cas9.

### Immunoelectron microscopy is a valid method for tracking SpCas9 in transfected primary cells *in vitro* over time

To track SpCas9 at different times after transfection, we introduced PX458 plasmid in OPCs and fixed the cultures after 10 h, 24 h, 72 h, and 5 days (Fig. 3A–L). Then, we performed IF and IG-TEM detection to identify the subcellular localization and dynamics of SpCas9 over time. At 10 h, we did not detect SpCas9 by either IF or IG (Fig. 3A–C). This was also the case for GFP after IF detection (Fig. 3A), suggesting that the plasmid was not expressed at the shortest time point analyzed in our study. Interestingly, 24 h after transfection, the label

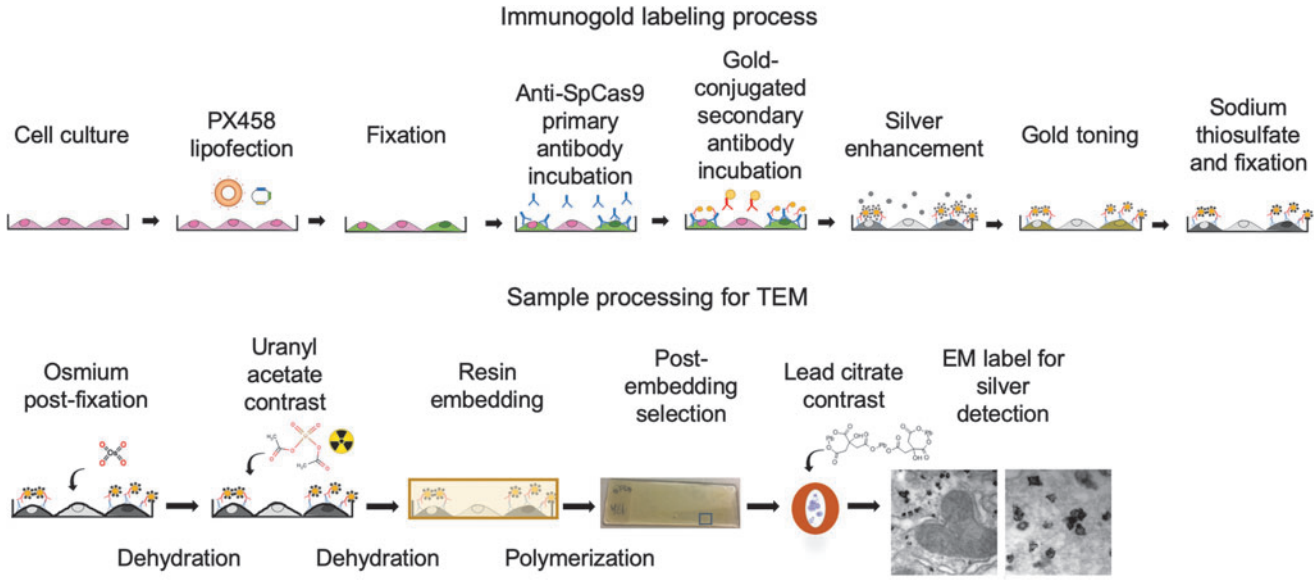


**FIG. 1.** Step-by-step diagram describing the procedure followed from cell culture to transmission electron microscopy analysis. See Materials and Methods.

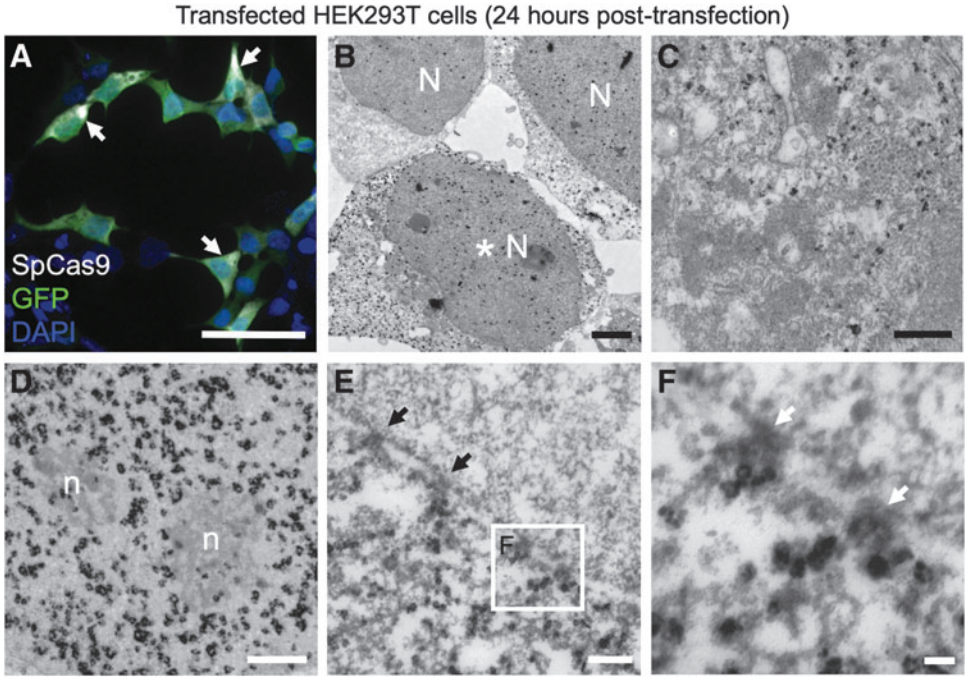


**FIG. 2.** Expression of green fluorescent protein (GFP) and *Streptococcus pyogenes* Cas 9 (SpCas9) in HEK293T cells transfected with PX458 24 h after transfection. **(A)** Immunofluorescence (IF) analysis of transfected HEK293T cells shows SpCas9 expression broadly distributed in the nucleus and cytoplasm (white arrows). Interestingly, GFP tag does not perfectly co-localize with SpCas9. **(B)** SpCas9 immunoelectron detection (immunogold [IG]) results in cells with different amounts of label. Intensely labeled cells, with signal in both the nucleus and cytoplasm (asterisk), contrasts with cells presenting a less abundant labeling. **(C)** Detail of the cytoplasm of a SpCas9-labeled cell. **(D)** High-power image of the nucleus of a SpCas9-labeled cell. Remarkably, the label is found throughout the nucleus but not in the nucleolus. **(E)** Gold-particle labeling can be frequently found associated to nuclear pores (black arrows). **(F)** High-magnification photomicrograph showing the presence of labeling in the nuclear pore boundary (white arrows). N, nucleus; n, nucleolus. Scale bars: **(A)** 100 $\mu$m; **(B)** 1 $\mu$m; **(C)** 500 nm; **(D)** 1 $\mu$m; **(E)** 200 nm; and **(F)** 50 nm.

was detected by IF and IG in small cytoplasmic vesicles surrounding the nucleus (Fig. 3D–F) and in the perinuclear space only detectable by IG (Fig. 3E and F). Intriguingly, at this time point, we were able to detect only one cell in which Cas9 presented a nuclear localization (Fig. 4A), indicating that the lack of nuclear label in the majority of the cells is not due to a methodological limitation. IF analysis of the cells 72 h post transfection suggested that Cas9 was expressed in specific areas of the cytoplasm (Fig. 3G). We corroborated this observation by IG-TEM, which allowed us to determine that Cas9 compartmentalized into small cytoplasmic vesicles (Fig. 3H and I). To investigate the role of the vesicles that packed the enzyme in this cell type further, we tracked

**FIG. 3.** Expression of GFP and SpCas9 in oligodendrocyte precursor cells (OPCs) transfected with PX458. **(A–C)** No expression of SpCas9 is detected 10 h after transfection by **(A)** immunofluorescence or **(B** and **C)** immunogold transmission electron microscopy (IG-TEM). **(D, G,** and **J)** SpCas9 immunofluorescent labeling in the cytoplasm of OPCs after 10 h, 24 h, 72 h, and 5 days upon transfection (white arrows). **(E, H,** and **K)** IG followed by TEM images showing SpCas9 labeling within small vacuoles or vesicles 24 and 72 h after SpCas9 transfection (black arrows in **E** and **H**), while 5 days post transfection, the label is confined to dense vacuoles with lysosomal morphology (black arrows in **K**). **(F, I,** and **L)** High-magnification photomicrographs of the vacuoles and lysosomes (white arrows) where the label is detected 24 h, 72 h, and 5 days post transfection, respectively. **(M** and **N)** Quantification of **(M)** GFP- or **(N)** SpCas9-positive cells 10 h, 24 h, 72 h, and 5 days after transfection. Data shown are mean ± standard error of the mean. ** indicates a statistical $p$-value < 0.01. *** indicates a statistical $p$-value < 0.001. Scale bars: **(A, D, G,** and **J)** 10 $\mu$m; **(B, E, H,** and **K)** 1 $\mu$m; **(C, F,** and **I)** 500 nm; **(L)** 200 nm.

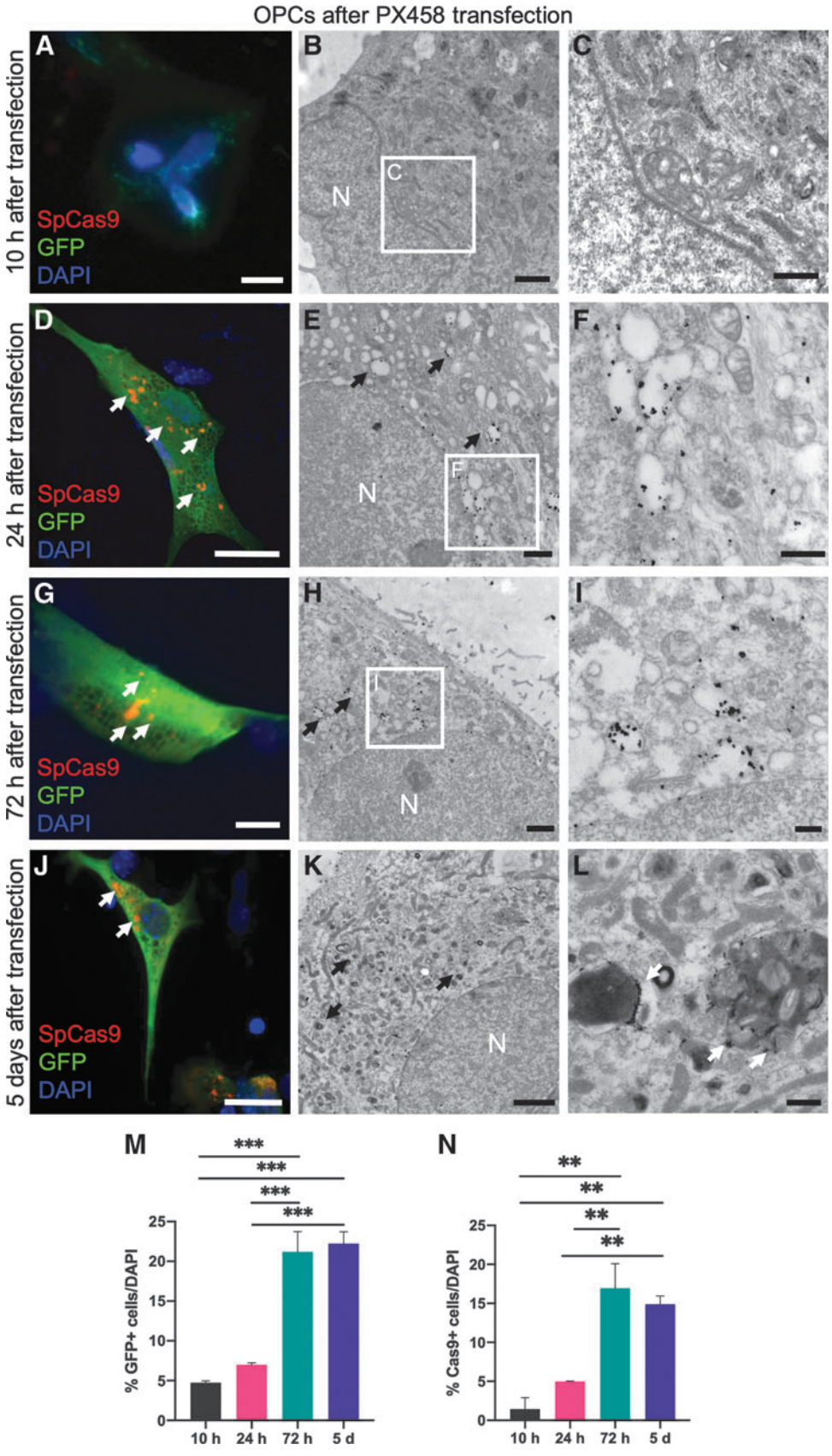

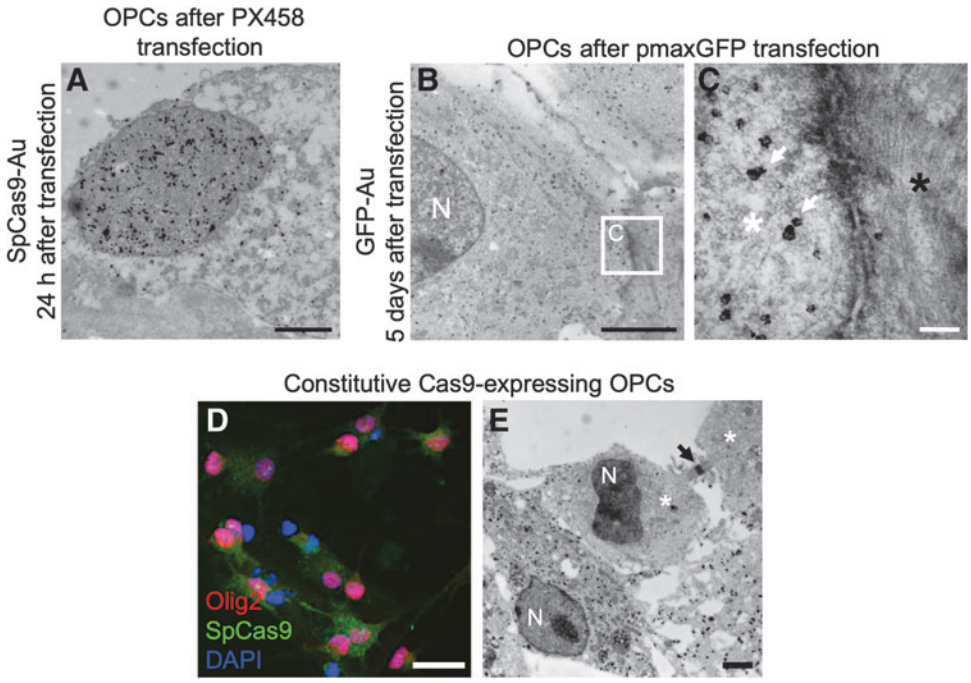


**FIG. 4.** SpCas9 is distinctly localized in OPCs. **(A)** A minority of OPCs display nuclear localization of SpCas9. **(B)** GFP IG-labeling in pmaxGFP-transfected OPCs. The expression of this plasmid does not induce the formation of vacuoles or GFP vesicle packaging. **(C)** High-magnification photomicrograph showing the cytoplasm of a GFP-labeled OPC (white asterisk) and a non-labeled OPC (black asterisk) showing no vacuoles. Gold particles are highlighted by white arrows. **(D)** IF analysis of OPCs derived from H11-Cas9 mice showing SpCas9 expression the cytoplasm. **(E)** TEM analysis reveals SpCas9 label widely distributed in the cytoplasm of OPCs. This labeling is not confined to vesicles. Interestingly, cells going through cell division do not express Cas9 (asterisk). In this photomicrograph, a mitotic cell in telophase can be observed. The black arrow points to the mitotic spindle. Scale bars: **(A)** 1 $\mu$m; **(B)** 5 $\mu$m; **(C)** 500 nm; **(D)** 25 $\mu$m; **(E)** 1 $\mu$m.

SpCas9 5 days after transfection. At this time point, we observed by IF that SpCas9 was still present in discrete regions of the cytoplasm, as we observed at 24 and 72 h (Fig. 3D, G, and J). By combining IG labeling and TEM, we detected that the enzyme localized to electron-dense lysosome-like structures and also autophagosomes, which displayed mitochondria and membranous structures in their content (Fig. 3K and L).

Quantitative analysis of $GFP^+$ and $Cas9^+$ cells relative to the total number of cells showed an increase with time until 72 h post transfection, which was sustained at similar levels 5 days after transfection (Fig. 3M and N). We found statistically significant differences in the number of $GFP^+$ cells between 10 h ($4.75 \pm 0.23\%$; $n = 83$ cells) and 72 h post transfection ($21.20 \pm 2.55\%$; $n = 110$ cells, $p = 0.0002$); 10 h and 5 days post transfection ($22.25 \pm 1.47\%$; $n = 67$ cells, $p = 0.0001$); 24 h ($6.99 \pm 0.25\%$; $n = 517$ cells) and 72 h post transfection ($p = 0.0006$); 24 h and 5 days post transfection ($p = 0.0004$; Fig. 3M). The number of $Cas9^+$ cells also increased in a similar trend. We found significant differences between 10 h ($1.45 \pm 1.45$; $n = 83$ cells) and 72 h post transfection ($16.95 \pm 3.14\%$; $n = 110$ cells, $p = 0.0013$); 10 h and 5 days post transfection ($14.90 \pm 1.05\%$; $n = 67$ cells, $p = 0.0033$), 24 h ($4.98 \pm 0.06\%$; $n = 517$ cells) and 72 h post transfection ($p = 0.0068$); 24 h and 5 days post transfection ($p = 0.0194$; Fig. 3N).

To elucidate further whether the specific packaging of Cas9 was due to a transfection issue, we transfected pmaxGFP (Lonza) into OPCs. This plasmid is used as a control for transfection when using GFP as a fluorescent marker. As this plasmid does not express Cas9, we performed IG to detect GFP. Our results indicate that GFP is extensively expressed in the cytoplasm and is not packaged into vesicles (Fig. 4B and C), supporting the notion that vesicle packaging is a specific feature of Cas9-induced expression in this cell type.

Overall, using IG-TEM provides a detailed view at a single-cell and subcellular level, allowing Cas9 to be detected, even in discrete organelles. Our results also suggest that Cas9 expression via lipofection in OPCs can result in enzyme degradation in lysosomes.

### IG-TEM favors the validation of an efficient expression method in primary cultures

One of the main issues reported by CRISPR users is the validation of the expression method in primary and hard-to-transfect cell cultures. As a proof of principle to endorse that ultrastructural analysis contributes to validate an optimal expression method for this type of cultures, we isolated cells that endogenously express SpCas9 to compare their ultrastructure to that of transfected cultures. For this purpose, we isolated OPCs from P0 H11-Cas9 mice and performed the same detection protocols as for transfected OPCs. In this case, using IF, we found that Cas9 is widely expressed throughout the cell cytoplasm (Fig. 4D). Still, IG-TEM allowed us to confirm that cells express Cas9 in the cytoplasm. Strikingly, mitotic cells, even those in cytokinesis, did not express Cas9, suggesting that OPCs undergoing cell division do not express the enzyme (Fig. 4E). Thereby, we corroborated that ultrastructural studies are significant to ascertain the basic biology of different cells expressing the CRISPR-Cas9 system.

### IG enhances specificity of label detection in the liver

To set up the methodology for Cas9 IG detection and TEM processing, we performed IF and IG-TEM on liver and brain tissue of P60 H11-Cas9 mice ($n = 6$).

First, we used IF to study the expression of SpCas9 by astrocytes and oligodendrocyte progenitors within the motor cortex of the brain (Fig. 5). In the case of Olig2-positive OPCs, Cas9 was expressed within the cytoplasm. This result is consistent with our results in OPC cultures *in vitro*, indicating that Cas9 is in most cases in the cytoplasm in this specific cell type (Fig. 5E–H). To identify astrocytes, we used immunolabeling for the glial fibrillary acidic protein (GFAP) together with Cas9 immunolabeling. Using this approach, we determined that astrocytes do not express Cas9 in this animal model (Fig. 5I–L). Interestingly, we found Cas9-positive cells with neuronal morphology in the cortex of the brain, with both cytoplasmic and nuclear signal. On the contrary, using immunoelectron microscopy, we were not able to detect Cas9 expression in any brain structure after trying several different conditions.

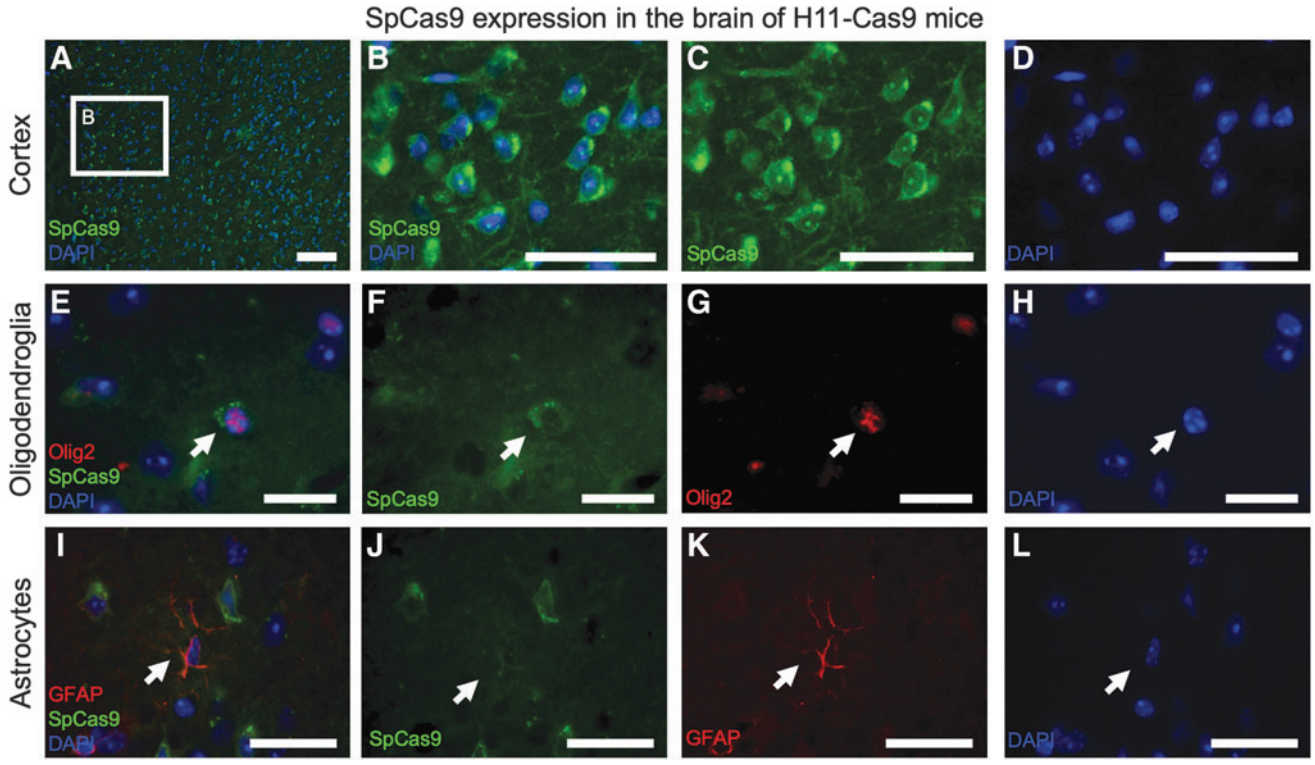


**FIG. 5.** Immunofluorescence detection of SpCas9 in the brain of H11-Cas9 mice. **(A–D)** Abundant SpCas9-positive cells with neuronal morphology can be observed in the brain cortex. The labeling can be observed in the cytoplasm and in specific areas of the nucleus. **(E–H)** Olig2-positive cells display a cytoplasmic SpCas9 distribution (white arrows in **E–H**), while other glial cells such as GFAP-positive astrocytes **(I–L)** do not express the enzyme (white arrows in **I–L**), indicating some variability in SpCas9 expression among cell types in this transgenic mouse line. Scale bars: **(A)** 100 $\mu$m; **(B–D)** 50 $\mu$m; **(E–L)** 10 $\mu$m.

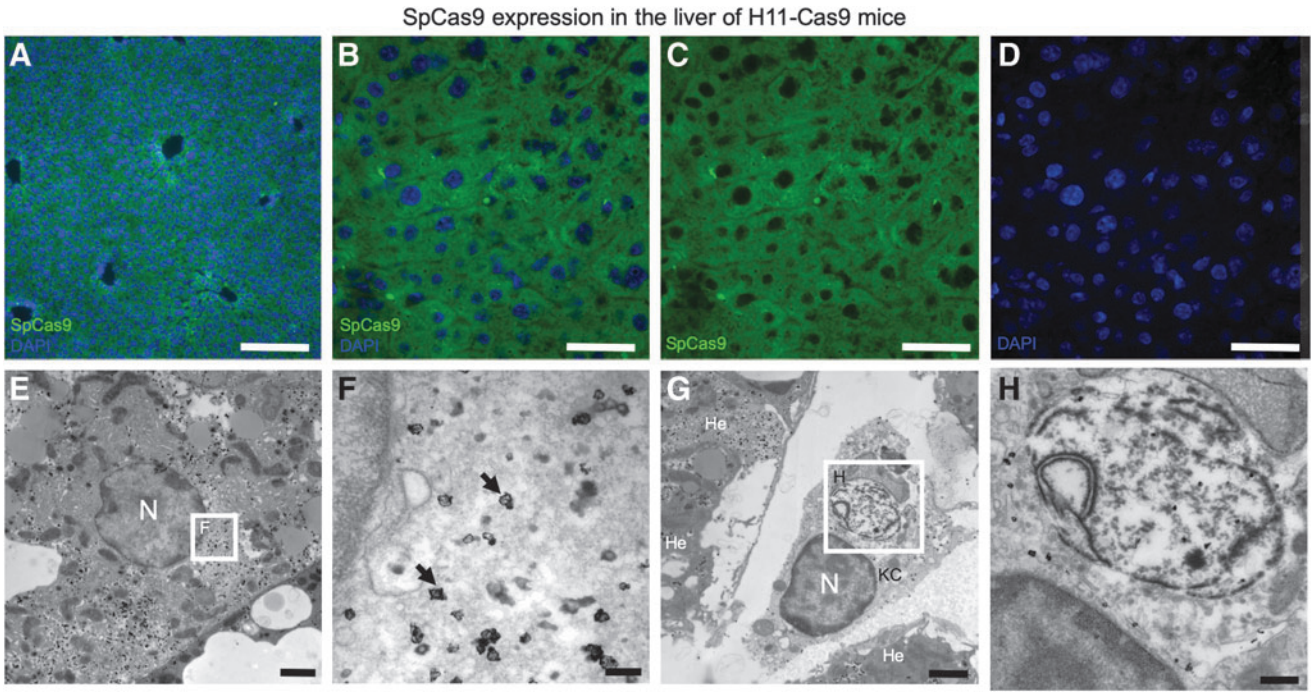


**FIG. 6.** Immunofluorescence detection of SpCas9 in the brain of H11-Cas9 mice. **(A–D)** IF detection of SpCas9 in the liver exhibits a ubiquitous cytoplasmic labeling in most cells. **(E)** IG-TEM analysis displays a hepatocyte presenting a homogenous distribution of SpCas9 throughout the cytoplasm. **(F)** High magnification photomicrograph of the labeled cytoplasm shown in **(E)** (arrows point to gold particles). **(G)** Kupffer cell labeled with SpCas9. **(H)** High-magnification micrograph of the labeled cytoplasm shown in **(G)**. He, hepatocyte; KC, Kupffer cell. Scale bars: **(A)** 250 $\mu$m; **(B–D)** 50 $\mu$m; **(E)** 2 $\mu$m; **(F)** 200 $\mu$m; **(G)** 2 $\mu$m; **(H)** 500 nm.

IF of the liver displayed a wide distribution of the label across the tissue (Fig. 6A–D). Intriguingly, IG in the liver allowed us to detect the gold labeling broadly distributed in the cytoplasm of some hepatocytes and Kupffer cells (Fig. 6E–H). This is an interesting fact, given that the liver is a highly autofluorescent organ, and IG can be a tool to discard autofluorescence while providing a high-resolution image.

The fact that IG can efficiently detect Cas9 in liver but not brain tissue suggests that not all tissues may be optimal for IG processing and analysis.

## Discussion

Cutting-edge studies have transformed the bacterial defense system CRISPR-Cas into a potent tool for genome editing,[3,23,24] not only for nuclear but also for extranuclear DNA.[2,4,17,25,26] However, to our knowledge, there are no studies that present ultrastructural data for CRISPR applications. Conventional techniques, such as IF Cas9 detection, do not allow for subcellular tracking, nor do they provide super-resolution images that facilitate the understanding of the dynamics of this bacterial enzyme within the eukaryotic cell.

Therefore, the purpose of this study was to develop a tool to achieve Cas9 identification and high-resolution imaging for individual cells. Accordingly, we used different *in vitro* and *in vivo* studies to assay IG combined with TEM in order to analyze different cellular features of Cas9 expressing cells.

We transfected HEK293T with PX458 Cas9 expressing plasmid as a control and proof of principle for cell-line experimentation. In this aspect, our results using IF show that 24 h after transfection, these cells display a broad distribution of the enzyme throughout the nucleus and cytoplasm. Still, IG provides a better resolution for subcellular localization. TEM analysis allows the detection of the enzyme within the nucleus but not in the nucleolus, and furthermore, it permits the visualization of Cas9 in the proximity of nuclear pores, suggesting its nuclear translocation.

As a proof of concept for Cas9 detection in primary cell cultures, we used oligodendrocyte progenitors isolated from P0 mice from control and transgenic animals that constitutively express Cas9. TEM analysis allowed us to detect Cas9 mostly in vesicles and in the perinuclear space, while this effect was not observed when these

cells were transfected with GFP. However, recent articles achieve genome editing in OPCs by using either human-induced pluripotent stem cells together with lipofection[27] or viral vectors in primary OPCs.[28] This indicates that the method of isolating or inducing OPC production and the transfection method is rather important in this cell lineage. Our results suggest that nuclear internalization and/or enzyme availability in the nucleus of OPCs is scarce and therefore undetectable, opening the field to more studies that take into account aspects to understand and correlate the efficiency of genomic edition with nuclear availability and nuclear transportation in primary oligodendroglial lineage cell cultures.

Taking into account the broad cytoplasmic distribution of GFP in PX458 and pMAX GFP transfections, together with our quantitative analysis showing an increase in GFP expression over time, we suggest that GFP is a stable protein in OPCs. We found a similar increase in the number of Cas9-positive cells with time. Nevertheless, the subcellular distribution of this protein appeared to be restricted to the perinuclear space and cytoplasmic vesicles at the short and medium term after transfection (24 and 72 h, respectively). Furthermore, in the longer term (5 days after transfection), Cas9 appeared mostly confined to lysosomal vesicles and autophagosomes, suggesting that the enzyme is degraded by OPCs after lipofection. In contrast, Cas9-expressing OPCs displayed a wide cytoplasmic distribution of the enzyme in nondividing cells. These findings reveal the potential of immunoelectron microscopy to provide complementary information to that offered by other techniques, such as IF or Western blot, to elucidate the final fate of proteins at the subcellular level. Additionally, IG-TEM favors the comparison of transfected versus non-transfected and dividing versus nondividing cells within the same culture.

Finally, we also demonstrate that IG-TEM can be successfully used for Cas9 detection in mouse tissues such as the liver. Conversely, while IF was able to reveal Cas9 expression in the brain, IG-TEM was not effective for this purpose. While we cannot rule out the possibility that enhanced methods could improve Cas9 detection in difficult tissues, there is evidence supporting the fact that antibody–antigen interactions can be complex and unpredictable, especially in applications such as immunoelectron microscopy.[29] Technical improvements in antibody design, tissue processing, and Cas9 expression will help to overcome these limitations.

## Conclusion

In conclusion, we have adapted a classic method such as TEM with a state-of-the-art tool such as the CRISPR-Cas system to potentiate this technique in the cell biology field and give a clearer vision and a more exact validation for CRISPR users. Ultrastructural studies together with IG labeling contribute to a deeper comprehension of Cas9 biology at the subcellular level. Nevertheless, further research is needed in this field to understand CRISPR-Cas9 dynamics better in a wider spectrum of cell types and tissues.

## Acknowledgments

The authors acknowledge the support of Susana González-Granero at the Laboratory of Comparative Neurobiology of the University of Valencia and the electron microscopy service at the Centro de Investigación Príncipe Felipe (Mario Soriano-Navarro) for their valuable help.

## Author Disclosure Statement

The authors declare no competing financial interests.

## Funding Information

This study was funded by the *Nano-scaffolding for neuronal migration and generation* project (PCI2018-093062) granted by the Spanish Ministry of Science, Innovation and Universities to V.H-P. and by Red de Terapia Celular (TerCel-RD16/0011/0026) to J.M.G-V. M.J.U-N. was supported by a McDonald Fellowship from the Multiple Sclerosis International Federation.

## Supplementary Material

Supplementary Figure S1

## References

1. Hsu PD, Lander ES, Zhang F. Development and applications of CRISPR-Cas9 for genome engineering. *Cell* 2014;157:1262–1278. DOI: 10.1016/j.cell.2014.05.010.
2. Jinek M, Chylinski K, Fonfara I, et al. A programmable dual-RNA-guided DNA endonuclease in adaptive bacterial immunity. *Science* 2012;337:816–821. DOI: 10.1126/science.1225829.
3. Barrangou R, Fremaux C, Deveau H, et al. CRISPR provides acquired resistance against viruses in prokaryotes. *Science* 2007;315:1709–1712. DOI: 10.1126/science.1138140.
4. Cong L, Ran FA, Cox D, et al. Multiplex genome engineering using CRISPR/Cas systems. *Science* 2013;339:819–823. DOI: 10.1126/science.1231143.
5. Sander JD, Joung JK. CRISPR-Cas systems for editing, regulating and targeting genomes. *Nat Biotechnol* 2014;32:347–355. DOI: 10.1038/nbt.2842.
6. Roth DB, Lindahl T, Gellert M. Repair and recombination. How to make ends meet. *Curr Biol* 1995;5:496–499.
7. Soutoglou E, Dorn JF, Sengupta K, et al. Positional stability of single double-strand breaks in mammalian cells. *Nat Cell Biol* 2007;9:675–682. DOI: 10.1038/ncb1591.
8. Symington LS, Gautier J. Double-strand break end resection and repair pathway choice. *Annu Rev Genet* 2011;45:247–271. DOI: 10.1146/annurev-genet-110410-132435.
9. Glass Z, Li Y, Xu Q. Nanoparticles for CRISPR-Cas9 delivery. *Nat Biomed Eng* 2017;1:854–855. DOI: 10.1038/s41551-017-0158-x.
10. Yu JH, Schaffer DV. Advanced targeting strategies for murine retroviral and adeno-associated viral vectors. *Adv Biochem Eng Biotechnol* 2005;99:147–167.
11. Epstein BE, Schaffer DV. Combining engineered nucleases with adeno-associated viral vectors for therapeutic gene editing. *Adv Exp Med Biol* 2017;1016:29–42. DOI: 10.1007/978-3-319-63904-8_2.

12. Weltner J, Balboa D, Katayama S, et al. Human pluripotent reprogramming with CRISPR activators. *Nat Commun* 2018;9:2643. DOI: 10.1038/s41467-018-05067-x.
13. Fogarty NME, McCarthy A, Snijders KE, et al. Genome editing reveals a role for OCT4 in human embryogenesis. *Nature* 2017;550:67–73. DOI: 10.1038/nature24033.
14. Koo B-K. Generation of FLIP and FLIP-FlpE targeting vectors for biallelic conditional and reversible gene knockouts in mouse and human cells. *Methods Mol Biol* 2018;1842:255–264. DOI: 10.1007/978-1-4939-8697-2_19.
15. Jin W, Lin D, Nguyen AH, et al. Transfection of difficult-to-transfect rat primary cortical neurons with magnetic nanoparticles. *J Biomed Nanotechnol* 2018;14:1654–1664. DOI: 10.1166/jbn.2018.2604.
16. Vakulskas CA, Dever DP, Rettig GR, et al. A high-fidelity Cas9 mutant delivered as a ribonucleoprotein complex enables efficient gene editing in human hematopoietic stem and progenitor cells. *Nat Med* 2018;24:1216–1224. DOI: 10.1038/s41591-018-0137-0.
17. Jo A, Ham S, Lee GH, et al. Efficient mitochondrial genome editing by CRISPR/Cas9. *Biomed Res Int* 2015;2015:305716. DOI: 10.1155/2015/305716.
18. Wang H, Xu X, Nguyen CM, et al. CRISPR-mediated programmable 3D genome positioning and nuclear organization. *Cell* 2018;175:1405–1417.e14. DOI: 10.1016/j.cell.2018.09.013.
19. Sirerol-Piquer MS, Cebrián-Silla A, Alfaro-Cervelló C, et al. GFP immunogold staining, from light to electron microscopy, in mammalian cells. *Micron* 2012;43:589–599. DOI: 10.1016/j.micron.2011.10.008.
20. Gil-Perotin S, Cebrián-Silla A, Herranz-Pérez V, et al. Localization of GFP-tagged proteins at the electron microscope. In: *Neuromethods*. Totowa, NJ: Humana Press, Inc., 2016, pp. 179–190.
21. Nishiyama J, Mikuni T, Yasuda R. Virus-mediated genome editing via homology-directed repair in mitotic and postmitotic cells in mammalian brain. *Neuron* 2017;96:755–768.e5. DOI: 10.1016/j.neuron.2017.10.004.
22. Ran FA, Hsu PD, Wright J, et al. Genome engineering using the CRISPR-Cas9 system. *Nat Protoc* 2013;8:2281–2308. DOI: 10.1038/nprot.2013.143.
23. Mojica FJ, Díez-Villaseñor C, Soria E, et al. Biological significance of a family of regularly spaced repeats in the genomes of Archaea, Bacteria and mitochondria. *Mol Microbiol* 2000;36:244–246.
24. Jansen R, van Embden JDA, Gaastra W, et al. Identification of genes that are associated with DNA repeats in prokaryotes. *Mol Microbiol* 2002;43:1565–1575.
25. Qi LS, Larson MH, Gilbert LA, et al. Repurposing CRISPR as an RNA-guided platform for sequence-specific control of gene expression. *Cell* 2013;152:1173–1183. DOI: 10.1016/j.cell.2013.02.022.
26. Piatek AA, Lenaghan SC, Neal Stewart C Jr. Advanced editing of the nuclear and plastid genomes in plants. *Plant Sci* 2018;273:42–49. DOI: 10.1016/j.plantsci.2018.02.025.
27. Petersen MA, Ryu JK, Chang K-J, et al. Fibrinogen activates BMP signaling in oligodendrocyte progenitor cells and inhibits remyelination after vascular damage. *Neuron* 2017;96:1003–1012.e7. DOI: 10.1016/j.neuron.2017.10.008.
28. Scaglione A, Patzig J, Liang J, et al. PRMT5-mediated regulation of developmental myelination. *Nat Commun* 2018;9:2840. DOI: 10.1038/s41467-018-04863-9.
29. Griffiths G, Lucocq JM. Antibodies for immunolabeling by light and electron microscopy: not for the faint hearted. *Histochem Cell Biol* 2014;142:347–360. DOI: 10.1007/s00418-014-1263-5.